CHARLES UNIVERSITY IN PRAGUE

FACULTY OF MATHEMATICS AND PHYSICS

INSTITUTE OF PHYSICS

DOCTORAL THESIS

Development of room temperature CdTe gamma ray detectors for security and medical applications

Hassan Elhadidy

Supervisor: Assoc. Prof. Ing. Jan Franc, DrSc.

Specialization: Semiconductor Physics - Optics and Optoelectronics

2008

Acknowledgements

At the outset, I would like to express my deep gratitude and thanks to my supervisor, Assoc. Prof. Ing. Jan Franc, DrSc. for his support throughout my time at the institute of Physics. His excellent guidance has extensively contributed to successful finish of my Ph. D. thesis. His talent, dedication, and enthusiasm have been my source of inspiration.

I'm so glad to have the beneficial opportunity to work in the group of Prof. RNDr. Pavel Hoschl, DrSc. and I'm very grateful to him for his valuable advices, continuous help and fruitful discussions.

I am very thankful to Assoc. Prof. Roman Grill, for his helpful suggestions, critical comments, and providing with software of the TEES simulation. I really appreciate the theoretical background that was given to me by him. Indeed, I'm grateful to Assoc. Prof. Pavel Moravec for the great experimental experience and support that was offered to me by him me with his beneficial advices, continuous help and fruitful discussions.

I would like to acknowledge Doc. Ing. Petr Praus, CSc. for his help with the temperature controller design and Dr. Michael Fiederle for providing PICTS measurements device in Freiburg.

For their support, guidance, and friendship over the past three years, I'm also indebted to Ing. Eduard Belas, CSc, Mgr. Jan Kubát and other colleagues from the Institute.

Last but not least, I want to take this opportunity to express my gratitude to my parents, wife, brothers, sisters, and my lovely baby. I dedicate this thesis to them.

I hereby state that I have written this doctoral thesis by myself using only the cited references. I agree to lend it

Prague, 29 May 2008 Hassan Elhadidy

Table of Contents

Title page……………………………………………………………………………… 1
Acknowledgements ……………………………………………………………….. 2
Table of contents ………………………………………………………………... 3
Abstract…………………………………………………………………………….. 5

Chapter 1: General Survey……………………………………………………….. 6
1.1 Introduction……………………………………………………………….... 6
1.2 Goal of the Study………………………………………………………... 8
1.3 Basic characteristics of CdTe………………………………………………. 8
1.3.1 Not intentionally doped CdTe………………………………………. 8
1.3.2 Intentionally doped CdTe…………………………………………… 10
1.3.2.1 Doping with transition metal elements……………………... 11
1.3.2.2 Doping with elements from groups I, III, IV, V and VII…… 12
I- Shallow doping……………………………………………… 12
II- Deep doping…………………………………………………… 13
1.4 Study of defect states in CdTe compounds……………………………… 16
1.4.1 Methods used to study the defects states……………………………. 16
1.4.2 Defect levels in SI CdTe... 17

Chapter 2: Theory…………………………………………………………………… 20
2.1 Shockley-Read-Hall model………………………………………………… 20
I- Low concentrations of centers………………………………………. 22
II- High center concentrations……………………………………...... 22
2.2 PICTS theory…………………………………………………………….. 22
2.2.1 Two-gate methods for PICTS evaluation…………………………… 24
2.2.2 Four gate methods for PICTS evaluation…………………………... 24
2.3 Evaluation of electron trapping parameters
from conductivity glow curves……………………………………….. 25
1- Grossweiner's method……………………………………………… 26
2- Variation of the heating rate method……………………………….. 26
3- The initial rise method……………………………………………… 27
4- Haering and Adams method………………………………………… 27
2.4 Resistivity mapping……………………………………………………… 28

Chapter 3 : Experimental……………………………………………………….. 30
3.1 Crystal descriptions………………………………………………………… 30
3.2 Sample preparations……………………………………………………….. 30
3.3 Measuring methods
3.3.1 Thermoelectric Effect Spectroscopy method………………………. 31
3.3.2 Photo-induced current transient spectroscopy method…………….. 34
3.3.3 Resistivity mapping method……………………………………….. 35
3.3.4 Photoluminescence method………………………………………… 37
3.3.5 Photocurrent spectroscopy (PCS) methods………………………… 37

Chapter 4: Results and discussion…………………………………………… 39
4.1 Comparative study of CdTe doped by shallow and deep impurities……. 39
4.1.1 Content of the impurities………………………………………….. 40

4.1.2. TEES measurements…………………………………………….. 41
4.1.2.1 Samples doped with shallow donors………………………. 41
4.1.2.2 Samples doped with deep donors………………………….. 44
4.1.3 PICTS measurements……………………………………………… 47
4.1.4 Summary………………………………………………………… 48
4.2 Complex study of CdTe:Sn crystals…………………………………… 50
4.2.1 Content of impurities………………………………………………. 50
4.2.2 Resistivity and photoconductivity mapping………………………….. 52
4.2.3 Defect levels in bandgap of CdTe:Sn………………………………… 52
4.2.3.1 Photoluminescence and Photocurrent spectra……………… 54
4.2.3.2 Photoluminescence mapping………………………………. 58
4.2.3.3 PICTS measurements……………………………………… 59
4.2.4 Summary………………………………………………………………. 60
4.3 Dependence of TEES of CdTe:Sn on Fermi level position…………….. 61
4.3.1 Measurement of the types of conductivity…………………………… 61
4.3.2 Resistivity map…………………………………………………… 61
4.3.3 Calculation of the position of the Fermi level……………………….. 62
4.3.4 Fermi level position and the TEES of CdTe:Sn……………………… 63
4.3.4.1 Fermi level position…………………………………….. 63
4.3.4.2 TEES spectra………………………………………………. 64
4.3.5 Summary………………………………………………………………. 65
4.4 Detailed characterization of defects in CdTe:In by TEES……………… 66
4.4.1 TEES measurements………………………………………………… 66
4.4.2 Origin of the traps…………………………………………………... 71
4.4.3 Traps and the charge collections properties…………………………. 71
4.4.4 Summary…………………………………………………………….. 72
4.5 Photoluminescence study of CdTe:Sn and CdTe:In
by Ti-sapphire laser and HgCdTe detector………………………………. 73
4.5.1 Experimental Results………………………………………………… 73
4.6 Numerical simulation of TEES………………………………………….. 79
4.6.1 Outlines of the model……………………………………………….. 79
4.6.1.1 Theory……………………………………………………… 79
4.6.1.2 Model output………………………………………………. 80
4.6.1.3 Model Inputs……………………………………………….. 80
4.6.1.4 Model Approximations…………………………………….. 81
4.6.2 Validity of the some glow curves evaluations methods…………….. 81
4.6.3 Study the influences of trapping parameters on the TEES signal…… 82
4.6.3.1 The influence of the concentration
of the traps on their TEES signals…………………………. 82
4.6.3.2 The influences of the capture radii of the deep level on
the TEES signal from donor and acceptor level………….. 83
4.6.3.3 Influences of the midgap level position on the TEES
signal from donor and acceptor level……………………. 84
4.6.4 Summary……………………………………………………….. 85
CONCLUSION……………………………………………………………. 87
List of publications Related to the Thesis……………………………………… 89
Reference…………………………………………………………...................... 90

Abstract

Defect structure in high resistivity CdTe samples doped with shallow (In, Cl) and deep (Sn, Ge) donors from crystals grown by vertical gradient freeze method have been investigated by several characterization techniques, to identify which defects act as strong traps or recombination centers that deteriorate the mobility-lifetime product ($\mu\tau$) of the carriers in order to eliminate them from the technological process.

Thermoelectric effect spectroscopy (TEES) and photo-induced current transient spectroscopy (PICTS) methods have been used in comparative study of various samples and showed that near midgap levels in samples doped with shallow donors (Cl, In) have a low value of capture cross-section and are hole traps. Traps in samples doped with a deep donor (Ge, Sn) have higher capture cross section of the midgap level, and act as an electron trap which results in a substantial deterioration of detector performance. TEES measurement using Fermi-level scanning revealed the conversion of the Sn defect from the electron trap in the lower resistivity sample to the hole trap in the higher resistivity one.

Photoluminescence (PL), Photocurrent (PC), PICTS, and resistivity and photoconductivity techniques have been used in a complex study of Sn doped CdTe samples. It was found out that the middle-gap Sn related donor level is responsible for pinning of Fermi-level and for both compensation and photoconductivity. Two deep acceptor levels located lower in the band gap than the Sn donor level were found to be responsible for the photoconductivity at room temperature. While two deep electron traps, which deteriorate the detector ability of CdTe were identified as native complex defects

A detailed study of In doped CdTe samples using TEES and the mobility-lifetime product values have shown , that deterioration of the mobility-lifetime product of electrons can be caused by electron trap at E_C-(0.6-0.7)eV, which clarifies why some In doped CdTe samples are good detector and others are not detecting samples even both have hole midgap level. This electron trap was identified as a native defect. Therefore, annealing is expected to eliminate it from the technological process and this way to improve the yield of usable material. Maximum concentrations of these levels in the samples were estimated based on a combination of TEES and mobility-lifetime product measurements.

A comparative study of CdTe:Sn and CdTe:In using the PL and mobility lifetime measurements were done. A very intensive PL luminescence on deep levels is observed in case of CdTe:Sn samples. The intensity is approximately two orders of magnitude higher, than in In doped samples. Approximately 7-15% of radiative recombination occurs through deep levels in case of CdTe:Sn samples and 0.2-1% in case of CdTe:In . A correlation between the detection ability and the integral PL intensity at deep levels was observed.

A correlation between integral PL intensity of A-centers and deep levels in CdTe:In samples was found out. This fact supports the idea, that deep levels in these samples are primarily complexes formed together with A-centers.

TEES simulation model was presented based on the numerical solution of a set of kinetic equations introduced in the Shockley-Read-Hall model. The influences of trap parameters on the simulated TEES were investigated. Checking the validity of different methods for analysis of glow curves showed that the Variation of the heating rate method which ignored the retrapping process is the best method to analyze the TEES glow cures.

Chapter 1

General Survey

1.1 Introduction

The interest in non-cooled and portable spectrometric X and gamma-ray detectors increased remarkably in the last years. There are two reasons for this development:
1. Medical applications developed as a result of more strict demands on secure radiation dose and a necessity to improve image resolution. It was clearly demonstrated, that semiconductor detectors having ability to use advanced integration technology exhibit a key device for mapping of human organs.
2. Possible terrorist attacks represent huge risks due to a possible application of a "dirty" nuclear bomb. Only a sufficiently dense and sensitive monitoring system based on semiconducting detectors in places, where large amounts of people are concentrated, can remove this type of risk.

Semi-insulating CdTe and CdZnTe have long been known to have great potential in room-temperature X-ray and gamma ray semiconductor detector applications [1, 2]. The high atomic number and density of these compounds provide strong absorption and high detection efficiency of high energy photons. The wide band gap of the materials allows the fabrication of highly resistive devices enabling large depletion depths and low leakage currents, when the material is brought into the semiinsulating state with electrical compensation techniques. The moderately high mobility and lifetime of charge carriers (particularly electrons) allow good charge transport in devices depleted to several mm or even cm thickness. The full potential of these compounds for high-energy photon detection applications, however, was not exploited for many decades due to the limited commercial availability of high-quality crystals [3] . This situation has changed dramatically during the mid nineties with the emergence of few small companies committed to the advancement and commercialization of the CdZnTe based radiation detector technology. The main crystal producers are concentrated in USA (eV Products, Saxonburg, PA), Japan (Nikko), France (LETI, Eurorad) and Canada (Redlen).

Semiconductor detectors, Fig. 1-1, consists of a slab of a semiconductor material with electrodes on the opposite faces, which can be both ohmic or one of them is Schottky in order to further decrease the dark current. High-energy photons from an outside radioactive source or X-ray tube induce electron-hole pairs in the semiconductor volume through photoelectric or Compton interactions, with numbers proportional to the photon energy (for the photoelectric effect). The electrons and holes are separated and moved in the outside applied electric field, creating a current through the device. This current is typically integrated by a charge sensitive preamplifier to measure the total charge induced by the outside radiation and produces a voltage pulse, which collected as a histogram in a multi-channel analyzer (MCA). Photons with various energies produce voltage pulses in the preamplifier with various amplitude and individual peaks with various peak positions in MCA. Charge loss in the detector due to trapping or recombination results in reduced pulse amplitude and a low energy tail in the energy peak.

In order to transport the charge carriers through devices several mm or cm thick, the mobility (μ) and lifetime (τ) of the carriers has to be sufficiently high to avoid carrier trapping and recombination. While the electron mobility (μ_e = 1000–800 cm^2/Vs) and lifetime [τ_e = (1–5) $x10^{-6}$ s] are relatively high, the hole mobility (μ_h = 80–30 cm^2/Vs) and

lifetime (τ_h =10^{-6}–10^{-7} s) are typically very low in CdTe and CdZnTe [3]. In most applications requiring good spectral resolution, CdZnTe detectors with read-out schemes that use only (or largely) the electron signal and suppress the hole contribution are used [4-6].

For detectors with good signal to noise ratio working at room temperature, the leakage current should not exceed few nA. This requires free carrier concentration in the 10^5 cm^{-3} range and/or semi-insulating crystals with bulk electrical resistivity in the 10^{10} Ωcm range. In practice, barrier devices are fabricated using semi-insulating crystals. Most of the devices fabricated today use semi-insulating CdTe and CdZnTe crystals with metal electrodes (Pt, Au, In) that form Schottky-barrier devices [3].

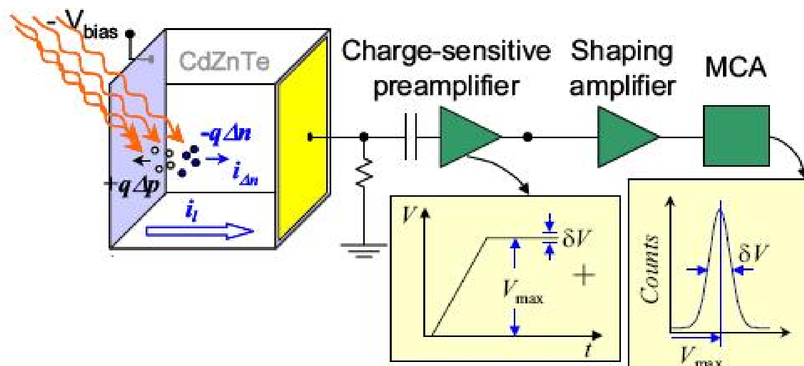

Fig. 1.1 Operation principle of semiconductor detectors [3]

The performance of room temperature semiconductor detectors is determined by *the charge transport* and *structural properties* of the available crystals.

The charge transport properties determine the collection efficiency of free carriers induced by the incident high energy photons and the various sources of noise in the crystals. There are two aspects of the charge transport properties that are extremely important for room temperature semiconductor detector devices. The materials have to be semi-insulating and the concentration of residual electrically active defects has to be low to provide sufficiently high carrier mobility and lifetime.

Structural properties of the materials control the uniformity of the charge transport. Non-uniform distribution of structural defects causes non-uniform charge trapping and electric field distribution, and lead to charge transport non-uniformity in detector. The various structural defects that adversely affect charge transport in CdZnTe [7, 8] are grain boundaries, twins, Te inclusions, dislocations and sub-grain boundaries. These defects can act as sites for the impurities and native defects segregation. This phenomenon deteriorates significantly the condition of a strong compensation in the working volume of material.

1.2 Goal of the Study

To make the design of detectors more scientific a lot of information has to be collected about the defects in the fabricated material. Defects in the bandgap of such material are controlling the charge transport properties of the material which reflects the performance of the detector.

The goal of study of this thesis is to investigate in detail the defect levels in the bandgap of high resistivity CdTe doped with shallow and deep donors for detector applications. Determination of the different trapping parameters of these defect levels and their correlation to the charge collection properties of the material are looked for. The goal is to analyze and to identify which defects act as strong traps or recombination centers that deteriorate the mobility-lifetime product ($\mu\tau$) of the carriers in order to eliminate them from the technological process and this way to improve the yield of usable material.

1.3 Basic characteristics of CdTe

CdTe has been known for a long time as a promising semiconductor with applications as gamma and x-ray detectors. The lattice match and chemical compatibility between CdZnTe and various compositions of HgCdTe make CdZnTe prime candidate as substrate material for HgCdTe epitaxy. CdTe is also one of the leading semiconducting materials in photovoltaic research. It demonstrated more than 15% efficiency in various laboratories and more than 10% efficiency measurement in industrial applications.

Many physical properties are controlled to some extent by the relative position of the energy levels within forbidden gap associated with the native defects or impurities. Both energy levels close to the band edges and deep levels play an important role in determining the electrical and optical properties of the material. It was observed that majority of these defect levels form several bands in the band gap with each band consisting of many discrete levels. Even though it is difficult to draw a clear line to distinguish between shallow and deep levels, we considered the trap levels having activation energy more than 0.2eV as a deep level and those levels with energies lower than 0.2eV as a shallow level.

1.3.1 Not intentionally doped CdTe

Not intentionally CdTe samples, prepared on the Te part of the phase diagram (low Cd pressure), have normally p-type conductivity with carrier concentrations typically about $10^{15}cm^{-3}$. CdTe in uncompensated form is a low-resistivity semiconductor due to the intrinsic defects and residual impurities. In undoped CdTe we can observe several native defects, which can be donors or acceptors. The high resistivity of undoped CdTe indicates relatively few electrically active impurities. In general, the simplest native defects are vacancies, antisites and interstitial atoms and their complexes such as vacancy-antisite pairs.

An equilibrium ab initio defect study found that under Te rich conditions, CdTe at high temperatures is a highly compensated p-type with cadmium vacancy, V_{Cd} , as the dominant acceptor and tellurium on cadmium site, Te_{Cd}, as the compensating donor [9].

Under Cd rich conditions, interstitial Cd_I is expected to dominate and make the material n-type. Complexes of native defects are formed due to the native acceptors (e.g.

V_{Cd}) and native donors (e.g. Te_{Cd}). Overview of the native level and native complexes energies in undoped CdTe recently calculated using the first-principles band-structure methods [10, 11] is illustrated in Fig1-2.

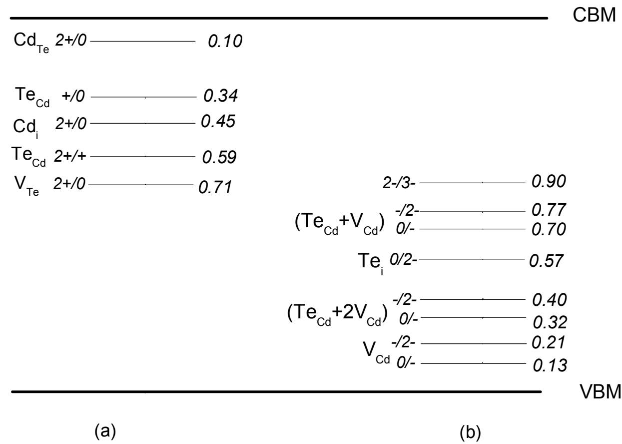

Fig. 1-2. Forbidden bandgap of the undoped CdTe with native defects (a) donor transition energy levels, and (b) acceptor transition energy levels, calculated theoretically using the first-principles band-structure methods.

However, the most recent (2008) first-principles calculations show that intrinsic defects may not have a significant effect on the carrier compensation either due to the lack of deep levels near midgap or to low defect concentration [12]. It was demonstrated, also, that an extrinsic defect, O_{Te}-H complex, may play an important role in the carrier compensation in CdTe because of it induces a (+/-) transition level near the midgap (E_C-0.73 eV) with amphoteric character and reasonably high concentration. The clear discrepancy between two latest ab initio studies shows that this type of calculations should be taken with caution mainly due to a relatively large computational error.

Experimentally, various methods were used to levels detection: Photo-EPR (photo electron paramagnetic resonance), DLTS (deep level transient spectroscopy), PICTS (photo induced current transient spectroscopy), TEES (thermoelectric effect spectroscopy), PL (photoluminescence), ODMR (optically detected magnetic resonance), SPS (surface plasmon spectroscopy), CPM (constant photocurrent method), TSC (Thermally stimulated current spectroscopy), Hall (Hall measurement) or TDL (tunable diode laser spectroscopy). Review about these experimental methods will be given in 1.4.1. List of levels observed in undoped samples is shown in Table 1-1. Main native defects presented in samples are $V_{Cd,}$, Te_{Cd}, Te_I , V_{Te} , Cd_I, and the complex of Te_{Cd} - $V_{Cd.}$

Both the isolated Cd and Te vacancies were identified in CdTe [13, 14] by EPR and photo-EPR methods. The Cd and Te vacancy concentrations in CdTe were found to be less than $1x10^{16}$ cm^{-3}. The $V_{Cd^-}^{2-}$ position was found be less than 0.47 eV above the valence band, the uncertainty being due to lattice relaxation energy.

Positron lifetime spectroscopy was used to measure the neutral and negatively charged vacancy concentrations in CdTe grown by vertical Bridgmann technique [15] and found mostly neutral V_{Cd} complexes in the high 10^{16} cm^{-3} range.

Table 1-1. Energies related to native defects in CdTe

Defect	Energy [eV]	Capture cross-section [cm^2]	Donor / Acceptor	Method	Reference
V_{Cd}	<0.47		Acceptor	EPR, Photo-EPR	[13, 14]
V_{Cd}	0.100		Acceptor	DLTS, PICTS	[16]
V_{Cd}	0.100	(6.4-8.4) x 10^{-16}	Acceptor	TEES	[11]
V_{Cd}	0.21		Acceptor	TEES	[17]
V_{Cd}	0.23-0.25	(1.8-9) x 10^{-16}	Acceptor	TEES	[11]
V_{Cd}	0.400		Acceptor	DLTS, PICTS	[16]
V_{Cd}	0.430		Acceptor	TEES	[18]
V_{Cd}	0.730		Donor	TEES	[17]
V_{Cd}	0.730		Acceptor	TEES	[19, 20]
V_{Cd}	0.760		Acceptor	DLTS, PICTS	[16]
V_{Cd}	0.78	4 x 10^{-13}	Acceptor	PICTS	[21, 22]
Te_{Cd}	0.39-0.43	(2.3-4.9) x 10^{-13}	Donor	TEES	[11]
Te_{Cd}	0.74		Donor	TEES	[19, 20]
Te_{Cd}-$2V_{Cd}$	0.43-49	1.1 x 10^{-14}	Acceptor	TEES	[11]
Te_{Cd}-$2V_{Cd}$	0.69-0.71	(1.8-4.7) x 10^{-14}	Acceptor	TEES	[11]
Te_{Cd}-V_{Cd}	0.85-0.73	1.58 x 10^{-12}	Acceptor	TEES	[11]
V_{Te}	1.400		Donor	Photo-EPR	[23]
V_{Te}	1.100		Donor	DLTS, PICTS	[16]
V_{Te}	0.400		Donor	Theory	[9]
V_{Te}	0.500	1 x 10^{-16}	Donor	Theory	[24, 25]
Cd_I	0.640	4 x 10^{-12}	Donor	DLTS, PICTS	[16, 22]
Cd_I	0.540		Donor	PICTS	[26]
Unknown	0.250	2-3x10^{-19}			[25]
Unknown	0.240	2-6x10^{-17}		DLTS	[27]
Unknown	0.880	1.2 x 10^{-12}			[25]

1.3.2 Intentionally doped CdTe

Many applications of the CdTe, like electro-optical devices, require that the material has high resistivity and minimum concentration of carrier traps that contribute to incomplete charge collection and broadening in the photopeak for radiation detector applications. While the resistivity above 10^9 Ωcm is desirable, the minimum resistivity approximately 10^8 Ωcm is acceptable [28]. For most materials, the achievement of high resistivity material by purification is unrealistic, where even in the crystals prepared from high purity (7N) materials, still there are several part per billion (ppb) of chemical impurities and the deal of native defects, introducing localized levels in the gap acting as donors or acceptors. Therefore it is necessary to introduce dopants or defects that compensate the existing impurities. There are two main manners to the doping of samples

1.3.2.1 Doping with transition metal elements

Doping with these elements is promising for the material photorefractive effect and applications in optoelectronics. For materials used as radiation detectors, they appear to be important in making the material semi-insulating [29]. Such dopants, normally occupy the Cd site, act as deep donors and form near midgap levels. As a result of doping the residual acceptors are compensated, the Fermi level is pinned at the midgap position which results in high resistivity material. A summary of the ionization energies of transition metal impurities is given in Table 1-3.

Vanadium, V, doping study showed that doping with V in the range of (1-10) $x10^{18}$ cm^{-3} can make CdZnTe semi-insulating with resistivities in the 10^{9}-10^{10} Ωcm range [29]. Overview of defect levels connected to deep dopants in CdTe is given in Ref. [30].

Due to the fact that both its diffusivity and solid solubility is high [21] Cu has potential role in compensation and trapping in CdTe. The role of Cu in CdTe was in detail investigated in many Refs, e.g. [21, 26, 31]. It was shown that, the level with energy 0.35 - 0.37eV above the valence band corresponds to Cu occupying Cd sublattice and acts therefore as an acceptor, resulting in substantial improvements in the resistivity, but it reduced the carrier lifetimes [21]. Clearly, Cu doping leads to a deep state that is effective at trapping of charge and help to pin the Fermi-level closer to the mid bandgap position.

Theoretically, ab intio calculations of the defect levels in the bandgap of the doped CdTe with some extrinsic impurity from these elements including the formation of complexes are illustrated in Fig. 1-3.

Table 1-2. Energies of transition metal elements in CdTe

Dopant	Energy [eV]	Donor / Acceptor	Experimental method	Reference
Ag	0.108	Acceptor	PL	[32]
Au	0.263	Acceptor	PL	[33]
Co	1.250	Acceptor	EPR, ODMR,PL	[34]
Cr	1.340	Acceptor	EPR, ODMR,PL	[35]
Cu	0.146	Acceptor	PL	[36]
Cu	0.360	Acceptor	PICTS	[31]
Cu	0.370	Acceptor	PICTS	[26]
Fe	0.150	Acceptor	SPS	[37]
Fe	0.200	Acceptor	CPM	[30]
Fe	0.350	Acceptor	EPR, ODMR,PL	[38]
Fe	0.430	Acceptor	TSC	[30]
Fe	1.450	Donor	Photo-EPR	[39]
Mn	0.050	Donor	Hall	[40]
Mn	0.730	Donor	Hall	[40]
Ni	0.760	Donor	CPM	[30]
Ni	0.920	Acceptor	EPR, ODMR,PL	[38]
Sc	0.011	Donor	PL	[32]
Ti	0.730	Donor	PL, TDH	[32]
Ti	0.830	Donor	DLTS	[41]
V	0.510	Acceptor	TSC	[30]
V	0.670	Donor	Photo-EPR	[42]
V	0.740	Acceptor	Theory	[43]
V	0.950	Donor	DLTS	[44]

1.3.2.2 Doping with elements from groups I, III, IV, V and VII

Due to the fact, that the dopants used in this thesis belong to these groups, especially the elements In and Sn, the features of this doping will be discussed here in detail. Energy levels related to major impurities of elements from groups I, III, IV, V and VII and their complexes with native defects are shown in Table 1-3. Theoretically, defect levels in the bandgap of the doped CdTe with some extrinsic impurity from these groups including the formation of complexes is calculated [10] using the first-principles band-structure methods and illustrated in Fig.1-3.

III- Shallow doping

Due to the small ionization energy of the elements from groups I, III, V and Vll (< 0.2 eV) their doping can be referred to as shallow doping. Group I elements, like Li and Na act as acceptors when occupying the Cd sites, but, on interstitial sites, they act as donors [45]. Group III elements, like In, Ga and Al, on the Cd sites and VII elements like Cl, Br and I, on the Te sites are donor states. Substitutional group V elements, like P, Sb, and Bi, on Te sites are acceptor states. Therefore, doping with these elements (groups I, III, V and VII) creates either shallow donors, or acceptor states, which should compensate the impurities and native defect in the pure material.

The most important feature of the shallow donor doping in CdTe is the formation of the donor-vacancy (V_{Cd}) complex, which is called an A-center, and the self-compensation process. It was observed that for In-doped CdTe, In_{Cd} is a shallow donor. The free carrier concentration, n, increased linearly with N_{In} indicating 100% doping efficiency at low In concentrations. At above N_{In} of $2x10^{18}$ cm^{-3} the increase stops [46]. Since the solubility limit of In is known to be $1x10^{19}$ cm^{-3} or higher, this effect is seen as evidence of self-compensation, that is, by creation of Cd-vacancies when high concentration of Indium is introduced. A more detailed study of this phenomenon has shown, that at high In concentration the Fermi level is positioned close to the C-band and the electron energy is sufficient to form the Cd vacancy. The A-center consisting of Cd vacancy and In_{Cd} was supposed to be created $(In_{Cd}^{+} - V_{Cd}^{2-})^{-}$ [47].

The same results were also reported in a MBE study of In doping of CdZnTe under Cd over - pressure. In donor of 100% activation efficiency was found between $2x10^{16}$ and $1x10^{18}$ cm^{-3}, but strong self-compensation behavior was observed for higher concentrations [48]. The formation of the In-V_{Cd} complex is also confirmed in [19, 49, 50] and showed, by using the positron lifetime measurements, that it is either neutral or negatively charged. The acceptor level of this complex in CdTe:In was found out by PL measurements at E_C-1.465 [47]. The chemical structure of Indium based A-centers in CdTe was confirmed by X-ray methods [51].

For compensation to work without excessive trapping there must be a mechanism by which a delicate balance between donors and acceptors can be achieved. In most material, including CdTe, there is no easy way to achieve a precise balance between shallow donors and acceptors. In spite of this high resistivity state is often observed with shallow donor doing. A theoretical model explaining the role of shallow donors in formation of high resistivity state, when a midgap level with a very low concentration $N_{deep}<10^{13}cm^{-3}$ is present, was proposed [52]. The model is based on processes of self-compensation and precipitation of Cd vacancies in CdTe doped with shallow donors (In, Cl) during cooling to room temperature.

At the same time the compensation is achieved by the presence of deep levels, they may also act as carrier trapping centers and thus the study of both compensation and carrier traps is critical in determining the potential of this material as a radiation detector [53].

A detailed investigation of distribution of point defects in high resistivity In doped CdTe prepared by vertical gradient freeze method was performed by Franc et al [54] by a set of optical, photoelectrical and electrical methods. It was found, that the defect located 1.05eV below the conduction band represents a center of photosensitivity. A deep level probably responsible for pinning of the Fermi level near the middle of the gap was found by PICTS at 0.8 eV.

Cl has been employed in CdTe to produce high resistivity material [21], where Cl_{Te} is a shallow donor with a level detected at 0.14 eV below the E_C. In addition, PL showed the chlorine A-center at energy E_V+0.12 eV, and optically detected magnetic-resonance technique verified the A-center to consist of a V_{Cd} vacancy and a Cl_{Te} donor [55]. A near proportionality was found between the concentration of A-centers and the concentration of Cl using positron lifetime measurements [50].

Because of the importance of compensation and trapping in CdTe for nuclear detector applications, and because of a broader interest in semi-insulating materials for applications for epitaxial substrates and electro-optical devices, there is considerable interest in this thesis in trying to understand the mechanism of compensation, including the origin, concentration, and the trapping properties of these deep levels in the case of shallow donors doping.

IV- Deep doping

The possibility to prepare high-resistivity CdTe by doping with IV group elements (Ge, Sn) was demonstrated in the past [56, 57]. These elements appear to introduce both shallow and deep levels. Si and C doped CdTe were also prepared, but showed little electrical activity [58]. Electron paramagnetic resonance (EPR) measurements [59] directly registered the Ge^{2+}/Ge^{3+} and the Sn^{2+}/Sn^{3+} donor levels 0.95 eV and 0.85 eV below the conduction band, respectively. Therefore, both dopants are potentially interesting for fabrication of detector grade CdTe in case that shallow acceptors prevail over shallow donors. Also, EPR studies of Pb and Ge doped CdTe have been reported [60]. Observation of many shallow and deep levels in Sn, P, Cs doped CdTe as characterized by DLTS, PICTS and PC has been reported [61].

A complex investigation of defect structure of high-resistivity, Sn-doped CdTe grown by vertical-gradient freeze and Bridgman methods by a number of optical, photoelectrical, and electrical methods was performed by Franc et al [62] and concluded that, besides Sn, which naturally acts as a deep donor and plays a major role in pinning of the Fermi level near the mid-gap, Fe related defects and Cd vacancies act as principal recombination and trapping centers.

There is an interest in this thesis to study the defect structure of Sn doped CdTe with special attention paid to deep levels substantially influencing the mobility-lifetime product and response time of the material, which can be considered as a promising one for fabrication of x-ray detectors.

Table 1-3. Energies of elements from groups I, III, IV, and VII in CdTe

Dopant	Energy [eV]	Capture cross-section	Donor / Acceptor	Experimental method	Reference
Al	0,014		Donor	PL	[63]
As	0,092		Acceptor	PL	[64]
Cl	0,014		Donor	EPR	[65]
Cl	0,015		Donor	PL	[63]
Cl-DX1	0,220		Donor	Theory	[66]
Cl-DX2	0,470		Donor	Theory	[66]
Cl-DX3	0,210		Donor	Theory	[66]
Cl-VCd	0,120		Acceptor	PL, ODMR	[55]
F	0,014		Donor	PL	[63]
Ga	0,014		Donor	PL	[63]
Ge	0,730		Acceptor	Photo-EPR	[64]
Ge	0,950		Donor	Photo-EPR	[38]
In	0,014		Donor	PL	[63]
In	0,220	$8.6x10^{-13}$	Acceptor	DLTS	[27]
In	0,230	2×10^{-15}	Acceptor	QTS	[22]
In	0,230	$3\text{-}4x10^{-13}$	Acceptor		[67]
In	0,280	$2x10^{-13}$	Acceptor		[67]
In	0,320	$2x10^{-14}$	Acceptor	QTS	[22]
In	0,340	$1\text{-}5.5x10^{-13}$	Acceptor	DLTS	[27]
In	0,340	$1x10^{-13}$	Acceptor		[67]
In	0,380	$4.9x10^{-14}$	Acceptor		[67]
In	0,470	2×10^{-15}	Acceptor		[67]
In	0,580	2×10^{-15}	Acceptor	DLTS	[27]
In	0,680	3×10^{-13}	Acceptor	DLTS	[27]
In	0,800	5×10^{-13}	Acceptor	QTS	[22]
In, undoped	0,210	5×10^{-14}	Acceptor	DLTS	[27]
In, undoped	0,280	$6.5x10^{-13}$	Acceptor	DLTS	[27]
In, undoped	0,380	$3x10^{-9}$	Acceptor	DLTS	[27]
In, undoped	0,460	4×10^{-14}	Acceptor	DLTS	[27]
In, undoped	0,740	$1\text{-}6 \times 10^{-14}$	Acceptor		[67]
In, undoped	0,860	2×10^{-12}	Acceptor	DLTS	[27]
Li	0,058		Acceptor	PL	[68]
N	0,056		Acceptor	PL	[64]
Na	0,059		Acceptor	PL	[68]
P	0,068		Acceptor	PL	[64]
Pb	1,280		Donor	Photo-EPR	[38]
Sn	0,380	$0.9x10^{-13}$	Acceptor	QTS	[22]
Sn	0,430	4×10^{-14}	Donor	QTS	[22]
Sn	0,510	1×10^{-14}	Acceptor	QTS	[22]
Sn	0,550		Acceptor	TEES	[19]
Sn	0,850		Donor	Photo-EPR	[38]
Sn	0,890	5×10^{-12}	Donor	QTS	[22]
Sn	0,900		Donor	DLTS	[61]

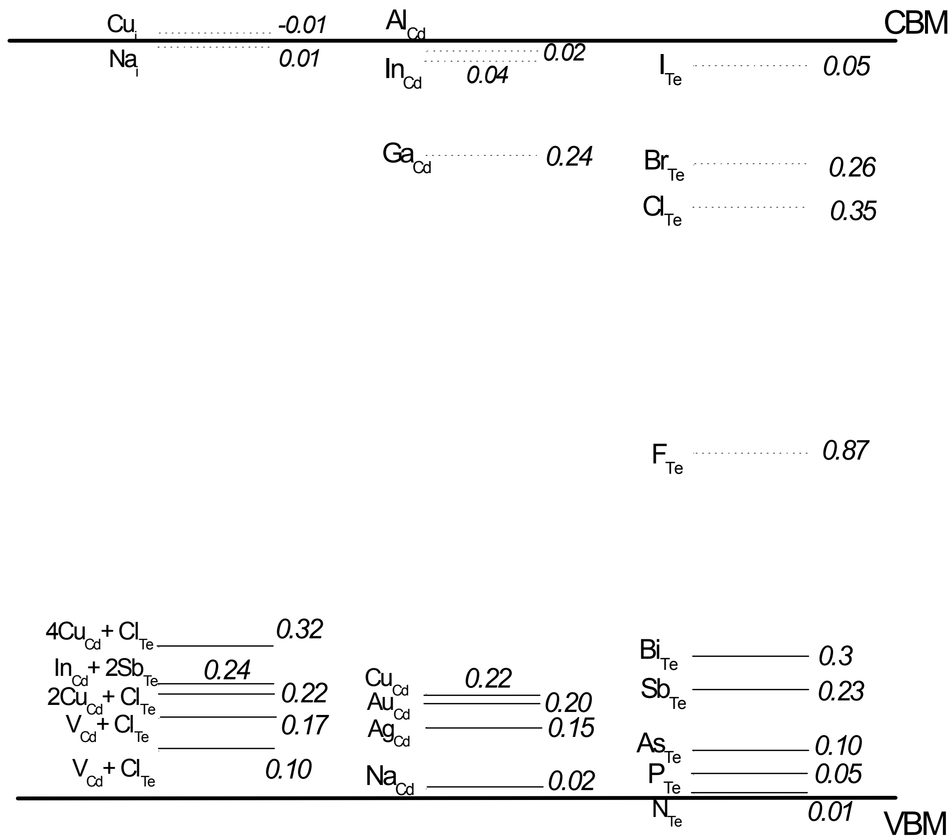

Fig. 1-3. Theoretically calculated energy levels using the first-principles band-structure methods in doped CdTe with extrinsic impurities, where (.....) are energy of donor levels with (+/0) transition, and (—) are acceptor energy levels with (0/-) transition,

1.4 Study of defect states in CdTe compounds.

1.4.1 Methods used to study the defects states.

There are many methods used for defect studies. A brief review of some of the most popular methods used to study CdTe is presented here.

Electron paramagnetic resonance (EPR) has been used for both the shallow and the deep levels to infer the electronic states of the impurities. However, photoluminescence (PL) has been used with a large degree of success to measure the ground state and excited state energies of the *shallow levels*.

Many methods were applied to study the deep levels, but the investigations are made difficult by the high resistivity of the material, difficulty with determination of the trap types (whether electron or hole), and difficulty of making metal/semiconductor contacts. Some of the most widely used methods are thermally stimulated current (TSC) and related methods [69, 70], thermoelectric emission spectroscopy (TEES) [71], deep level transient spectroscopy (DLTS) [72], photo-DLTS [73], photoinduced current transient spectroscopy (PICTS) [74], temperature-dependent Hall-effect (TDH) [75] and thermoelectric voltage spectroscopy (TEVS) [76].

However, for n-type SI CdTe, their high resistivity are on the order of 10^9 Ω cm and their typical RT electron mobility is about 1000 cm^2/V s, implying free carrier concentrations on the order of 6x 10^6 cm^{-3}. Methods such as DLTS and TDH cannot be used for samples with these resistivities since these methods require the free carrier concentration to exceed the impurity concentration. To circumvent this problem, photo-DLTS was developed, and it allows study of deep levels when combined with optical spectroscopy [73]. PICTS has also been used to study defects in CdTe and CdZnTe [16, 26, 31, 54, 62, 77-83],

In addition to the difficulties posed by high resistivity, the trap types are difficult to establish. TSC is a well-established method for studying SI materials, however, it is difficult to recognize the trap type from TSC because both electron and hole traps give signals having the same polarity. By using Schottky contacts and biasing, one can try to measure only majority carrier traps, but defects due to the contact electrodes compete with the bulk defects of interest [84, 85] . Furthermore, the Schottky contact resistance increases exponentially with decreasing temperature, which can severely distort the TSC spectra. The same considerations apply to DLTS and other methods. TSC has been used to study SI CdTe and CdZnTe materials [11, 18, 19, 58, 76, 77, 82, 86-90].

TEES [71] is described to be suitable for the study the deep levels in SI materials. It gives similar information on the energy position and the concentration of the traps as TSC, but in addition TEES is also capable to resolve hole traps from electron traps. It is also shown that the combination of TEES and TSC can reveal the trap influence on peculiar transit phenomena of some other quantities like photoconductivity [71]. TEES has proven to be a very powerful method for the study of deep levels defects in SI material. It was used in the investigation of SI-CdTe and CdZnTe samples in several Ref. [11, 17-20, 53, 76-78, 87-94]

1.4.2 Defect levels in SI CdTe.

Due to their important roles in various electrical and optical properties of semiinsulating CdTe and CdZnTe semiconductors, many groups have studied defect levels in the forbidden gap. Here, a brief review about the recent studies on the defect levels, in SI CdTe will be presented.

N. Krsmanovic et al. [19] used TEES method to study the effects of two intrinsic deep levels on electrical compensation in SI CdTe and CdZnTe crystals. The first level observed at E_V + 0.735 eV and assigned to V_{Cd}^{2-} acceptor, and the second level at E_V + 0.743 eV and identified as Te_{Cd} , which is thought to be complexed with a vacancy (V_{Cd}^{2-}). Therefore, they demonstrated that high-resistivity crystals can be grown by conventional Bridgman and high pressure Bridgman techniques from high-purity materials, such that either method reduces the Cd vacancy concentration during crystal growth, or by post-growth thermal processing, to a level at which it can be compensated by the second observed intrinsic defect (Te_{Cd}).

TEES and TSC methods have been used by N. Krsmanovic et al. [20] in the studies of deep trapping levels in undoped and Sn-doped CdZnTe. Temperature maximum, varying heating rate and initial rise methods were used to extract activation energies and trapping cross sections of the deep trapping levels in the samples. The pure sample had deep trapping levels with ionization energies of E_V + 0.73 eV and E_V + 0.74 eV, which were assigned to intrinsic defects due to Cd vacancies and Te antisites respectively. In the Sn doped samples deep levels at E_V + 0.34 eV, E_V + 0.55 eV and E_V + 0.73 eV were observed. The level at E_V + 0.55 eV was assigned to Sn, while the other levels to Cd vacancies. The pulse height measurements on these samples indicated that Sn doping did not improve the detector performance.

TEES and TSC were used by S. Awadalla et al. [90] to investigate trapping levels in SI CdTe and CdZnTe crystals grown by vertical Bridgman with over pressure control and high-pressure Bridgman methods. The thermal ionization energies of these levels were extracted using both the variable heating rate and initial rise methods. It was reported that the shallow levels observed at 0.11 and 0.17 eV are intrinsic and the latter level is most likely related to the dislocation density and better control of these levels is required to produce high resistivity crystals.

TSC and PICTS techniques were used in another study related to shallow defect levels in CdTe material [82]. It was reported about the origin of the 0.15 to 0.20 eV defect levels in undoped, chlorine and copper doped CdTe crystals grown by THM, and some of the studied samples were irradiated by a strong γ-ray source. The results showed that the defects origin is more complicated than generally considered.

TEES and TSC techniques were used to identify the defect levels in undoped and Al doped CdTe samples grown by high-pressure Bridgman [11]. Together 10 defect levels were identified in the crystals, such that their ionization energy and trapping cross section were extracted using the initial rise and variable heating rate methods. The ionization energy values obtained were compared to theoretical values of the transition-energy levels of intrinsic and extrinsic defects and defect complexes in CdTe determined by first-principles band-structure calculations. On the basis of this comparison, the observed defect levels were assigned to various native defects and impurity complexes.

By using TEES and TSC experiments, Cs. Szeles et al. [18] have observed hole trapping and thermal emission from a deep acceptor level created during thermal annealing of CdZnTe crystal grown by the high-pressure Bridgman technique. This deep level was assigned to the 2-/- acceptor level of isolated Cd (Zn) vacancies. The thermal ionization

energy of the level is 0.436 eV, and the trapping cross-section was found to be $2x10^{-16}$ cm^2.

The TEES method was used to investigate the role of cadmium vacancy-related defects in CdTe nuclear detectors by Z.C. Huang et al. [17]. It was reported on the deep level which is responsible for the degrading performance of CdTe nuclear detectors. Three CdTe wafers, undoped, Al-doped, and Zn-alloyed (Zn = 10%) were prepared by high pressure Bridgman technique. The cadmium vacancy (V_{Cd})-related defects, behaving as electron trap at E_C - 0.73 eV, was found to be responsible for the degrading performance of the detectors. The best detector was found to be from the material with the lowest concentration of this defect. This electron trap acts as hole recombination center, decreasing the hole collection efficiency in the photocurrent measurement. A V_{Cd}-related hole trap, at E_V + 0.21 eV, was also observed in these samples. It was suggested that alloying with zinc could be effective in eliminating these V_{Cd}-related deep levels, and hence improving the detector performance. On the other hand, deep electronic levels were studied as a function of Zn concentration in CdZnTe crystals grown by the high-pressure Bridgman technique using TEES [91]. It was reported that, hole traps are the dominant deep levels and a strong increase of the thermal ionization energies of hole traps was observed with increasing Zn content of the compound. The higher ionization energies explain the observed stronger hole trapping and much shorter hole lifetime in CdZnTe as compared to CdTe. The behavior also suggests increased carrier recombination and explains the strong deterioration of electron collection in detectors fabricated from CdZnTe of high Zn concentration.

Another effect of the Zn have been reported by S. Awadalla et al. [93]. Data obtained by TEES together with the first-principles total-energy calculations were used to investigate the cation vacancy–isoelectronic oxygen pair ($V_{(Cd/Zn)}$ -O_{Te}) in CdZnTe crystals compared to it is behavior in CdTe. It was reported that, the thermal ionization energy $E=E_V$ + 0.184 ±0.011 eV and trapping cross section $S=(7 \pm 4)10^{-17}$ cm^2 of the (−/2-) transition for the V_{Cd}-O_{Te} pair are identical to those found in CdTe. In addition the concentration of the pair is much smaller in CdZnTe than in CdTe crystal for samples with the same nominal oxygen concentration, due to the formation energy of substitutional O_{Te} is larger in CdZnTe than in CdTe. This indicates that the addition of Zn to CdTe reduces the O_{Te} concentration that form $V_{(Cd/Zn)}$-O_{Te} pair.

The TEES, TSC, and PICTS methods were used by M. Ayoub et al. [77] to investigate the defects in the CdTe:Cl crystals grown by traveling heater method under different annealing conditions. It was observed that an increase of the resistivity after a thermal treatment of samples under argon pressure.

A. Castaldini et al. [16] investigated the deep levels present in semiconducting CdTe and SI CdTe:Cl and CdZnTe by complementary spectroscopic techniques, where cathodoluminescence, DLTS, PICTS, and photo-DLTS were used. The latter two methods, which can be applied to SI materials, allow characterizing of the deep traps located up to midgap. Together 12 different traps were identified, some common to all the investigated samples, some peculiar to one of them. The analysis the SI compounds enlightened the role played by the defects involved in the compensation process namely A center and the deep traps located near midgap.

A. Castaldini et al. [80] studied the role which such deep traps play in the control of the electrical properties of the material. The combination of the PICTS, and photo-DLTS have been used to determine the character of deep trap, labeled H, as an acceptor at E_V+0.76eV, and an electron trap, labeled E, at E_C - 0.79eV. Level H was common to all investigated compounds and has been attributed to a deep acceptor complex related to V_{Cd}^{2-}, while E is present only in CdTe:Cl samples. This provides clear experimental

evidence of the presence of a deep trap in CdTe:Cl, which could be a good candidate for the deep donor level needed to explain the compensation process of SI CdTe:Cl.

On the other hand, A. Cavallini et al. [95] studied the compensation processes in CdTe-based compounds. In this study, PICTS and P-DLTS analyses together with DLTS analyses were carried out to deepen understanding the behavior of the these deep levels as a function of the position of the Fermi level since they are critical for the compensation process. They concluded that, in CdZnTe the level H at E_V+0.75 eV has a donor-like character. The possible extension of the donor-like character of this defect to CdTe:Cl should be positively considered.

A. Cavallini et al. [81] have used the PICTS techniques to identify the defect states induced in SI- CdTe:Cl and CdZnTe detectors by high and low energy neutron irradiation. Together 14 deep traps were observed, such that their relative concentration varies significantly as does their behavior under increasing neutron fluence. By correlating the evolution of each trap in the two investigated materials, it was possible to discuss hypotheses on the origin of most of the observed deep levels and on the role they play in the charge collection and material compensation properties.

Formatted: English (U.S.)

Defect levels in CdTe doped with Bi were studied [79] by low temperature PL, PICTS, PC measurements, and optical absorption. Two centers associated with the doping with Bi were reported. The first one, a deep level located at E_V+0.71 eV, only present at low dopant concentrations, has donor character and hole-trap properties, and is mainly responsible for the high resistivity and very high photoconductivity of the samples. The second one, an acceptor center located at E_V+0.30 eV, assigned to Bi_{Te} species, is only present at high dopant concentrations and is mainly responsible for the low resistivity and poor photoconductivity of these samples.

Franc et al. [96] investigated the defect structure of CdTe doped with Yb and co-doped with Ge, grown by Bridgman method, by a set of optical (PL, absorption, PC), galvanomagnetic and thermoelectric methods. It was explained that Yb acts as a deep donor with the energy level at E_V+0.3 eV corresponding to the $Yb^{2+/}Yb^{3+}$ electronic transition. Introduction of Yb with concentration 10^{19} cm^{-3} in the melt results in a decrease of electrically and optically active acceptor defects in the as-grown crystals and causes a decrease of electrical resistivity of CdTe:Ge

In this thesis, defect structure of shallow (In, Cl) and deep (Sn, Ge) doped CdTe will be studied in details by performing a set of complementary measuring techniques. We will analyze the mechanism of compensation, including the origin, concentration, and the trapping properties of these defects with special attention paid to deep levels substantially influencing the mobility-lifetime product and response time of the material, which can be considered as a promising one for fabrication of x-ray and gamma ray detectors.

Chapter 2

Theory

2.1 Shockley-Read-Hall model

The band diagram of the perfect single crystal semiconductor consists of a valence band and a conduction band separated by the forbidden band. When the periodicity of the single crystal is perturbed by foreign atoms or crystal defects, discrete energy levels are introduced into the band gap. Each energy level created from such defects can be represented by energy E_T and concentration of centers N_T. The Shockley-Read-Hall (SRH) model [97] was introduced to describe the statistics of generation-recombination of electron-hole pairs in crystal semiconductors occurring through the trapping mechanism of electrons on the generation-recombination centers in the forbidden band (deep-level impurities).

The transfer of electrons from the valence band to the conduction band is referred to the generation of electron-hole pairs (or pair-generation process), since not only a free electron is created in the conduction band, but also a hole in the valence band which can contribute to the charge current. The inverse process is the thermal recombination of electron-hole pairs. A third event, which is neither recombination nor generation, is the trapping event. In either case, a carrier (electron or hole) is captured and subsequently emitted back to the band from which it came. Only one of the two bands and the center participate. The basic mechanisms are illustrated in Fig. 2-1.

Generally, the center can act as a recombination center when there are excess carriers in the semiconductor and as a generation center when the carrier density is below its equilibrium value. These centers can be obtained due to metallic impurities or as the result of the crystal imperfections (dislocations, precipitates, vacancies or interstitials), most of them are undesirable [97, 98]. The electron emission rate for centers in the upper half of the band gap is much higher than the hole emission rate. This is in contrast with emission rates for centers in the lower half of the band gap. For most centers one emission rate dominates, and the other can frequently be neglected. The concentration of G-R centers occupied by electrons n_t, and holes p_t must equal the total concentration of centers N_T.

$$n_t + p_t = N_T \tag{2.1}$$

Basic assumptions of SRH model are:

1) free charge carriers can be only described with concentration and mid-thermal velocity
2) all crossings are immediate processes
3) parameters of trapping centers do not depend on state of surrounding system and correspond to equilibrium states
4) the drift-diffusion is assumed for the transport of electrons and holes
5) one trap level in the forbidden band
6) the dynamics of the trapped electrons is quasi-stationary, which can be motivated by the smallness of the density of trapped states compared to typical carrier densities

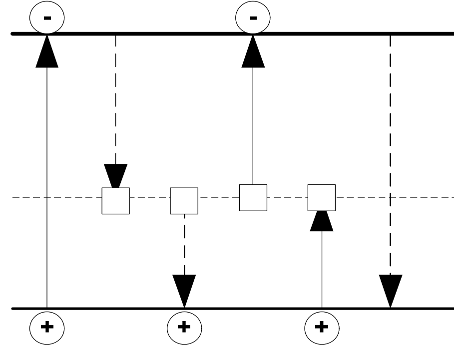

Fig. 2-1. Bandgap model with six basic processes of recombination with one deep level (1-generation of e^-h^+ pair, 2-capture of electron on trap, 3-capture of hole on trap, 4-excitation of electron from trap, 5-excitation of hole from trap, 6- bandgap recombination)

The rate equations for the densities of electrons in the conduction band, n, holes in the valence band, p, and trapped electrons on the center, n_t, due to the generation-recombination process after taking account the band to band process [99] are described as:

$$dn/dt = G + S_e v_e n_t n_l - S_e v_e (N_t - n_t)n + C_B(n_i^2 - np) \tag{2.2}$$

$$dp/dt = G + S_h v_h (N_t - n_t)p_l - S_h v_h n_t p + C_B(n_i^2 - np) \tag{2.3}$$

$$dn_t/dt = S_e v_e (N_t - n_t)n - S_e v_e n_t n_l + S_h v_h (N_t - n_t)p_l - S_h v_h n_t p \tag{2.4}$$

$$\Delta n + \Delta n_t = \Delta p \tag{2.5}$$

Where

$S_{e(h)}$ is electrons (hole) capture coefficient of the center.

$v_{e(h)}$ is electron (hole) thermal velocity

n_l (p_l) is electron (hole) concentrations when $E_F = E_t$.

G is the generation rate; C_B is the direct G-R rate between VB and CB.

Since there are excellent references of this model, e. g. [97, 98, 100], we outline only some of its basic conclusions, which are related to the carriers lifetime.

In thermal equilibrium, where the densities of electrons and holes in bands is n_o and p_o respectively, the relaxation time of free electrons (hole) on trap is defined as

$$\tau_{e(h)} = \frac{1}{S_{e(h)} v_{e(h)} p_t(n_t)} \tag{2.6}$$

In non-thermal equilibrium, there are two cases

1- Low concentrations of centers:

In this case, it is assumed that the majority carrier density under equilibrium conditions is large compared to the center density, so that we may neglect the change in charge density produced by changing concentrations in the trap center. This case is valid if any one of the four quantities n_o, p_o, n_l, p_l is large compared to N_t. So the deviation of electrons and hole densities from their thermal equilibrium must be equal to preserve electrical neutrality. If Δn represents this deviation, then

$$n = n_o + \Delta n, \qquad p = p_o + \Delta n (= \Delta p) \tag{2.7}$$

And the lifetime for both electrons and holes on the trap is

$$\tau = \tau_{h_0} \frac{n_0 + n_l + \Delta n}{n_0 + p_0 + \Delta n} + \tau_{e_0} \frac{p_0 + p_l + \Delta p}{n_0 + p_0 + \Delta n} \tag{2.8}$$

Where $\tau_{e0}(\tau_{h0})$ correspond to lifetime for electrons (holes) to totally empty (totally full of electrons) level.

Different formulas were obtained from eqn. (2.8) in Ref. [97] depending on whether the sample is n-type ($n_o \rangle\rangle p_0$) or p-type ($p_o \rangle\rangle n_0$), and the position of the center in the bandgap.

2- High center concentrations:

In this case, the concentrations $\Delta n \neq \Delta p$, and consequently, the electron and hole lifetimes are unequal. The lifetime of the minority carrier has the form:

$$\tau_e = \tau_{e_0}(1 + \frac{p_l}{p_0}) \text{ (p-type)} \qquad \tau_h = \tau_{h_0}(1 + \frac{n_l}{n_0}) \text{ (n-type)} \tag{2.9}$$

2.2 PICTS theory

PICTS (photo-induced current transient spectroscopy) is one of the methods used for investigation of deep levels in high-resistivity bulk materials. The method is based on storing and processing data of photocurrent decay after illumination by laser LED diode for various temperatures. In this theory we consider single trapping level configuration and negligible retrapping, which is the ideal model. We assume that period of darkness is long enough so that traps are empty at time of new beam flash. The current $i(t_\infty)$ is thus the dark

current. According to the assumption made the current induced by de-trapping can be written as [101]

$$i(t) = qAE\mu_h\tau_h p_t(0)\frac{1}{\tau_t}\exp[-\frac{t}{\tau_t}] + i(t_\infty)\,, \tag{2.10}$$

Where $p_t(0)$ is the initial density of filled traps (here holes are considered), μ_h and τ_h are respectively the mobility and recombination lifetime of free holes, q is the electronic charge, E the applied electrical field. The constant A depends on the illumination surface between the electrodes and on the penetration depth of the light. The relaxation time of holes τ_t is related to the depth of the light E_t of the level (with respect to the top of the valence band) and to capture cross section of trap centers S_t by the expression

$$\frac{1}{\tau_t} = S_t v_h N_V \exp[-\frac{E_t}{kT}]\,, \tag{2.11}$$

Where N_V is the effective density of states in the valence band and, v_h is the thermal velocity of the holes. Similar expressions are valid for the case of electrons ([102]).

In reality current decay is the sum of more than one exponential. There can be seen three regions of decay in the Fig. 2-2.

a) Rapid decay region corresponds to the carriers released by the traps with large emission cross section – needn't to be the finest as there can be artifacts due to the non-zero cut-off time of the exciting light beam.
a) Intermediate decay region that is relied to the traps which are in the thermal resonance at the measuring temperature.
b) A slow decay region corresponds to the carriers released by traps with small emission cross- section – Evaluation of this part is often problematic due to interference of the weak signal with the background.

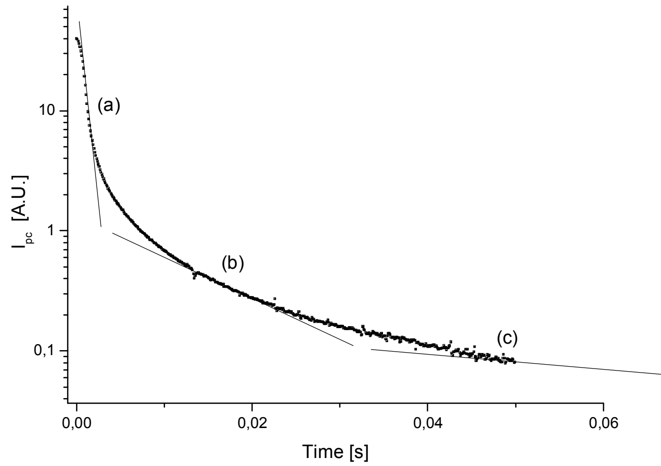

Fig. 2-2. Semilogarithmic plot of a transient signal received from an Au/CdTe contact at 95K

2.2.1 Two-gate methods for PICTS evaluation

The basic two-gate method for transient's evaluation consists of plotting of the difference

$$\Delta_{12}i(T) = i(t_1) - i(t_2) \quad (2.12)$$

as a function of temperature, where t_1 and t_2 are two delay times at which the readings are taken from transient. Usually t_2 is chosen large with respect to t_1. After processing we get set of spectra from which we need to get temperature T_m of maximum; they can be expressed as

$$\Delta i_{12}(T_m) = qA\overline{E}\mu_h\tau_h p_t(0)\frac{1}{\tau_m}\frac{t_2 - t_1}{t_2 - t_m}\exp[-\frac{t}{\tau_t}] \quad (2.13)$$

The dependence of the amplitude of the maximum on the temperature T_m may provide an independent method for determination of the trap parameters.

The important point for using double-gate processing is to make sure, that the initial filling $p_t(0)$ of the traps remains constant over the temperature range of interest. This condition may in principle be fulfilled by using high photo-excitation in order to saturate the traps. One of the most important problems in bulk samples is that the lifetime and possibly the mobility of the thermally released carriers may depend on temperature in a manner, which cannot be expressed in a simple analytical form.

2.2.2 Four gate methods for PICTS evaluation

The way to solve this problem is to compute the ratio $\Delta i_{12}(T)/\Delta i_L(T)$, which means to normalize PICTS signal. The heights of the peaks in a normalized spectrum then reflect the relative concentrations for the various types of traps present in the material.

For data evaluation I used this method (4-gate) PICTS signal processing. The double-gate method has the following drawbacks:

a) It is, in general, not easy to take into account possible thermal variations of mobility and recombination lifetime, especially if the thermally released carriers are not of the same type as the photocarriers.
b) One cannot be sure that $p_t(0)$ remains constant over the whole temperature range.
c) Owing to some uncertainty concerning the presence or absence of the $1/\tau_t$ in the pre-exponential factor.

Four-gate processing consist in the recordings at four different times t_0, t_1, t_2, t_3 and in computing the ratio

$$Y[\tau_t(T)] = \frac{i(t_1) - i(t_2)}{i(t_0) - i(t_3)}, \quad (2.14)$$

Where optional parameters $t_1/t_0 = 2$ and $t_2/t_0 = 3$ were fixed for the data processing.

For plotting the Arrhenius diagram it is necessary to compute the relaxation time τ_m for each PICTS spectrum corresponding to the temperatures T_m at which the maximum occurs.

$$\tau_m = \frac{t_2 - t_1}{\ln[(t_2 - t_0)/(t_1 - t_0)]}, \tag{2.15}$$

Points in Arrhenius diagram ($10^3/T_m$ as x axis, $T_m^2\tau_m$ as y axis) are then interlaid by the linear apparent fit from which we can acquire values of capture cross sections S_t and activation energies of the traps $\Delta E = E_C - E_T$ for electrons and $\Delta E = E_V - E_T$ for holes [102]. This apparent fit can be expressed by formula

$$y = A + Bx \tag{2.16}$$

Activation energies can be computed from equation

$$\Delta E = B.k.10^3 \tag{2.17}$$

where k is Boltzmann constant. Capture cross sections for electrons and holes are calculated from

$$S_e = \frac{h^3}{\sqrt{96}k^2 m_e}\exp(-A) \tag{2.18}$$

$$S_h = \frac{h^3}{\sqrt{96}k^2 m_h}\exp(-A) \tag{2.19}$$

where h is Planck constant and m_e, m_h are effective masses of electrons and holes.

2.3 Evaluation of electron trapping parameters from conductivity glow curves

The plot of current versus temperature of semi-insulting materials, as in Fig. 2-3, is described as either a 'thermally stimulated current' or a 'conductivity glow' curve. In principle the measurement of a single glow curve suffices to determine the entire trapping parameters, i.e. trap depth, E_t, and trap capture cross section for electron (hole), S_t. In practice the evaluation of glow curve data can be very complicated, and is often accompanied by uncertainties which render the method of greater qualitative than quantitative value [103].

To analyze the glow curves it is necessary to make various simplifying assumptions. Many analyzing methods are published depending on these assumptions, and on nature of the recombination process, which depends on the relative magnitudes of the capture cross sections S_t and S_R of the trapping and recombination centers. Since there is very good summary about these methods [103], and, recently, discussions with numerical calculations are in many Ref. (e.g. [104]), a brief summary about the methods we have utilized to evaluate our results is presented here.

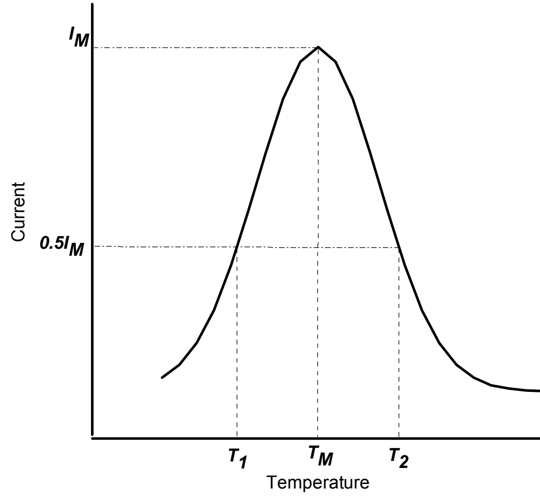

Fig. 2.3 Conductivity glow curve when including trap level of depth E_t, with S_T, and heating rate R . The parameters of the curve are the temperature, T_M, of the maximum current, I_M, and the temperatures T_1 and T_2 at which the current attains the value $0.5I_M$ on either side of T_M

1-Grossweiner's method [105]:

This method supposed no retrapping occurs, and recombination is assumed (i.e. $S_t \ll S_R$). To obtain the trap depth E_t it is only necessary to determine T_M and T_1, as

$$E_t = 1.5kT_M T_1 /(T_M - T_1) \tag{2.20}$$

And the expression for the S_t is

$$S_t = 3kT_1 EXP(E / kT_M) / 2N_C \nu_e (T_M - T_1) \tag{2.21}$$

Where, N_C is the effective density of states in the conduction band, ν_e is the electron thermal velocity

2-Variation of the heating rate method [106]:

Also, this method ignored the retrapping and assumed recombination process, (i.e $S_t \ll S_R$). The relation between E_t, S_t, and R is

$$E_t = KT_M \ln(S_t \nu_e N_C KT_M^2 / RE_t) \tag{2.22}$$

This can be rewritten as

$$\ln(T_M^2 / R) = (E_t / kT_M) - \ln(S_t \nu_e N_C k / E_t)$$

If several heating rates are used and T_M is determined as a function of ***R***, It is possible to derive ***E_t*** from the slope of the straight line which should be obtained by plotting $\ln(T_M^2 / R)$ against $1/KT_M$. Knowing ***E_t***, the carrier cross section values can be obtained from eqn. (2.22)

3-The initial rise method [107]*:*

This method is independent of the *recombination mechanism.* It depends on the fact that, when the traps begin to empty as the temperature is raised, and the current is described as,

$$I = A\exp(-E_t / kT_M) \tag{2.23}$$

Where A is constant.
Eqn. (2.23), can be rewritten as

$$\ln(I) = (-E_t / kT\ ) + Const. \tag{2.24}$$

In practice the initial portion only of the peak is measured, i.e. doesn't depend on T_m. A plot of the **ln(I)** against **1/T** should yield a straight line with a slope of $-E_t$.

4-Haering and Adams method [108]:

They deduced expression for the peak maximum I_M, in the two extreme cases of no retrapping (i.e. $S_t \ll S_R$) and fast retrapping (i.e. $S_t \gg S_R$). They concluded that at both limits

$$I_M = A\exp(-\frac{E_t}{kT_M} - 1) \tag{2.25}$$

Where A is a different constant in each limit.
Eqn. (2.25), can be rewritten as

$$\ln I_M = (-\frac{E_t}{kT_M} - 1) + Const. \tag{2.26}$$

Application of this method requires the measurement of a number of glow curves at a variety of heating rates, after which ***$\ln(I_M)$*** is plotted as a function of ***$1/T_M$*** to produce a straight line.

2.4 Resistivity mapping.

The resistivity mapping instrument uses a contactless, consequently, non destructive method, based on the capacitive relaxation of the sample called «Time Dependent Charge Measurements» (TDCM) invented by Stibal et al [109]. It is well known that a homogenous semiconductor material can be characterized by the dielectric relaxation (τ_r), which is related to the dielectric constant (ε) and the resistivity (ρ) of the material and expressed by

$$\tau_r = \varepsilon_0 \varepsilon \rho \qquad (2.27)$$

Where ε_0 is the dielectric constant of vacuum. The planar semiconductor sample, Fig. 2-3, is represented by the parallel association of a capacitor C_S and a resistor R_S as

$$C_S = \varepsilon_0 \varepsilon \frac{A}{d} \ , \qquad R_S = \rho \frac{d}{A}$$

Where A and d are the area and the thickness of the sample. In this case, the relaxation time is simply expressed by $\tau_r = R_S C_S$ and the resistivity becomes, according to (2.27)

$$\rho = \frac{R_S C_S}{\varepsilon} \qquad (2.28)$$

By applying a voltage step to the detector, through the additional capacitance C_a, the total charge flowing into the capacitors is represented [109] by

$$Q(t) = \frac{C_a^{\ 2}}{C_a + C_S} V (1 - e^{t/\tau_E}) + Q(0) \qquad (2.29)$$

Where

$$\tau_E = RS(C_a + C_S) \ , \qquad Q(0) = \frac{C_a C_S}{C_a + C_S} V$$

and C_a represents the total series capacitance of the contact resulting from the space between the sample and the electrode. With the above relations, (2.27) can be rewritten as

$$\rho = \frac{C_S \tau_E}{(C_a + C_S)} = \frac{Q(0)\tau_E}{Q(\infty)\varepsilon_0 \varepsilon} \qquad (2.30)$$

Where $Q(\infty) = C_a V$.

Experimentally, measuring the charges, $Q(\infty), Q(0)$, and the time τ_E corresponding to $Q(\tau_E) = 0.63[Q(\infty) - Q(0)] + Q(0)$, from charge time dependence signal, resistivity can be evaluated

The TDCM model was validated by Stibal et al. [109], who demonstrated the correlation between the resistivity data measured by TDCM and that of the Van de Pau Hall technique. A very satisfactory correlation between TDCM and the classical ohmic contact measurements was also studies in Ref. [110].

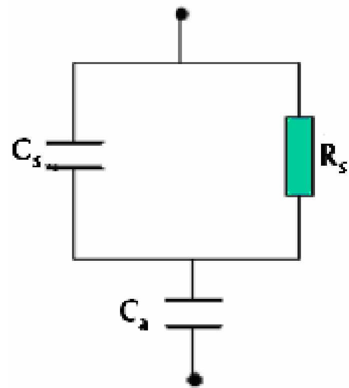

Fig. 2-3. Parallel capacitor C_S and a resistor R_S equivalent to a planar semiconductor sample, C_a represents the total series capacitance of the contact resulting from the space between the sample and the electrode.

Chapter 3

Experimental

3.1 Crystal descriptions

CdTe crystals of diameter 50 mm doped with various dopants were grown from melt by the vertical gradient freeze (VGF) method, at our laboratory, at Institute of Physics, Charles University (Prague, Czech Republic). The CdTe was synthesized from stoichiometrically mixing 6N-purity Cd and Te in the same ampoule. The optimal Cd pressure for CdTe growth was 1.2 atm at an axial temperature gradient of 5 °C/cm and a cooling rate of 0.5 °C/h.

3.2 Sample preparations

All the high-resistivity CdTe crystals investigated in this PhD thesis were prepared by vertical gradient freeze method, and by growth from Te solvent. They were doped by various dopants (In, Cl, Sn, Ge). Wafers for different mapping (resistivity, photoconductivity, photoluminescence) had dimensions about 50 × 40 mm^2. They were obtained by cutting the as-grown ingots along the direction of growth, after which they were mechanically lapped, polished, and finally chemically-mechanically polished with a bromine/methanol solution.

Samples for measurement of thermoelectric effect spectroscopy (TEES), Photoluminescence (PL), Photo-induced current transient spectroscopy (PICTS), and Photocurrent spectroscopy (PCS) had dimensions about 10x10x1.5mm^3. The samples were chemically and mechanically etched in 1% Br-methanol solution prior to contact fabrication. Ohmic contacts on both the front and back surfaces were fabricated by chemical deposition using of a 0.5% $AuCl_3$ solution applied for 15s.

V-A characteristics of contacts in dark were ohmic with a maximum deviation of 1% from ideal course as is shown in the Fig. 3-1.

The CdTe sample with Au contacts on front and back sides was fastened to a plate in different measuring setups by high heat conductivity Ag paste and then to the cryostat handle with high vacuum grease.

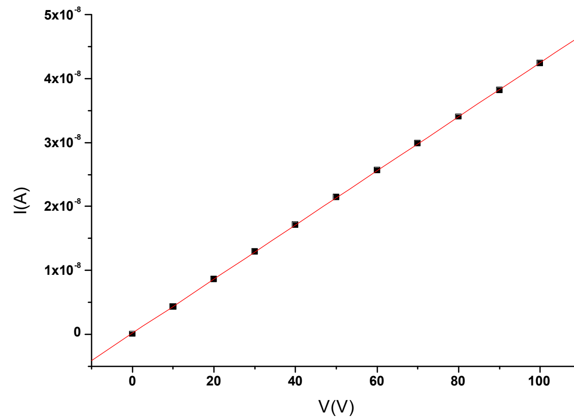

Fig. 3- 1. V-V characteristic for Au contacts in dark

3.3 Measuring methods*:*

3.3.1 Thermoelectric Effect Spectroscopy method:

The basic idea of the Thermoelectric Effect Spectroscopy (TEES) method [71] is based on the temperature gradient induced diffusion of free charge carriers towards the electric contact at the cold end of the sample. If the deep traps are filled by illumination at low temperature, the subsequent rise of temperature causes the release of trapped carriers. Therefore, application of the thermal gradient across the sample results in "thermoelectric current" (I_{TEE}) in the outer circuit. TEES spectrum shows the dependence of I_{TEE} current measured as a function of the sample temperature (T). The different sign of peaks in TEES curves corresponds to the different types of charge carriers.

Due to the low thermal conductivity of our semi-insulating samples, sufficient natural temperature difference (2-10 K/cm) is obtained during heating the samples at heating rate below 0.16 K/s.

High performance temperature control system of liquid nitrogen cooled cryostat had to be designed to obtain good-quality TEES spectra at different temperature gradients. Temperature gradient stability for various rates which sustains in the whole measured range is the main prerequisite of highly resolved spectra recording. Data acquisition electronics system has also been assembled to record and store the spectra.

An experimental setup for TEES measurements (see Fig. 3-2) is based on a liquid nitrogen cooled cryostat operating in the temperature range of 80 – 400 K. High resistivity sample to be measured is placed inside of the cryostat by using a holder and its electrical contacts are fed via vacuum coaxial feed trough. The sample is cooled down to ≈ 90 K in the absence of light, where the traps are filled by optical excitation using a 25 mW He–Ne laser. The duration of irradiation was 1200 second. Temperature dependence of nascent thermoelectric current (I_{TEE}), which is generated by the temperature gradient during the sample warming up, is measured by using an electrometer (Keithley, model 6574). The sample temperature is precisely measured by milivoltmeter (Keithley, model 2000). Control computer is used for data acquisition and storing by using GPIB interface bus.

Temperature control system: Precise system was required for such a type of experiment. It has been designed at our institute by using a high grade PID type controller/setpoint programmer (see Fig. 3-3a). The controller is a modular assembly type with possibility of free wiring of the internal structure. The sample temperature to be controlled is measured by a linearized Si diode powered by 10 µA current source. Very precise and linear temperature warming up ramp with high rate is required to perform TEES measurement. It enables minimum deformation in the temperature dependence of generated thermoelectric current to be obtained. Relatively long and highly temperature dependent heating response time constant of the cryostat rather complicates the control task. However, the linearity deviation does not exceed 1 K ordinarily even in case of using the highest temperature change rates for a precisely tuned control system. PID parameters scheduling was inevitable for our control system to overcome the temperature dependence of the time constant. A linear high power DC amplifier has been constructed to transmit the controller DC output to the heating element. Different heating rates R have to be employed during the experiment.

Fig. 3-3b shows the performance of the temperature control system for different heating rates required to record TEES spectra. Excellent linear response of the control

system has been obtained. The Temperature deviation usually does not exceed 0.5 K in the heating rates between 5-15 K/min (see Fig.3-3b).

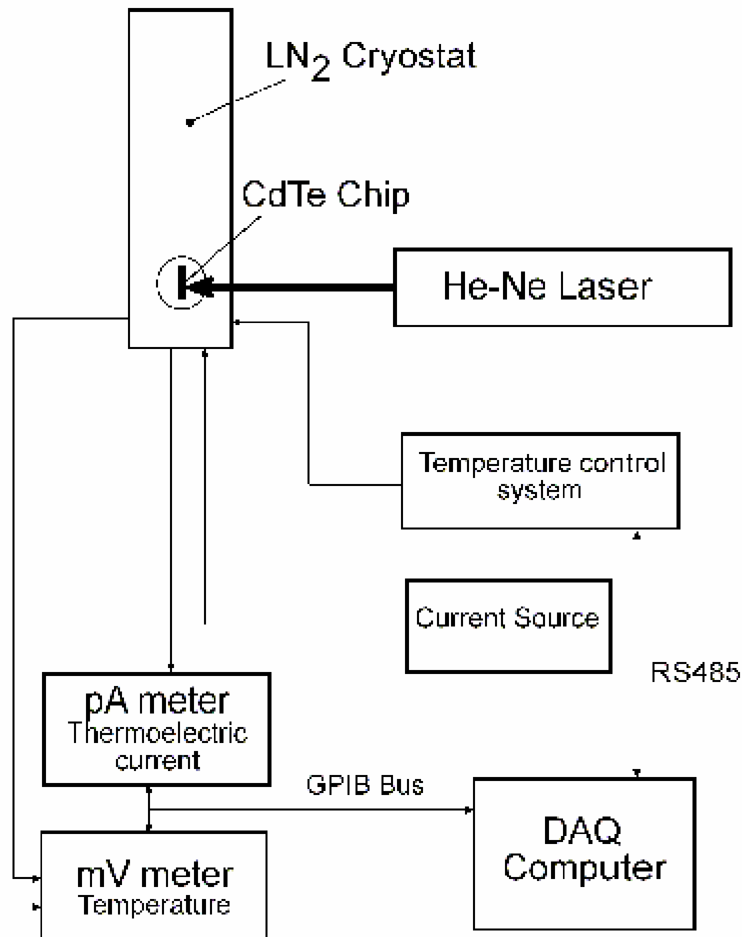

Fig.3-2. Schematic drawing of Thermoelectric Effect Spectroscopy experimental setup

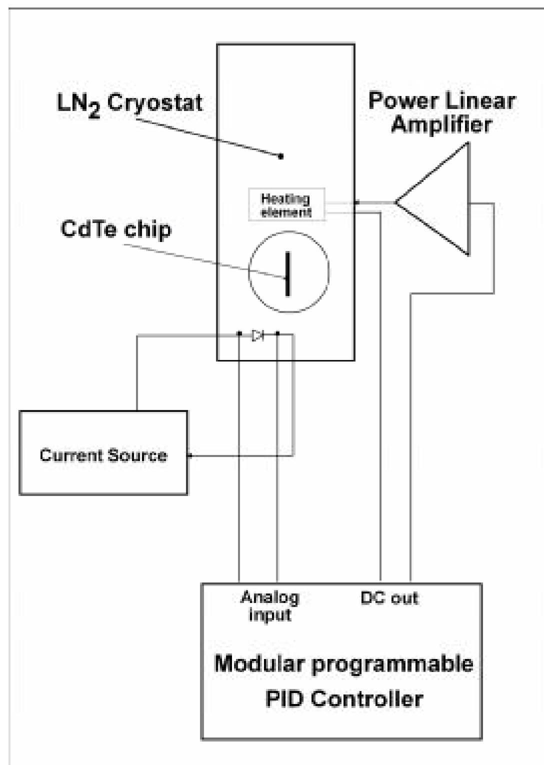

(a)

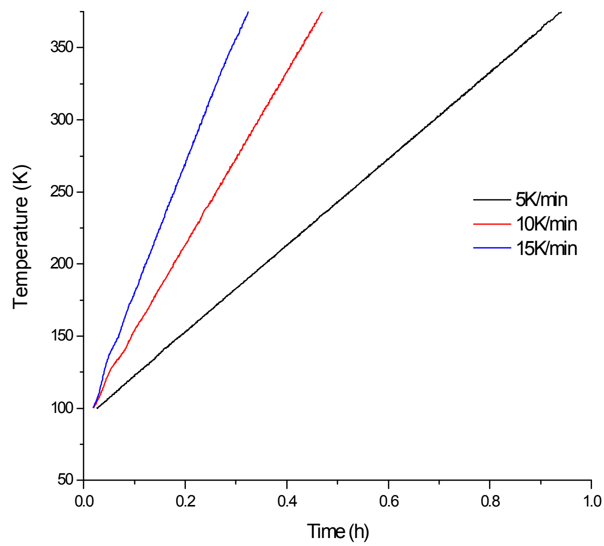

(b)

Fig. 3-3. a: Temperature control system of the cryostat, b: Temperature course in the cryostat for required rates, shows the performance of the temperature control system.

3.3.2 Photo-induced current transient spectroscopy method:

The Photo-induced current transient spectroscopy (PICTS) measurements were performed during my stay at Albert-Ludwigs-University in Freiburg. Figure 3-4. shows the scheme of the PICTS setup. It consists of a cryostat with a LED laser diode emitting light at 830nm, an amplifier and a computer for measurement control. The cryostat was cooled with liquid nitrogen. The maximum temperature range we could use for the PICTS measurement was from 77K to 380K. The sandwich configuration can be used for analyzing the transient signal under positive and negative polarities. Practically the metallic contact can be an ohmic or a blocking Schottky type. We used ohmic type of contacts, because it was difficult to make Schottky type of contacts on high resistivity material. Schottky type would be preferable for the advantage that PICTS measurement gives better results than in case of injecting contacts. This is due to the fact that in blocking contacts the baseline for the transient is low hence the ratio signal/noise is high. The applied electric field in sample at sandwich orientation was depending on the sample itself, the maximum value was 200V cm^{-1}. The sample with semitransparent Au contact was pressed down to copper part of cryostat functioning as well as bottom contact and fixed with liquid silver. Light from the LED diode was flashing near Au contacts with spot approximately $1mm^2$.

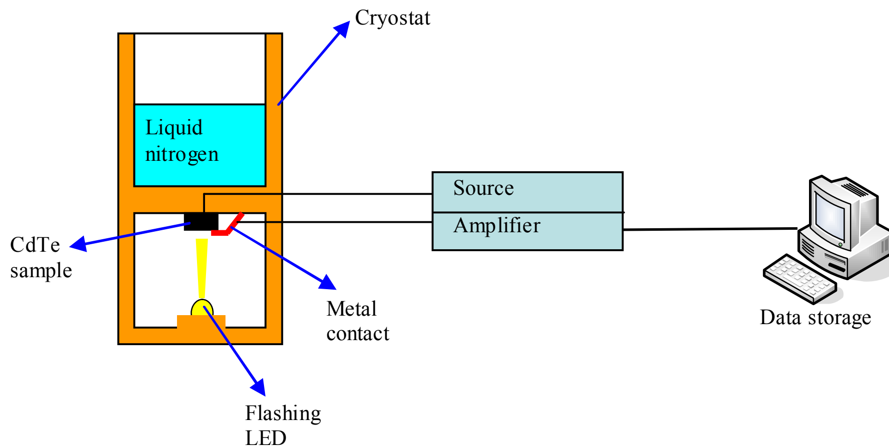

Fig. 3-4.Scheme of PICTS apparatus with cryostat cross-section

The transient signals during the dark interval were captured at each temperature so that one whole experiment could be realized in a single temperature scan and the transients' data were stored in the texts file. The behavior of the light from LED diode and current with time is shown in Fig 3-5.

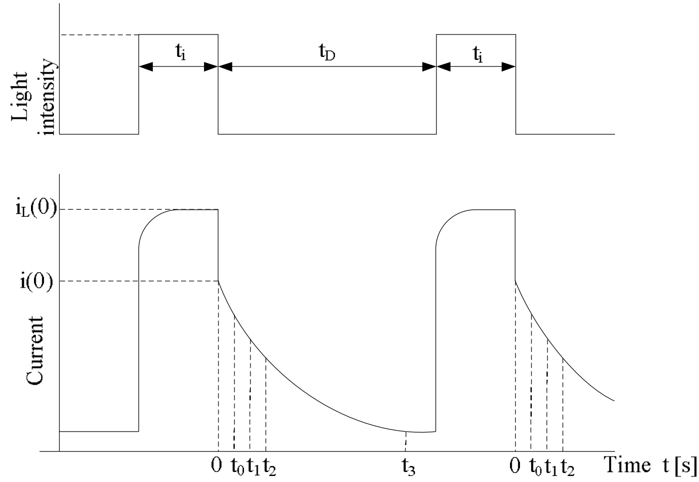

Fig. 3- 5.Light and current behavior in PICTS experiment [102]

3.3.3 Resistivity mapping method:

The resistivity mapping instrument uses a contactless, consequently, non destructive method, called «Time Dependent Charge Measurements» (TDCM) [109]. The sample acts as a capacitor and the resistivity is evaluated by measuring a time dependent charge transient observed after application of a voltage step. The measurement is contactless; it allows the examination of wafers without degrading surface quality.

The CdTe wafer is inserted between a 2.5 mm diameter measurement electrode, surrounded by an extended guard electrode, and a back electrode (Fig 3-6a). The equivalent circuit of this arrangement (see Fig 2-3) comprises a lossy dielectric capacitor C_s and an air capacitor C_a. The measurement routine is initiated with a voltage step instantaneously charging the capacitors connected in series. C_s is discharged with a characteristic time constant τ_E such that eventually the equivalent circuit is reduced to C_a. The charge redistribution is recorded as shown in Fig 3-6b. Using the measured charges Q(0) (after application of the step voltage), Q(∞) (after completed charge transfer to C_a) and τ_E the substrate resistivity can be evaluated according to

$$\rho = Q(0)\tau_E[Q(\infty)\varepsilon\varepsilon_0]^{-1} \tag{3.1}$$

Where ε is the dielectric constant of the sample, and ε_0 is the permittivity of vacuum. The measurement circuit of TDCM is schematically shown in Fig 3-7. The charge amplifier, essentially comprising an operational amplifier and feedback capacitor C_f provides an output voltage $U(t) = Q(t)/C_f$ proportional to the time-dependent charge Q(t).

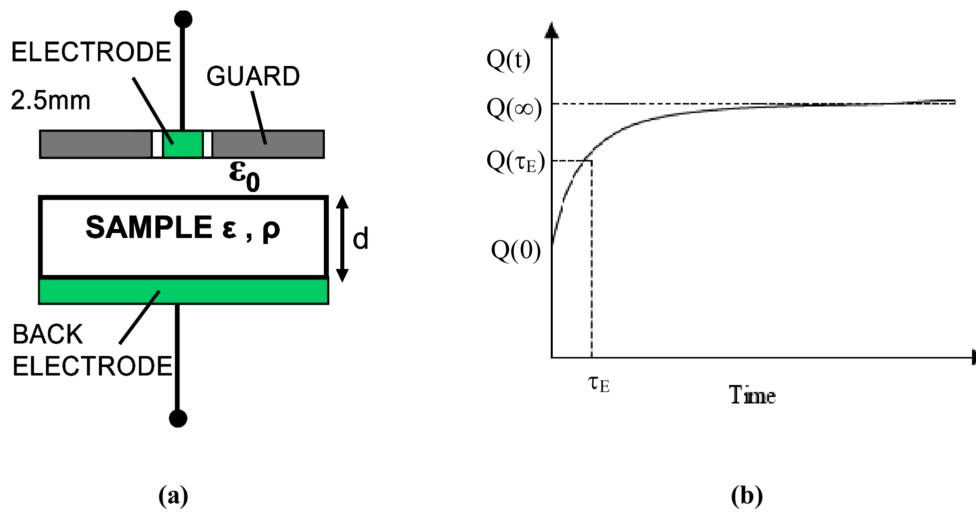

Fig. 3-6. Electrode configuration (a), equivalent circuit (b) The quantities to be measured are the instantaneous step Q(0), the asymptotic value Q(∞) and time τ_E corresponding to $Q(\tau_E)$, as shown in equation (3.1).

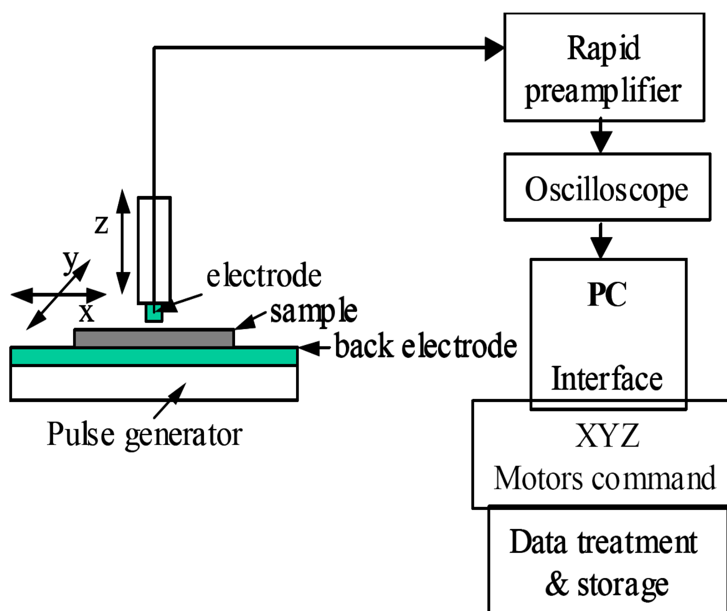

Fig. 3-7. Block diagram for TDCM measurements

3.3.4 Photoluminescence method:

Photoluminescence (PL) spectra were measured by cadmium mercury telluride (HgCdTe) detector in a configuration, when Ti-sapphire laser beam with energy ~1W used for exciting the samples, while the PL was collected in the Bruker Fourier spectrometer detector from backside. The reason for such a configuration was the fact that the sample itself served as a filter for the strong Ti-sapphire laser beam. The schematic setup for the photoluminescence is shown in Fig 3-8. The laser beam was reflected by a spherical mirror to illuminate the front part of the sample attached in the liquid Helium (4.2K) Cryostat Oxford instruments. Detection of low energy PL signal was available by using HgCdTe detector (small bandgap), typical 0.3 – 1.6 eV spectra range was measured.

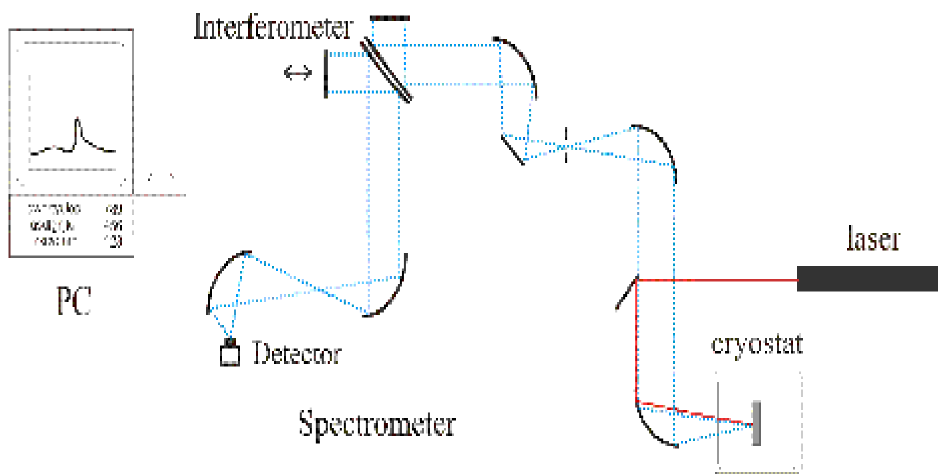

Fig. 3-8. Schematic setup for the photoluminescence (PL) measurements.

3.3.5 Photocurrent spectroscopy (PCS) methods:

The experimental set up used for the PCS is shown in Fig. 3-9. The source of the light we used was a high emission discharge lamp. The light beam from it was reflected by a spherical mirror to the chopper followed by the double grating monochromator. A light beam was chopped with a frequency 5-20Hz and the monochromator limited photons energy from 0.91eV to 1.9eV. Behind the monochromator output was the second harmonic (SH) filter. Behind the SH filter was the beam finally lead to the cryostat through the glass window. The closed-cycle He cryostat was used for measurement in the range of 10-300K.

The photovoltage values on the sample were received by the Lock-In amplifier and then read manually or by computer from the Keithley multimeter. The constant value of voltage on the sample was monitored by Keithley electrometer.

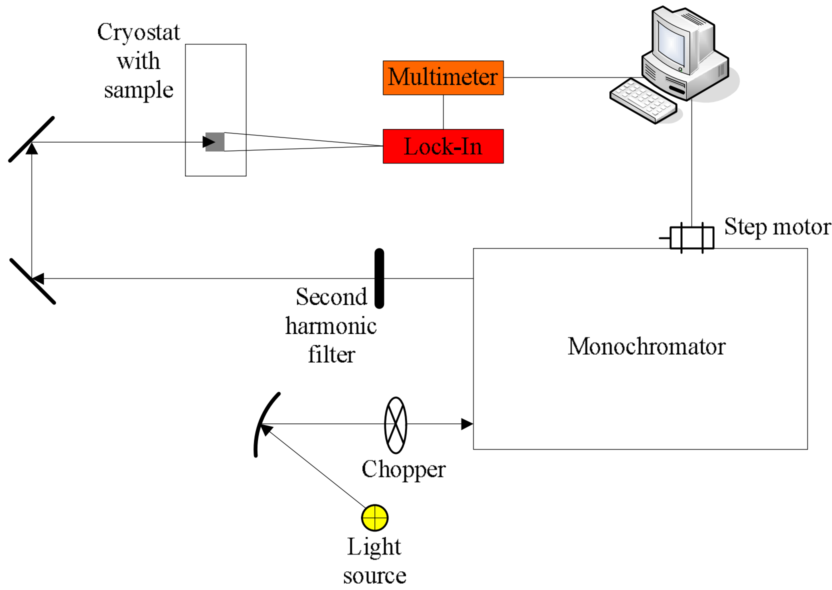

Fig. 3-9. The experimental setup with monochromator for PCS, and PL measurements

During our measurement the photovoltage U_{PC} on the sample was measured by Lock-In amplifier. To compute photocurrent values the following equation was used.

$$I_{PC} = U_{PC} \frac{(R_c + R_0)(R_C - R_0 - \Delta R)}{S.R_C.R_0(R_0 - \Delta R)}, \qquad (3.2)$$

Where R_0 is resistance of the sample in the dark and ΔR is change of sample resistance after area S illumination.

Chapter 4

Results and discussion

Generally, CdTe undoped crystals grown from a stoichiometric or slightly Te-rich melt exhibit a low p-type resistivity due to the presence of residual acceptors and native acceptor defects. One of the possible ways to increase resistivity of CdTe is the compensation of these acceptors by shallow or deep level donors (D) [111, 112] . Shallow donors are typically elements from the III group occupying Cd positions (like In) and elements of the VII group occupying Te positions (like Cl, Br, I). Deep donors are elements occupying Cd positions and have ionization energy in the midgap of CdTe like, Ge, Sn, V, Ti, Pb, etc. Depending on the concentrations of the dopants donors, they can compensate acceptors, e.g., a cadmium vacancy V_{Cd}, creating the A-center complex (V_{Cd}–D) [113]. Stabilization of the compensation condition against variation of the donor/acceptor concentration can be reached with a mid-gap native, or impurity donor level [56, 59, 114-121].

In this part of the thesis, the results of the study of defect levels in the band gap of CdTe doped by two shallow (In, Cl), and two deep (Sn, Ge), impurities will be presented. One can trace the results starting by the comparative study between the shallow and deep impurities, a complex study of one deep donor (Sn), and of one shallow donor (In). Discussion and summary followed every study, while the final conclusion will be at the end of this part.

4.1 Comparative study of CdTe doped by shallow and deep impurities

In this study, five CdTe ingots with different dopants (undoped, In, Cl, Sn, and Ge) have been grown by vertical gradient freeze method and labeled as (AV, A1, KA, VG3, and KV), respectively. The CdTe was synthesised from 6N purity Cd and Te in the same ampoule. The different dopants concentration in the melt is shown in table 4.1. The optimal Cd pressure for the CdTe growth was found to be of 1.2 atm at the axial temperature gradient of 5 °C/cm and cooling rate of 0.5 °C/h.

Table 4.1. Dopants concentrations in melt and solid phase of the CdTe crystals

Ingot (dopant)	Dopant conc. in melt (cm^{-3})	Dopant conc. in solid (cm^{-3})
AV	Undoped	
A1 (In)	10^{18}	$\sim 5x10^{16}$
KA (Cl)	10^{17}	$\sim 10^{16}$
VG3 (Sn)	10^{18}	$\sim 5x10^{14}$
KV (Ge)	10^{17}	$\sim 10^{16}$

4.1.1 Content of the impurities

Actual impurity content was measured in samples taken from the middle part of the ingots by glow discharge mass spectroscopy (GDMS). The concentration of impurities in the undoped, In (shallow donor), and Sn (deep donor) doped samples is presented in table 4.2

One can see that the concentration of residual impurities normally does not exceed the value of several ppb. The concentration of only two impurities, Na and Cu, reaches 100–200 ppb. Contamination with these impurities originates from the quartz, ampoule preparation process, or the starting 6N materials. The dopant elements were practically absent in the undoped AV ingot, while their concentration in the solid phase in their ingots are presented in table 4.2.

Table 4.2. Concentration of impurities.

N	**Crystal**	**Undoped (AV)**	**In doped (A1)**	**Sn doped (VG3)**
	Element	Conc. (ppb)	Conc. (ppb)	Conc. (ppb)
1	Li	<2	< 2	< 1.6
2	B	7	50	220
3	Na	160	200	100
4	Mg	20	90	50
5	Al	5	22	8
6	Si	<5	13	43
7	P	2	4	12
8	S	50	160	48
9	K	<8	< 4	< 3
10	Ca	<25	10	<15
11	V	<0.2	<0.2	< 0.1
12	Cr	7	2	5
13	Mn	<18	< 15	< 10
14	Fe	<30	30	26
15	Co	0.7	<0.2	< 0.2
16	Ni	8	2	0.7
17	Cu	120	13	30
18	Zn	5	170	2
19	Ge	<7	< 8	< 6
20	As	<100	< 300	< 70
21	Se	<8	< 6	<6
22	Br	<7	< 6	<8
23	Ag	<30	< 12	< 10
24	**In**	**<20**	**1600**	**< 15**
25	**Sn**	**<20**	**< 17**	**460**
26	Sb	<20	< 2	< 13
27	Hg	<1	< 2	< 0.7
28	Tl	<0.2	< 0.2	<0.1
29	Pb	<0.4	< 0.2	<0.4
30	Bi	<0.1	< 0.3	<0.1

However, the GDMS analysis provides only rough information about impurity and dopant concentrations in the studied ingots and certainly cannot describe their axial and radial distributions. More information about distribution of dopants and defects will be estimated from a set of maps *(next sections)* and characterization methods. For these purposes, all the prepared ingots were cut along the growth direction, and obtained wafers were mechanically lapped, polished, and finally chemo-mechanically polished with Br/methanol solution.

In this study, two spectroscopic methods, TEES (thermoelectric effect spectroscopy) and photoinduced current transient spectroscopy (PICTS) were used to study of deep levels in samples doped by shallow donors (In, Cl) and deep impurities (Sn, Ge) in order to get a deeper insight in midgap levels responsible for the pinning of the Fermi energy, and to compare the expected influence of these deep dependent dopants levels on the charge collection efficiency in detectors.

4.1.2 TEES measurements.

Four samples were cut from the wafers, whose origins were the A1, KA, VG3, and KV ingots. The undoped sample couldn't be characterized by this method, because it has a low resistivity value (10^3 Ω.cm), and TEES method is used for high resistivity materials. The samples had dimensions about 10 x 10 x 1 mm^3. Ohmic contacts were prepared by chemical deposition from 0.5% $AuCl_3$ on both the front and back surfaces. The samples were cooled in the absence of light to ≈ 90 K, where the traps were filled by optical excitation using a 25 mW He–Ne laser. The duration of irradiation was 1200 s. The samples were then warmed up with at least three different heating rates up to 400 K.

4.1.2.1 Samples doped with shallow donors.

Figure 4-1a. shows the results of TEES spectra measured at three different rates in CdTe:In. One can note that all observed peaks are positive, which means that all corresponding traps are hole traps. It is noted that that there is a shift of the peak positions towards the higher heating rate. Figure 4-1(b), (c), (d), and (e) show the Arrhenius plots, from which the trap's energy and hence their capture cross section can calculated using Eqn.(2.21). The calculated values of the energy and capture cross section of these traps are presented in table 4.3, and shown also in each Arrhenius graph.

The near midgap level (E_4 = 0.83 eV) responsible for pinning of the Fermi level has a relatively low value of the capture cross section (≈ 10^{-15} cm^2) and it is hole trap. i.e. it lies below the Fermi level, and therefore it is almost filled (or partially empty) by electrons.

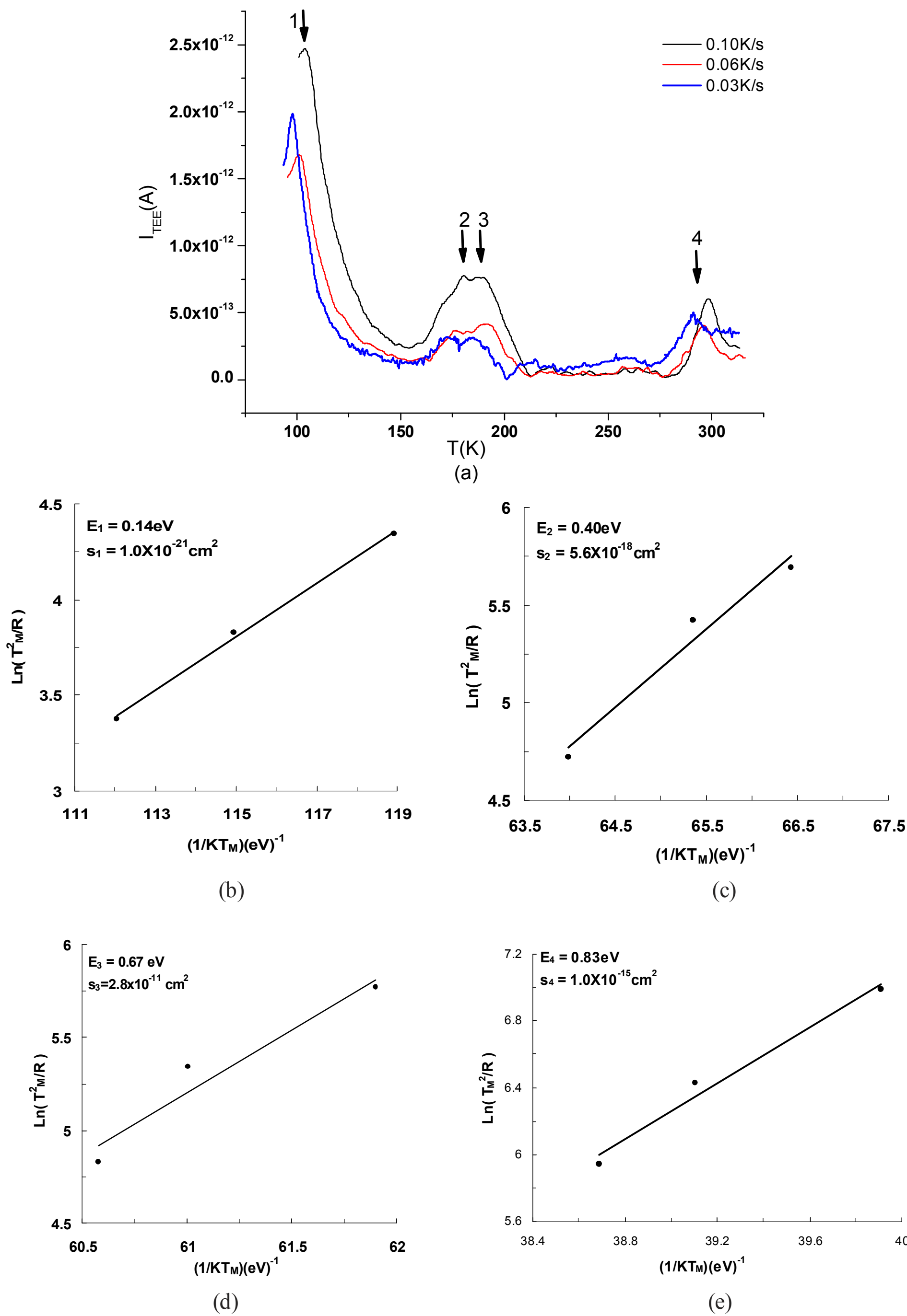

Fig. 4-1. (a) TEES spectra of CdTe:In at three different rates. Sample illuminated at 90K by 1.96eV photons for 1200s. (b), (c), (d), (e) Arrhenius plots showing the thermal ionization energy and trap cross section of peak 1, 2, 3, 4 respectively, in (a).

Results of measurements of TEES of the CdTe:Cl sample are given in figures 4-2 and 4-3, where two peaks shifting with the heating rate were observed. One is related to electron trap and the other related to hole trap. The energy and the capture cross section of these both traps are calculated and presented in table 4.3.

The near midgap level (0.63 eV) is again a hole trap with a small capture cross section ($\approx 10^{-17}$ cm^2). The differences in energies and capture cross sections of near midgap levels in samples doped by In and Cl indicate a different chemical origin of the corresponding defects.

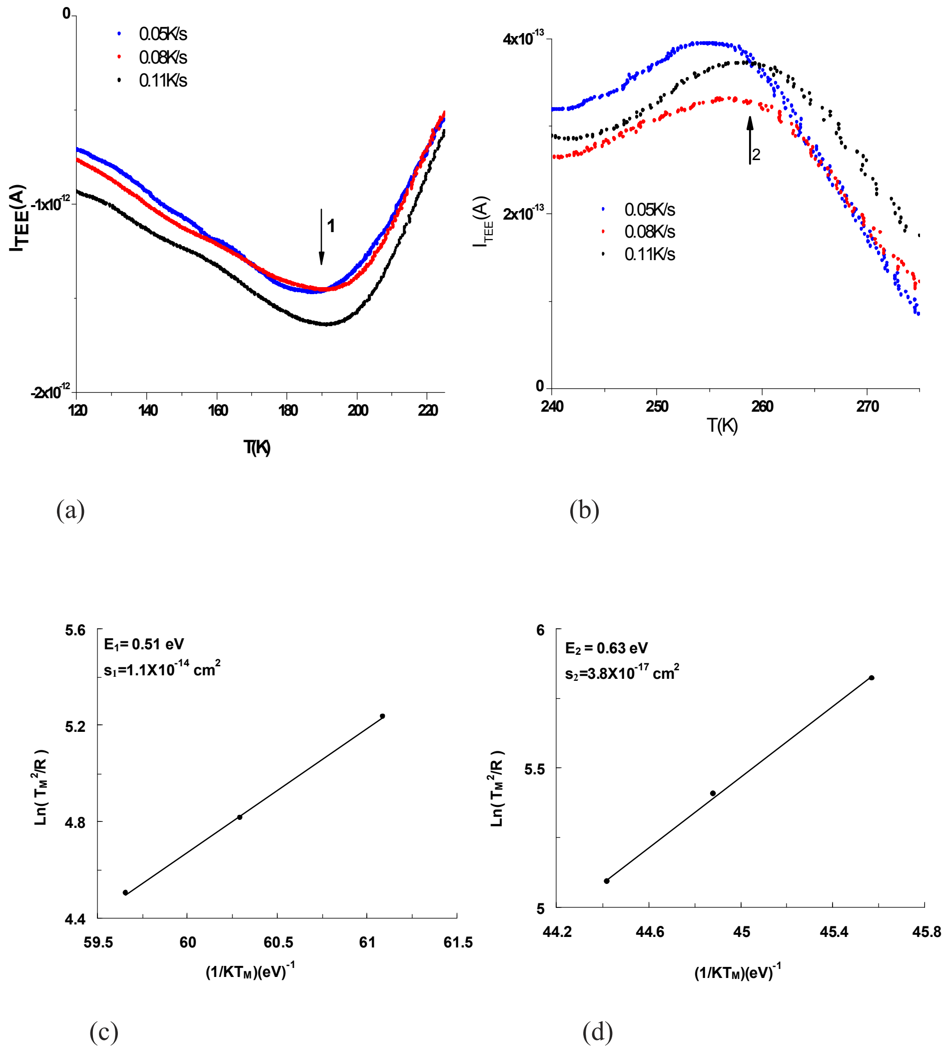

Fig. 4-2. Variable heating rate TEES plots of the current peak of the (a) electronic trap, (b) hole trap in sample CdTe:Cl . (c), (d) Arrhenius plots showing the thermal ionization energy and cross-section of the electron, hole trap, respectively.

4.1.2.2 Samples doped with deep donors.

The TEES spectra of the CdTe:Sn is shown in Fig. 4-3. It is characterized by two hole traps (L1, L2), electronic one (L3), and the near midgap is electronic trap (L4).

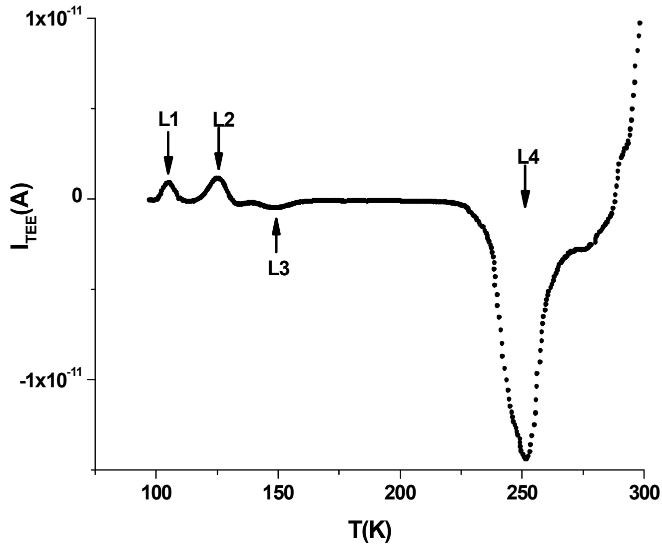

Fig. 4-3. TEES spectra at 0.166K/s from CdTe:Sn. Sample illuminated at 90K by 1.96eV photons for 1200s.

A Variable heating rate method was applied for all the observed traps, Fig. 4-4, to determine the trap's energy and capture cross section by using Arrhenius method. The calculated values are presented in table 4.3, and in the Arrhenius plots related to these traps in fig. 4-5.

One can note that, the near midgap level (E_4 =0.73 eV) is an electron one with a relatively high capture cross section $(10^{-13}cm^2)$. The same result is obtained when the other deep donor sample, CdTe:Ge, is investigated. The spectrum is dominated by signal from one trap. The result of measurements is shown in Fig. 4-6 (a) and (b). The trap is 0.76 eV deep and also electronic with a high capture cross section $(3.6x10^{-13}cm^2)$.

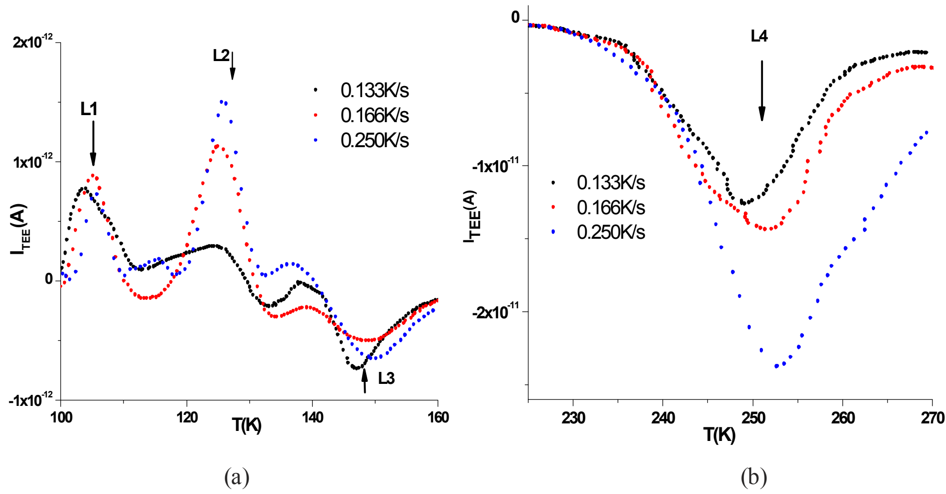

(a) (b)

Fig. 4-4. Variable heating rate TEES plots of the current peak of the (a) L1, L2, L3 , (b) midgap trap L4 in sample CdTe:Sn.

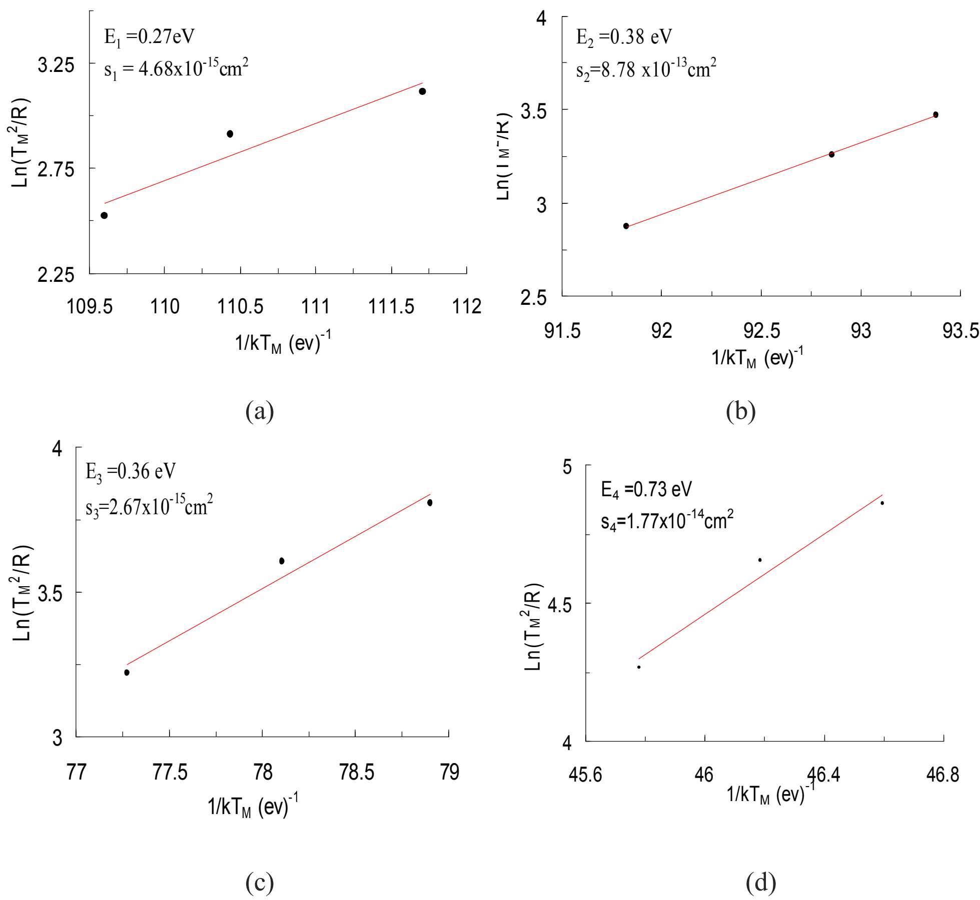

(c) (d)

Fig. 4-5. (a), (b), (c), ,(d) are Arrhenius plots of the trap levels L1, L2, L3, and L4 respectively in the TEES spectra from CdTe:Sn sample in fig 4.4.

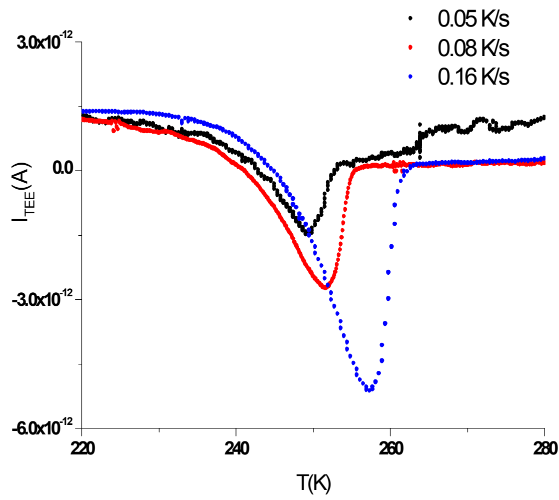

(a)

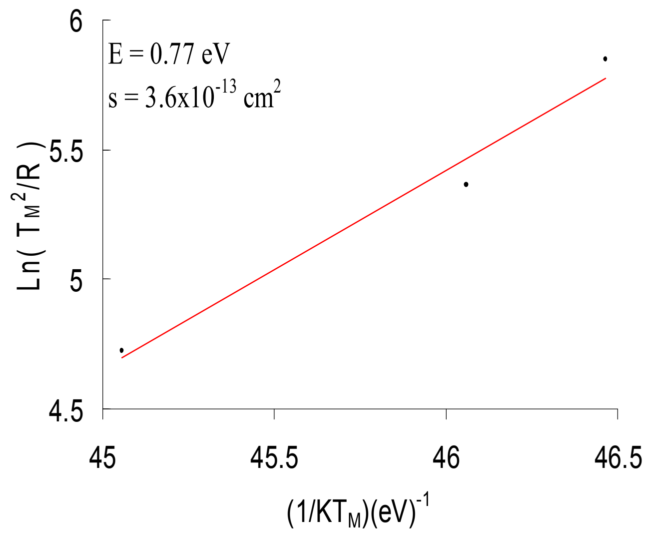

(b)

Fig. 4-6. (a) Variable heating rate TEES plot of the current peak of the unique trap in sample CdTe:Ge . (b) Arrhenius plot showing the thermal ionization energy and the cross-section of this trap.

4.1.3 PICTS measurements

To confirm the obtained values of both the energy and capture cross section in the different studied samples, the same four samples were measured by the PICTS technique. The operating temperature range of the PICTS setup was from 77K up to 350K. Practically we didn't start heating from the lowest reachable temperature, because it was timely demanding to reach it and only very shallow levels should be revealed in the temperature range 77-100K. Typical PICTS spectrum of the In (shallow donor) doped and Sn (deep donor) doped samples are shown in Fig. 4-7. The summary of energy levels and their capture-cross section for all samples is given in Table 4.3.

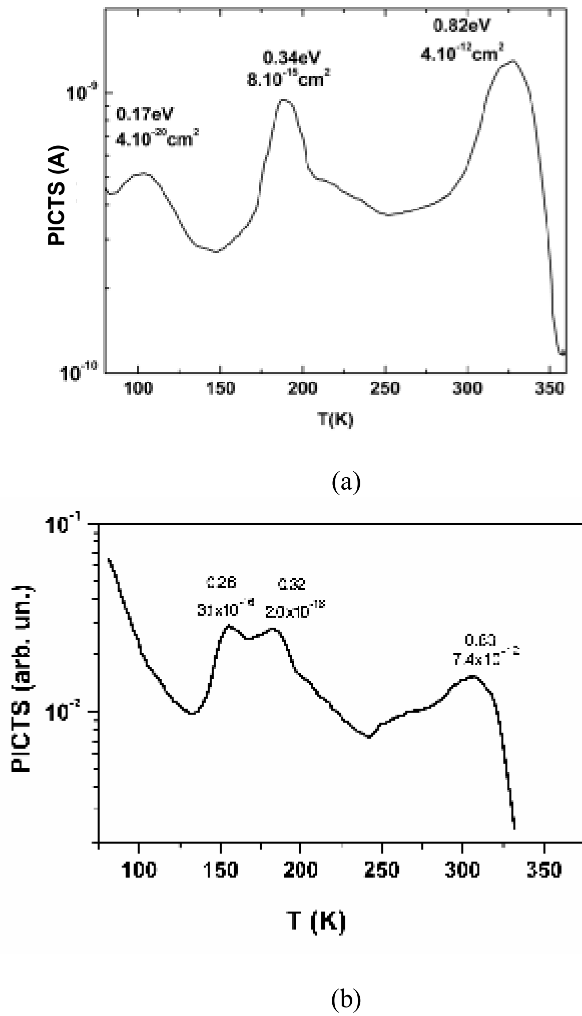

(a)

(b)

Fig. 4.7. Typical PICTS spectrum of the sample (a) CdTe:In , and (b) CdTe:Sn

Table 4.3. Ionization energy, trap's sign, and average capture cross-section for different studied samples.

Sample	E_t (eV) (TEES)	Trap's sign	Cross section s (cm^2) (TEES)	E_t (eV) (PICTS)	Cross section s (cm^2) (PICTS)
1. In	0.14	h	$1.0x10^{-21}$	0.17	$4.0x10^{-20}$
	0.40	h	$5.6x10^{-18}$	0.34	$8.0x10^{-15}$
	0.67	h	$2.8x10^{-11}$	Not observed	
	0.83	h	$1.0x10^{-15}$	0.82	$4.0x10^{-12}$
2. Cl	0.51	e	$1.1x10^{-14}$	0.50	$2.4x10^{-12}$
	0.63	h	$3.5x10^{-17}$	Not observed	
3. Sn	0.25	h	$6.7x10^{-16}$	026	$3.1x10^{-16}$
	0.29	h	$2.4x10^{-16}$	0.32	$2.0x10^{-16}$
	0.72	e	$9.7x10^{-14}$	0.83	$7.4x10^{-12}$
4. Ge	0.77	e	$3.6x10^{-13}$	0.75	$1.0x10^{-11}$
	Not observed			0.45	$6.5x10^{-8}$

The summary of energy levels and their capture-cross sections by both the TEES and the PICTS methods for all samples is given in Table 4.3. The results are in good agreement with the previously published data [54, 62] on CdTe:In and CdTe:Sn samples cut from crystals produced by the same preparation techniques in our lab.

4.1.4 Summary

It can be seen, that near midgap levels in samples doped with shallow donors (Cl, In) have a low value of capture cross-section $(\approx 10^{-17} cm^2)$ and are hole traps. Samples doped with a deep donor (Ge, Sn) have a much higher capture cross section of the midgap level $(\approx 10^{-13} cm^2)$, which acts as an electron trap. Both the higher capture cross-section and trap type (electron) in case of Ge and Sn doping are negative factors from the point of view of charge collection efficiency in detectors. Collection of holes is in general problematic due to their low mobility. Therefore detectors with read-out schemes that use only the electron signal and suppress the hole contribution are used [6]. Presence of an electron trap with a high capture cross-section, which was observed in CdTe:Ge sample No.3, results in a substantial deterioration of detector performance.

A comparison between results by TEES with that obtained by photo-induced current transient spectroscopy (PICTS) is also shown in Table 4.3. Good agreement of the trap energies obtained from both methods was found out. There is, however, a difference of the capture cross-section values up to two orders of magnitude. The answer why the capture cross-section by TEES is smaller than that by PICTS will be discussed in the next sections.

The deep trap near the middle of the gap was reported by a number of authors being common for doped and intentionally undoped CdTe and CdZnTe. It was attributed to a deep acceptor complex involving V_{Cd} acting as a recombination center (labeled H/H0 in the reference [80]). Another deep donor level (E) lying slightly above the H/H0 level was

found in CdTe:Cl samples [80]. Recently a midgap level (~0.7eV) in both undoped and Al-doped CdTe was identified as a complex of Cd vacancy and Te antisite based on ab-initio calculations [11]. The capture cross-section of this level is ~10^{-13}cm^2 and it is an electron trap. These results may seem to be contradictory to our data from In-doped CdTe, where a midgap hole trap with a small capture cross-section ~10^{-15}cm^2 was observed. Due to the midgap position of the level, however, emission of electrons or holes from the level can be seen in the TEES experiment in dependence of the filling factor of the level. Therefore the data from Ref. [11] and our results can correspond to the same level, if we suppose that in our samples the level is more filled by electrons and the emission of holes from the valence band therefore prevails in the TEES experiment.

It is generally accepted, that Ge and Sn occupy Cd position in the lattice and introduce deep levels near the midgap [59, 122], which compensate the residual acceptors (e.g. V_{cd}) and fix the Fermi level in the midgap position. Therefore, high resistivity (Semi-insulting) materials can be achieved. The distribution of the defects in the ingot and their influence on the Fermi level position and therefore, on the sign of the TEES signal and the charge collection need more discussion. It will be the goal of the complex study of deep donors in the next two sections (4.2, 4.3).

On the other hand, the compensation mechanism in case of shallow donor is not fully clear; especially it is not known what is the origin of the midgap levels fixing the Fermi level and what is their concentration, distribution in the ingots, and their correlation to charge collection properties. It will be the goal of the deep study of CdTe crystal doped by shallow donors in the 4.4 and 4.5 sections.

4.2 Complex study of CdTe:Sn crystals

In this part, a detailed study of the compensation of CdTe with Sn impurity, which has a donor level in the mid-gap, and whose atomic number (50) is between that of Cd (48) and Te (52)[59], will be given. The results obtained on several CdTe ingots grown with various Sn concentrations in the melt will be presented. The purpose of this study is to increase understanding of defect structure of CdTe:Sn with special attention paid to deep levels substantially influencing the mobility-lifetime product and response time of the material, which can be considered as a promising one for fabrication of x-ray detectors.

Four ingots were included in this study, three doped ingots VG2, VG3 and VG4, and the undoped AV from the previous study. There was a gradually increasing concentration of the Sn impurity in the ingots (see table 4.4). All ingots were cut along the growth direction. The obtained wafers were mechanically lapped, polished, and finally chemo-mechanically polished with Br/methanol solution. These wafers were characterized by several techniques to visualize the distribution of defects.

Table 4.4. General properties of the CdTe crystals.

	Sn concentration in melt(cm^{-3})	Max. resistivity (Ω.cm)	Photoconductivity σ_l- σ_d($\Omega^{-1}cm^{-1}$)	Type of Photoconductivity[a]
AV	Undoped	10^3	Not registered	…
VG2	$2x10^{17}$	$3x10^9$	$2x10^{-10}$	n-type
VG3	10^{18}	$6x10^9$	$1x10^{-9}$	n-type
VG4	10^{19}	10^{10}	$7x10^{-10}$	n-type

[a] *Type of photoconductivity in the area of maximum resistivity in dark (ρ_d).*

4.2.1 Content of impurities

Actual impurity content was measured in samples taken from the middle part of the ingots by glow discharge mass spectroscopy (GDMS). The concentration of impurities in CdTe samples is presented in table 4.5. The impurities in the AV, and VG3 were presented in table 4.2 in the last chapter. The overview is shown also here to complete picture of the impurities in all Sn doped CdTe studied samples. It is noted that the concentration of residual impurities normally does not exceed the value of several ppb. Again, the concentration of the two impurities, Na and Cu, reach 100–200 ppb. Contamination with these impurities originates from the quartz, ampoule preparation process, or the starting 6N materials. The VG4 ingot was occasionally contaminated with the B and Fe impurities. The Sn impurity was practically absent in the undoped AV ingot, and its concentration gradually increased in the VG2, VG3 and VG4 ingots due to its higher concentration in the melt according to the doping protocol (see Table 4.4).

The GDMS measurement shows that the incorporation of Sn to the crystal is poor. Sn content in the melt in the range 10^{17}–$10^{19}cm^{-3}$ results in the concentration of 10^{14}–$10^{15}cm^{-3}$ in the solid phase. The reason for this behavior is not clear. However, the low Sn melting point (231.9 °C) could lead to nonhomogeneous distribution and precipitation of this dopant, and this may influence the material properties throughout the ingot [102, 123]. The information about distribution of Sn will be estimated from the presented maps of

resistivity, photoconductivity, and photoluminescence based on the fact that the segregation coefficient of Sn is less than one. The Sn concentration is therefore supposed to increase along the growth direction.

Table 4.5. Concentration of impurities in the CdTe:Sn crystals.

N	**Crystal**	**Undoped (AV)**	**Sn doped (VG2)**	**Sn doped (VG3)**	**Sn doped (VG4)**
	Element	Conc. (ppb)	Conc. (ppb)	Conc. (ppb)	Conc. (ppb)
1	Li	<2	<1.5	< 1.6	<1.5
2	B	7	20	220	890
3	Na	160	130	100	130
4	Mg	20	15	50	25
5	Al	5	1.2	8	5
6	Si	<5	<5	43	8
7	P	2	2	12	<0.4
8	S	50	30	48	48
9	K	<8	<6	< 3	<7
10	Ca	<25	<20	<15	<12
11	V	<0.2	<0.1	< 0.1	<0.1
12	Cr	7	23	5	23
13	Mn	<18	<18	< 10	<16
14	Fe	<30	<20	26	100
15	Co	0.7	0.5	< 0.2	1.7
16	Ni	8	25	0.7	40
17	Cu	120	160	30	180
18	Zn	5	7	2	10
19	Ge	<7	<8	< 6	<8
20	As	<100	<100	< 70	<100
21	Se	<8	<6	<6	<6
22	Br	<7	<8	<8	<7
23	Ag	<30	<20	< 10	<15
24	In	<20	<20	< 15	<20
25	**Sn**	**<20**	**260**	**460**	**520**
26	Sb	<20	<30	< 13	<16
27	Hg	<1	<1	< 0.7	<1
28	Tl	<0.2	<0.2	<0.1	<0.2
29	Pb	<0.4	<0.4	<0.4	<0.3
30	Bi	<0.1	<0.1	<0.1	<0.1

4.2.2 Resistivity and photoconductivity mapping

Resistivity (ρ_{dark}) and photoconductivity (PCM), defined as $\Delta\sigma = \sigma_{light} - \sigma_{dark}$, were mapped by the non-contact time dependent charge measurements (TDCM) method [109]. The PCM mapping was performed at room temperature (RT) with band gap excitation (750 nm, 1–5 mW).

The conductivity type at light was measured at RT by thermoelectric effect measurements on samples cut from the area of maximum resistivity in dark (ρ_d), it was performed with ohmic contacts deposited onto the front and back surface of the samples from the $AuBr_3$ solution. The results are shown in table 4.4.

The undoped AV ingot was low resistivity CdTe ($\sim10^3$ Ωcm) with p-type conductivity. Resistivity of the VG2 ingot, grown with the lowest Sn concentration in the melt, was also low (10^4–10^5 Ω cm), except for the last-to-freeze zone with resistivity of 3 x 10^9 Ω cm and high photoconductivity (see table 4.4 and Fig. 4-8). Concentration of Sn was increased in the VG3 ingot. High resistivity and photoconductivity were obtained throughout the crystal (Fig. 4-9). The maximum resistivity of 9 x 10^9 Ω cm was reached in the last-to-freeze zone. Resistivity and photoconductivity in this crystal were rather inhomogeneous.

The VG4 crystal shows an improved uniformity of the resistivity and photoconductivity distributions (see Fig. 4.8). The maximum resistivity of 10^{10} Ω cm and photoconductivity 7×10^{-10} Ω^{-1} cm^{-1} was reached. The GDMS analysis shows that crystal VG4 was contaminated with B, which in the measured sample exceeded the concentration of Sn. The question therefore arises, whether boron can be responsible for high resistivity of crystal VG4 instead of Sn. Study of boron behavior in CdTe [124] at concentrations comparable and higher than the one present in the VG4 crystal has shown that boron is not electrically active and it is mostly concentrated in inclusions. Nuclear magnetic resonance (NMR) experiments [125] revealed that a fraction of about 20% of boron is incorporated on a substitutional site in the Te sublattice at room temperature and is supposed to act as an acceptor. We connect therefore the increase of resistivity in the crystals with the increasing content of Sn in the melt rather than with occasional contamination with boron.

In summary, the results of resistivity and photoconductivity measurements (Fig. 4-8) demonstrate that the high resistivity well correlates with photoconductivity in case of crystal VG4. We shall analyze the reasons for such behavior, namely, through the study of defect levels in the band gap of CdTe:Sn.

4.2.3 Defect levels in bandgap of CdTe:Sn

Photoluminescence (PL) spectra and mapping, Photocurrent spectroscopy (PCS), and Photo-induced capacity transit spectroscopy (PICTS) [102] were used with the previous maps to analyze the defect levels in the bandgap of Sn doped CdTe.

PL spectra were measured at 80 K in a cryostat attached to an X–Y translation stage with 0.5 mm step. An argon laser (488 nm) was used for excitation. PCS was measured in a conventional mode of excitation (1–5 mW) with the 20 Hz chopper. PCS and PICTS were performed with ohmic contacts deposited onto the front and back surface of the wafer from the $AuBr_3$ solution.

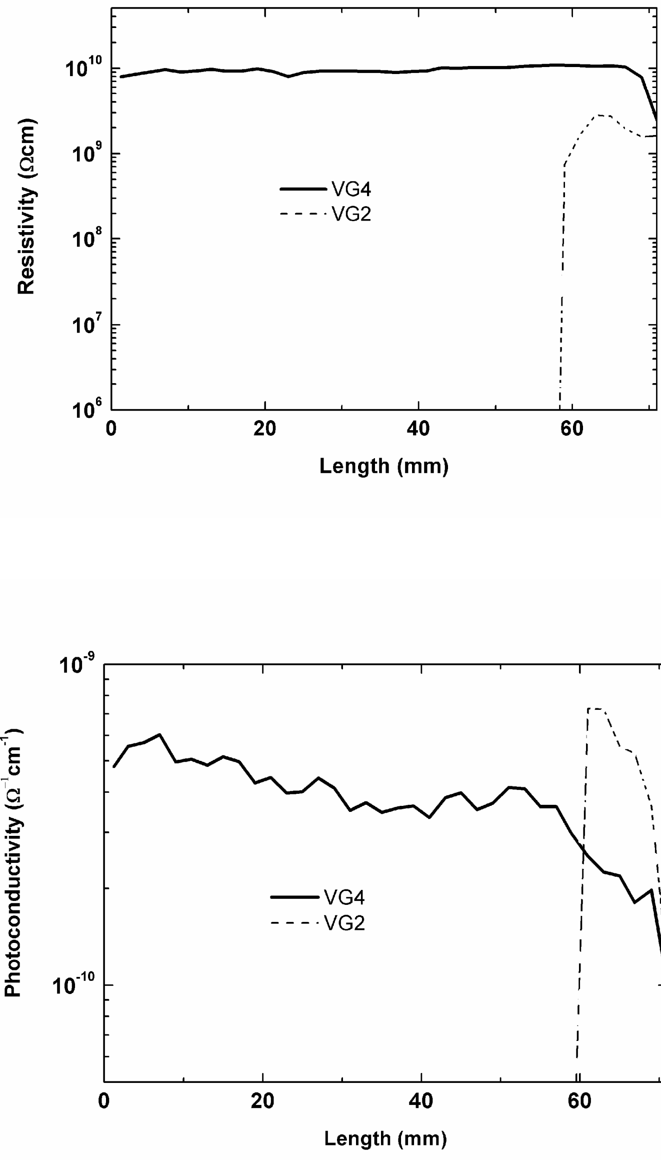

Fig. 4-8. Axial resistivity (ρ_{dark}) and photoconductivity ($\Delta\sigma$) profiles measured in the VG2 and VG4 ingots at room temperature.

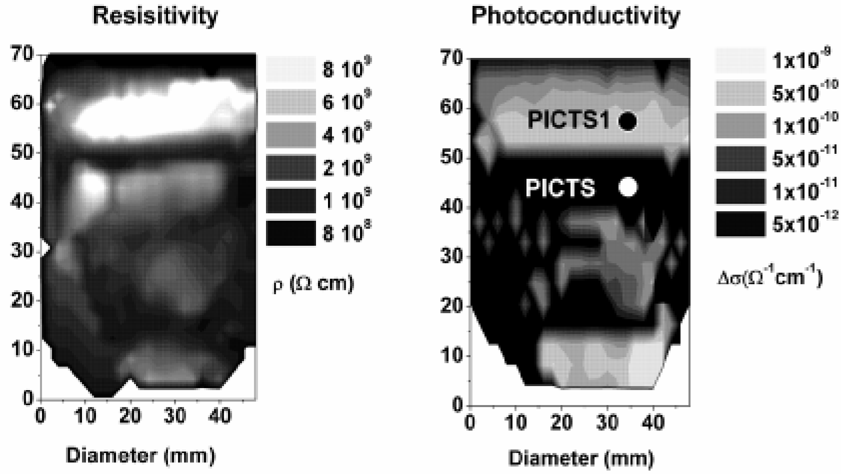

Fig. 4-9. Room-temperature resistivity (ρ) and photoconductivity (Δσ) maps of the long length cut of the VG3 ingot.

4.2.3.1 Photoluminescence and Photocurrent spectra*:*

The typical low – temperature PL spectra on wafers cut from the middle of the AV, VG2, and VG3 ingots are shown in Fig. 4-10. They contain two shallow and two deep emission bands, which are labeled as D-h, A-center, 1.06 eV, and 0.83 eV.

The intensity of the 0.83 eV transition, which is negligible in the undoped AV crystal, increases with the increasing content of Sn in the crystals. The zero phonon line (ZPL) [47] of this PL band is at E_C-0.94, i.e at E_V+0.66 eV. The origin of midgap level at E_V + 0.76 eV is often ascribed in the literature to complexes of Cd vacancy and foreign impurities [16, 126]. It seems therefore reasonable to connect the 0.83 eV PL band with a complex of Cd vacancy and Sn defect, e.g., (V_{Cd}–Sn_{Cd}). The difference of energies [i.e. ZPL of the 0.83 eV PL band, at E_V + 0.66 eV, from our PL data and E_V + 0.76 eV from PICTS and DLTS the literature] can be explained by interaction with lattice (absorption of phonons). Part of the difference can be also caused by an energy gap larger at 77 K (PL measurements) than that at 300–330 K (PICTS measurements).

The A-center band is due to the recombination of electrons from the conduction band with holes on the (V_{Cd}–D) acceptor [47], and the 1.06 eV band is due to Fe or Cu [125]. A significant signature of these samples is the D-h band, which dominated the PL spectra of crystals AV, VG2, and VG3. The D-h band arises due to the recombination of free excitons and of electrons on shallow donors with free holes [127].

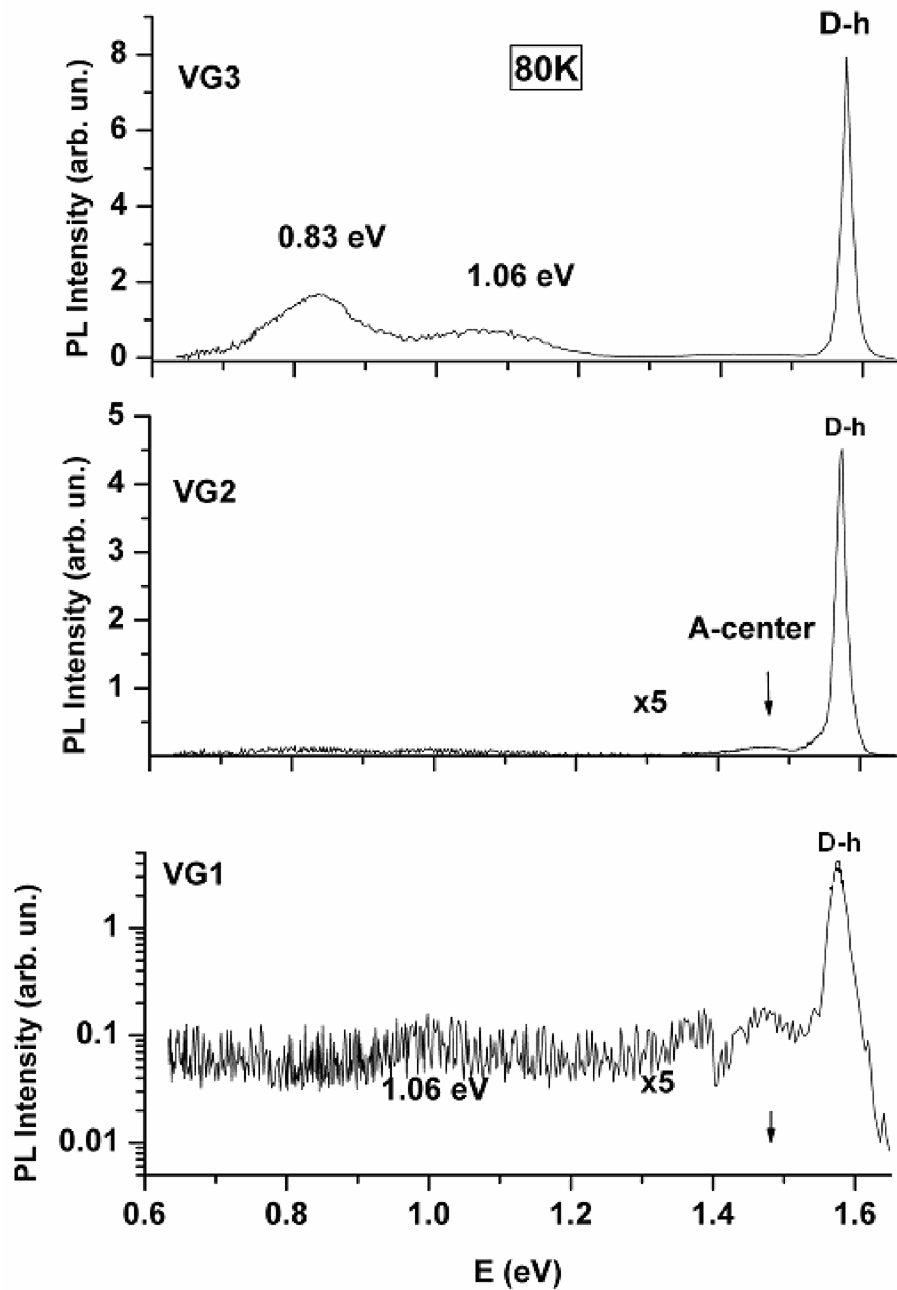

Fig. 4-10. Representative photoluminescence spectra of AV, VG2, and VG3 crystals at 80 K.

The PL and PC spectra measured in the most photosensitive part of the VG4 crystal are presented in Fig. 4-11. The PL spectrum of the VG4 crystal is dominated by the 1.06 eV emission (Fig. 4-11). This fact can be explained by a higher integral concentration of impurities having energy levels in this spectral region (Cu, Fe) in case of crystal VG4 (table 4.5).

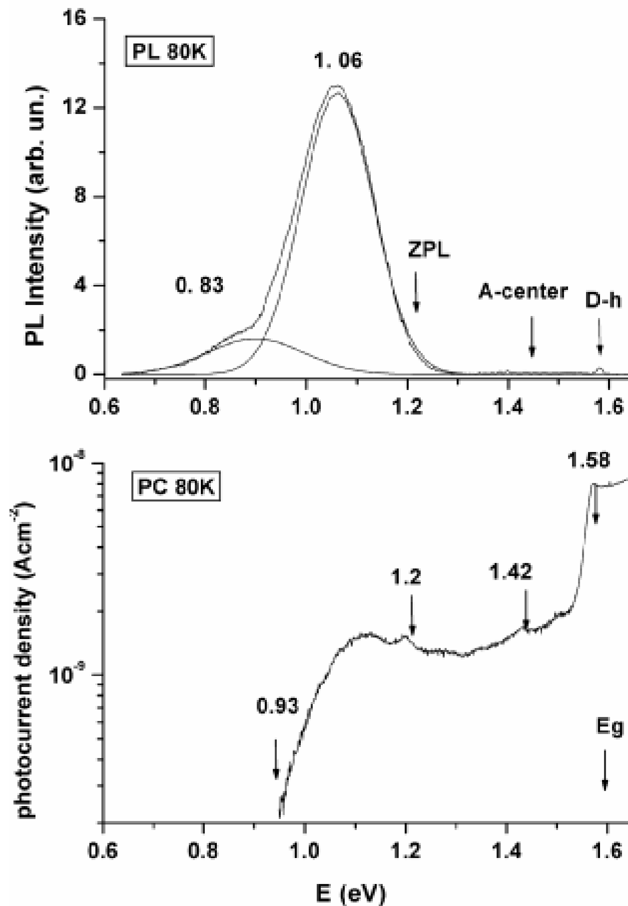

Fig. 4-11. Comparison of the photoluminescence and photoconductivity spectra of the VG4 crystal at 80K.

One can see in Fig. 4-11, that the PL emission is well resolved in the same spectral region, where the PCS signal is high (1–1.2 eV). In general, the zero phonon line (ZPL) of an emission corresponds to the photoionisation thresholds of the electronic level. Following the analysis made in Ref. [115], the position of the zero phonon line (ZPL) for 1.06 eV emission is at 1.2 eV (i.e. $E_V + 0.4$). The role of Cu in CdTe was in detail investigated in Ref. [128]. It was shown, that the level at $E_V + 0.35$ eV corresponds to Cu

occupying Cd sublattice and acting therefore as acceptor. We therefore suppose that part of the intensity of the 1.06 eV corresponds to electron transitions from conduction band to the E_V + 0.35 eV level of Cu_{Cd}. Transitions of electrons from conduction band to the $V_{Cd}^{2-/-}$ acceptor level (E_V + 0.43 eV) [102, 123] can also contribute to the observed PL signal. From the results of analysis of PL spectra, we attribute the 1.06 eV PL band to acceptor defects, which must be compensated by the introduced Sn to achieve high resistivity.

The ZPL of the 0.83 eV band is located at E_C-(0.9 – 0.95) eV. This deep level is revealed in the PCS spectrum as the photoionisation threshold for electrons at 0.93 eV. The hole trapping level, consequently, is at E_V + (0.65 – 0.7) eV. This energy of the level is shifted too far from the midgap to be responsible for the Fermi level pinning and the observed resistivity ~10^{10} Ω cm. We therefore suppose that Sn is mainly incorporated in the Cd sublattice and acts as a donor. The energy level of $Sn_{Cd}^{2+/3+}$ transition was determined by photo-electron paramagnetic resonance (EPR) at E_C-0.85 eV [59]. This energy is higher than the energy E_C-0.95eV observed from our photoluminescence and photoconductivity spectra. In this scheme, the deep Sn donor at E_C-0.85 eV compensates shallow acceptors like Na, Li, and deep acceptors (corresponding to 1.06 eV and possibly 0.83 eV PL bands) resulting in pinning of the Fermi level in the midgap and high resistivity. The scheme of midgap levels is shown in Fig. 4-12. The ZPL of the 1.06 eV band (E_C-1.2 eV) and 0.83 eV band (E_C-0.95 eV are used).

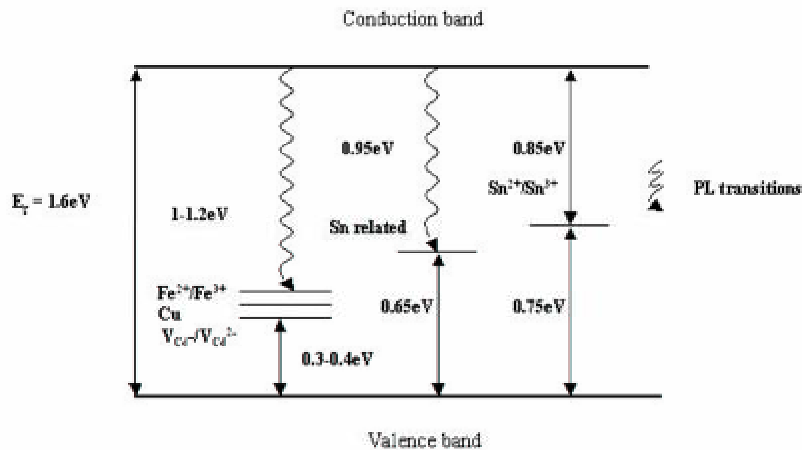

Fig.4-12. Schematic illustration of deep levels in CdTe:Sn deduced from photoluminescence and photoconductivity data of this paper and from Ref. [59].

4.2.3.2 Photoluminescence mapping:

The PL mapping was preformed and the results were compared with the resistivity and photoconductivity maps to establish whether any correlation exists between the PL band intensities and the resistivity.

Figure 4-13 shows the PL maps of the VG3 crystal, which were compared with the maps of resistivity and photoconductivity from Fig. 4-9. This comparison reveals that the 1.06 and 0.83 eV emissions correlate with resistivity and photoconductivity maps. The levels located at E_V + (Eg-1.06 eV) and E_V + (Eg-0.83 eV) are in the dark completely (1.06 eV) and at least partially (0.83 eV) filled with electrons. These levels lying below the dark Fermi level are the R-centers. They have a large probability of trapping for photoholes and a small one for photoelectrons because they are occupied with electrons in high-resistivity samples. They are negatively charged in photoconductive CdTe [129, 130].

These levels at light trap photoholes, which slowly recombine with photoelectrons from the C-band. Thus, resistivity at light decreases due to photoelectrons. The higher the concentration of photoholes trapped by these levels, the higher the photoconductivity of the sample is. The midgap level corresponding to the 0.83 eV transition is in the area of high resistivity more filled with electrons, and it can more easily trap photoholes resulting in the increased PL intensity.

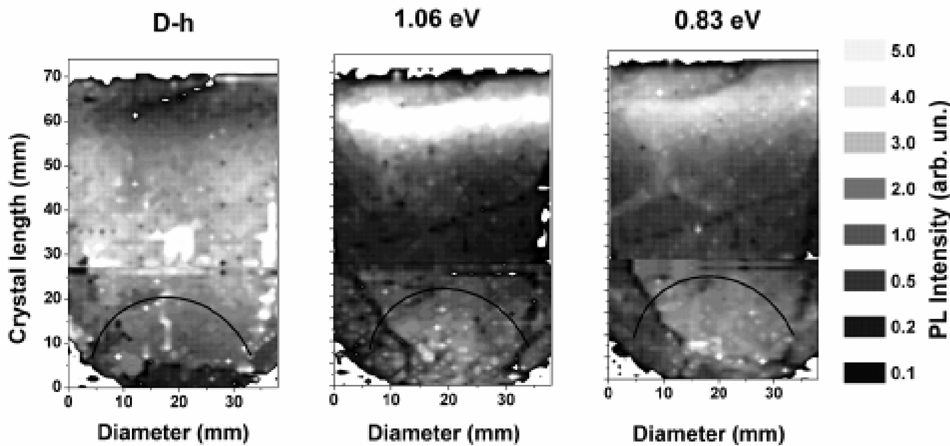

Fig.4-13.Photoluminescence map at 80 K of the long length cut of the VG3 crystal.

It has been mentioned already that high compensation of the VG2 crystal was achieved only at the very end. This is the region where concentrations of the deep Sn donor and of the shallow and deep acceptors reach maximum values. The VG3 and VG4 crystals with resistivity all throughout close to 10^{10} Ω cm were similar to this case. This is due to an increased concentration of Sn, which effectively compensated acceptors.

Our results demonstrate also (Fig. 4-9), that photoconductivity can be low in high resistivity CdTe. This is the case of low concentration of the R-centers populated with electrons, either due to low concentration of donors, which compensate these acceptors or

due to low concentration of acceptors in comparison with the concentration of photoholes. In this case, other defects are responsible for resistivity.

4.2.3.3 PICTS measurements*:*

To identify other defect levels, we present a comprehensive analysis of the hole and electron traps in the Sn doped CdTe. This analysis is based on the complementary data obtained with various techniques such as PICTS, DLTS, PL, and PCS.

The PICTS technique has been often used for characterization of high resistivity CdTe and results have been recently reviewed [131]. It is, however, difficult to make conclusion about the electron or hole character of the trap using only this technique. This difficulty can be overcome by the complementary study of the traps in low resistivity CdTe obtained by DLTS or photo-DLTS [22, 61]. In addition, we compared the PICTS spectra from the photosensitive and non-photosensitive areas of our CdTe:Sn crystals. The traps found in various CdTe crystals are listed in table 4.6.

Two normalized PICTS spectra from the VG3 crystal are shown in Fig. 4-14. The measurements were performed in the areas PICTS1 and PICTS2, which are shown on the photoconductivity map (see Fig. 4-9). They demonstrate that the 0.75 eV peak dominates the spectrum in a photosensitive area while the 0.52 eV peak is more pronounced in a non-photosensitive area. This tendency was found in all CdTe crystals doped with Sn.

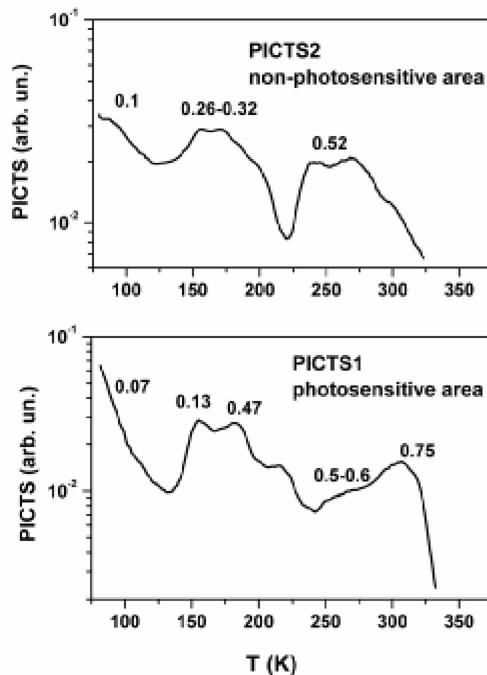

Fig. 4-14. Representative PICTS spectra from the photosensitive and non-photosensitive areas of the VG3 crystal

Four electron traps have been identified previously in the *n*-type CdTe:Sn, which can be classified according to Ref. [132] as P3 (0.32–0.38 eV), P4 (0.4–0.43 eV), P5 (0.5–0.56 eV), and P7 (0.75–0.85 eV). These traps are also present in our CdTe:Sn crystals (see table 4.6). An additional trap detected in our crystals is P2 (0.21– 0.25 eV) and it also has been identified in the past as an electron trap [27, 133-137].

Table 4.6. Identification of traps by comparison of PICTS, DLTS, and photo DLTS data.

		P0	P1	P2	P3	P4	P5	P7
PICTS (this work)	VG2 PC area	0.08	0.2	…	…	...	0.56	0.95
	VG3 PC area	0.073	0.13	…	....	0.47	0.51	0.75
	VG3 non PC	0.095	0.14	…	0.32	…	0.52	…
	VG4 PC area	….	0.11	0.21	0.32	…	…	0.85
	VG4 non PC	0.09	0.14	…	…	…	0.5	…
Identification		H-trap	H-trap	E-trap	E-trap [22]	E-trap[22]	E-trap[22]	E-trap[22]

The energies of the P7 trap found in the VG3 and VG4 crystals (0.75, 0.85 eV) coincide within the experimental error of the PICTS method with the energy of the $Sn^{2+/3+}$ transition [59]. The 0.95 eV transition revealed by PICTS in case of the VG2 crystals energetically coincides with the transition of the E_C-0.95 eV ZPL of the 0.83 eV PL band. The fact, that the E_C-0.85 eV transition was not observed in crystal VG2 can be explained by the lower concentration of Sn in this crystal.

4.2.4 Summary

In this part, four CdTe ingots, one undoped and three doped with Sn were grown by the vertical gradient freeze technique. The Sn concentration was gradually increased in this experiment. A thorough study of material properties was performed by a number of complementary techniques: analytical (glow discharge mass spectroscopy), electrical, thermo- and photo-electrical (resistivity, photo-induced current transient spectroscopy, and photoconductivity), and photoluminescence.

It was shown that the Sn impurity strongly influences the material properties. The concentration of Sn must be equal to or higher than the total concentration of uncompensated acceptors to reach precise compensation. The deep donor level of Sn located, at E_C–0.85 eV is responsible both for compensation and photoconductivity. The resistivity of 10^{10} Ω cm can be achieved at precise compensation. The Fermi-level is in this case pinned on the middle-gap donor level.

Electronic levels in the band gap were studied by several complementary techniques. Two deep acceptor levels are responsible for the photoconductivity at room temperature. They are located lower in the band gap than the Sn donor level, namely, at E_V + (0.66 to 0.7) eV and E_V + 0.39 eV. Two deep electron traps at E_C–0.47 eV and E_C–0.52 eV, which deteriorate the detector ability of CdTe were identified as native complex defects.

4.3 Dependence of TEES of CdTe:Sn on Fermi level position

In last sections, we used Sn impurities to demonstrate the importance of the concentration of chemical impurities and compensation in high-resistivity CdTe. It was concluded that the neutral deep donor level of Sn, Sn_{Cd}, is responsible for compensation and photoconductivity, resulting in pining of the Fermi level in the midgap and resistivity of 10^{10} Ω cm can be achieved.

In this section, we focus on the critical role of the Fermi-level position in the trapping of free charges. We also analyze, for the first time, the charge states of Sn_{Cd}, and its dependence on the Fermi level variation in high resistivity CdTe:Sn. Earlier works [138, 139] showed that the position of the Fermi-level energy across the gap is governed by variations in the axial segregation of the concentration of shallow impurities along the direction of growth.

In undertaking this work, we relied on the power inherent in a combination of the several spectroscopic methods. We used resistivity mapping and TEES methods.

The CdTe:Sn samples investigated in this study were from the ingot grown with 10^{18} cm^{-3} Sn concentration in melt. The content of impurities was measured by glow discharge mass spectrometer in samples taken from the middle of the ingot and presented in table 4.5. The concentration of Sn in the grown ingots varied along the direction of crystal growth because of axial segregation, resulting in a gradual change in the resistivity values from those that are usual for undoped p-type CdTe (10^3-10^4 Ω cm) to those typical of semi-insulating samples (5 x 10^9-10^{10} Ω cm).

4.3.1 Measurement of the type of conductivity

The conductivity type was determined from the thermoelectric- effect measurements obtained at room temperature. Here, it was necessary to consider thermal transitions from shallow acceptors into the C band, and the much higher mobility of electrons than that of holes. It was difficult to distinguish in semi-insulating samples the *p*-type conductivity due to a small concentration of free holes, or *n*-type due to band-to-band transitions. In the studied CdTe, crystal resistivity was relatively low in the parts taken from the beginning of the ingots (10^3-10^4 Ω cm), and gradually increased up to 5 x 10^9 Ω cm in those from the end of the ingots. In this case, it was easier to determine *p*-conductivity of the material. It means, that acceptors were not fully compensated by rhe deep donor Sn_{Cd}. The compensation was dependent on the deep donor concentration, N_{DD}, and the shallow impurity surplus, $N_A - N_D$, where N_A and N_D are the concentrations of shallow acceptors and donors, respectively. The increase in resistivity of crystal reflected the more favorable segregation coefficients for Sn (0.025) and the residual impurities present, compare to Na and Cu (~10^{15} cm^{-3})[140].

4.3.2 Resistivity map

A representative resistivity map of the CdTe:Sn wafer is shown in Fig. 4-15. A resistivity varies along the crystal length in the range of 5×10^8 - 8×10^9 Ω cm. The maximum resistivity was reached without overcompensation the sample with the deep donor level of tin. The conductivity of the whole sample was of the *p*-type, i.e even in the

area of highest resistivity the conductivity was of p-type. This fact was important for the calculation of the Fermi-level position in respect with the V-band maximum.

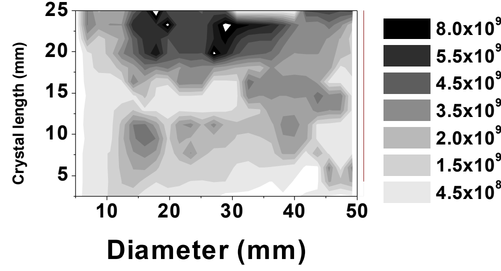

Fig. 4-15. Resistivity map of the p-type CdTe:Sn crystals measured at room temperature

4.3.3 Calculation of the position of the Fermi level

The Fermi-level position in respect with the V -band edge was calculated using the measured resistivity values, ρ, and the following set of equations:

$$\rho = \frac{1}{e(\mu_e n_0 + \mu_h p_0)}, \tag{4.1}$$

where e is the charge of an electron, n_0 and p_0, are the concentrations of free electrons and holes in equilibrium, μ_e = 0.1 m^2/Vs and μ_h = 8x10^{-3} m^2/Vs are the motilities of electrons and holes in CdTe, respectively. For the equilibrium concentration of electrons and hole the well known expressions are used:

$$n_0 = N_c \exp\left(-\frac{E_g - E_{F0}}{kT}\right), \qquad N_c = 2\left(\frac{2\pi m_e^* kT}{h^2}\right)^{3/2} ; \tag{4.2}$$

$$p_0 = N_V \exp\left(-\frac{E_{F0}}{kT}\right), \qquad N_V = 2\left(\frac{2\pi m_h^* kT}{h^2}\right)^{3/2} ; \tag{4.3}$$

where: N_C (300K) = 7. 925×10^{17} cm^{-3} , N_V (300K) = 1. 165×10^{19} cm^{-3} are the densities of states in C and V-bands, and E_g (300K)= 1.5 eV; k-is the Boltzmann constant, T-is absolute temperature. At room temperature the intrinsic carrier concentration is 2.8×10^5 cm^3, with values of m_e^* = 0.1 and m_h^* = 0.6; where: m_e^* and m_p^* are the electron and hole effective masses. The ranges of these values are m_e^* = (0.096- 0.1) and m_p^*= (0.4-0.8); see, for example [141].

From equations 4.1- 4.3 we get a solution for the Fermi-level

$$E_F = kT \ln\left(\frac{1-\sqrt{1-4e^2\rho^2\mu_n\,\mu_p n_i^2}}{2e\rho\mu_p N_V}\right). \qquad (4.4)$$

With this equation we calculated the Fermi-level position in all cross-sections of our samples. With the above mentioned parameters, the maximum value of resistivity in CdTe can reach 2×10^{10} Ω cm, when the Fermi level is located slightly above the midgap. The maximum value of resistivity in our *p*-type crystals was 8×10^{9} Ω cm, this means that the Fermi-level was located in the lower part of the bandgap.

4.3.4 Fermi level position and the TEES of CdTe:Sn.

4.3.4.1 Fermi level position

From the resistivity map and eq. 4.4, one can conclude that the position of the Fermi-level in respect to the V-band maximum varied along the length of the crystals. This variation influenced the population of deep levels of Sn, the position of which Jantsch and Hendorfer [59] had determined earlier from their photoelectron paramagnetic study. The graphical comparison of a change in the relative positions of the Fermi-level and the energy level of Sn is presented in Fig. 4-16. From this figure one can see that the Fermi-level crosses the energy level of Sn at energy E_V+ 0.63 eV.

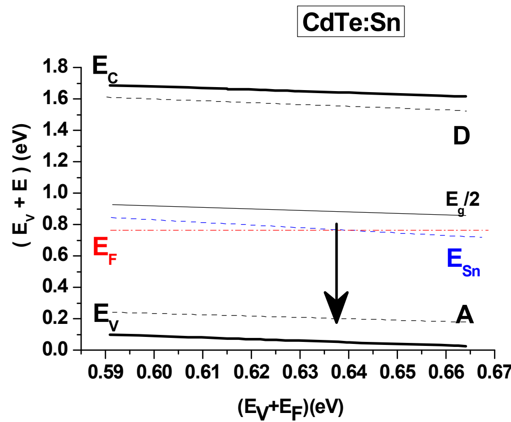

Fig. 4-16. A graphic representation of the band gap of CdTe:Sn comparing the positions of the Fermi level and the energy level of Sn. Here D and A are, respectively, shallow donors and acceptors, E_F is the Fermi level, and E_{Sn} represents the positions of deep donor Sn_{Cd}. The arrow shows the position at which the Fermi level crosses the position of E_{Sn}.

When a degree of occupation of a deep level is changed, a trapping rate is also changed, and a 'kink' in the measured characteristic (i.e., photo-current, photo-luminescence, photo voltage, or thermoelectric current) appears. So far, there have been few comprehensive studies on the compensation and trapping in CdTe and CdZnTe [88, 90, 142] and, to our knowledge no results was published on the dependence of trapping on

the Fermi-level position. In a recent study on deep levels in CdTe doped by various impurities (In, Cl, Sn, and Ge) we, in section 4.1, and others observed a correlation between the deep level peaks in the TEES and PICTS spectra for the case when the character of traps was well defined [143, 144].

The Fermi-level dependent conversion of a charge state of the midgap level $Sn^{0/+2}$ defect changing its ability to trap either an electron or hole, is demonstrated in the present work for the first time.

4.3.4.2 TEES spectra

Two samples were cut from the wafer in Fig. 4-15., the first sample, S_L, had lower resistivity, about $5x10^8$ Ω cm, while the other one, S_H, had higher resistivity, $5x10^9$ Ω cm. Therefore, the Fermi-level is at different position in the both samples, *i.e., it is located below and above the deep level of tin,* E_C – 0.85 eV (i.e, E_V + 0.63 eV , E_g(CdTe) = 1.48 eV at RT) in S_L and S_H, respectively.

The TEES spectra of the sample S_L was shown in the *Fig 4-3 (section 4.1)*, where this sample was studied in that section. Here, we present it again to compare it with the TEES spectra of S_H as in Fig. 4-17. One can see that besides several small peaks corresponding to shallow traps a strong emission with a maximum at ~ 250K dominates the spectrum in both samples. The measurements were repeated with several heating rates. Energy and capture cross section were found out by the heating rate method [144]. The hole trapping character of the deep level is obvious in the area of high resistivity (E_V+ 0.72 eV with $\sigma_{H3} = 9.7x10^{-14} cm^2$), while the same deep trap manifests itself as an electron trap in the area of lower resistivity(E_C- 0.73eV with $\sigma_{L4}=1.77x10^{-14}$ cm^2. This is an unequivocal evidence of the Fermi-level dependent conversion of the charge state of a Sn defect.

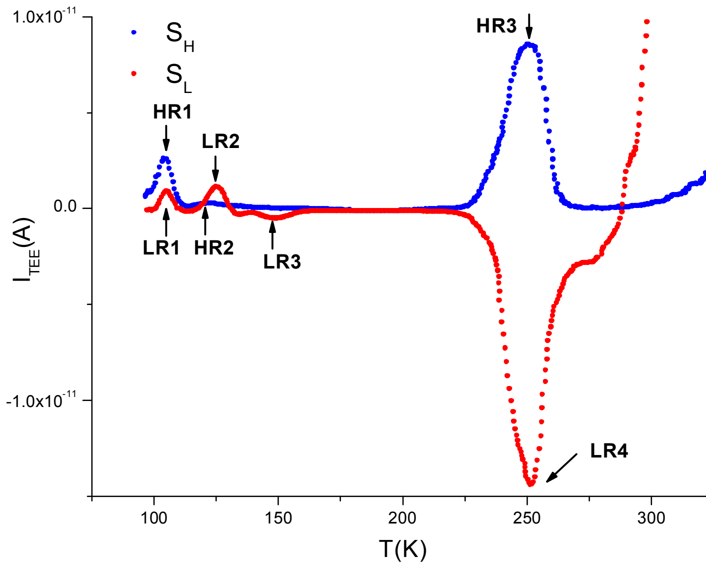

Fig. 4-17. Signal of the thermoelectric effect measured from the samples with lower resistivity, S_L, ($5x10^8$ Ωcm) and higher resistivity, S_H, ($5x10^9$ Ωcm).

4.3.5 Summary

Although the deep donor level, introduced by Sn, is needed to compensate for a surplus of acceptors in the CdTe; its concentration should be minimized as far as practical; otherwise, electron trapping is high. TEES measurement using Fermi-level scanning revealed the conversion of the Sn defect from the electron trap in the lower resistivity sample to the hole trap in the higher resistivity one.

4.4 Detailed characterization of defects in CdTe:In by TEES

It was observed in section 4.1, that the midgap level in the shallow donor (In, Cl) doped CdTe is hole trap with a relatively low capture cross section, which is one of the positive factors for detection properties of such material. But, still a lot of study is required to confirm the good charge collection in the shallow donor doped CdTe, especially, the compensation mechanism in this case is not fully clear. It is not known, also, what is the origin of the midgap level fixing the Fermi level and what is its concentration, its distribution in the ingots, and its correlation to charge collection properties.

In this section, the characterization of the defect level in the bandgap of the In doped CdTe will be studied in more detail. The primary goal to study of defects in high resistivity CdTe is to analyze and identify which defects act as strong traps or recombination centers in order to eliminate them from the technological process and this way to improve the yield of usable material. Deeper study of these materials will be also in the next section 4.5.

The material included in this study were three CdTe:In ingots, labeled as A, B, C, grown from the melt by the vertical gradient freeze method in our laboratory. The content of In in the doped crystals was analyzed by GDMS method. It was in the range of 5×10^{16}-$7\text{x}10^{17}$ cm^{-3}, while in an undoped crystal it was approximately ~2-4×10^{14} cm^{-3}. These values are valid for central parts of the ingots. The resistivity of doped crystals was in the range of (10^8-10^9 Ωcm). Therefore we can conclude that shallow acceptors in these crystals are compensated by the shallow donors-In_{Cd}. TEES technique was used to study the defect levels in a set of samples from the grown crystals. Correlation between the measured TEES spectra and the mobility-lifetime product of electrons is looked for

Results of the measurements

4.4.1 TEES measurements.

Figure 4-18a presents the TEES data of three samples S1, S2, and S3 from the same crystal A, and Figure 4-18b shows the TEES data of two samples S4 and S5 from the other two crystals B and C, respectively. We observed a set of different defect levels P00, P0, P1, P2, P3, P4 (electron traps) and P05, P5, P50 (hole traps). Only four or less of these defect levels were found to be present in one sample. The variable heating rate method was used to determine the ionization energy and capture cross section of traps [144]. Summary of the results is shown in the Table 4.7.

Figures 4-19(a) and (b) present the TEES data on the samples S1 and S2, respectively, at various heating rates. A shift of the peak to a higher temperature with an increase of the heating was observed for defect levels P1, P2, P3, P5 and P50. Using Arrhenius plot, the ionization energy and the capture cross section of these levels were calculated and presented in Table 4.7. Examples of Arrhenius plots are shown in Figures 4-19(c) (the level P1 in sample S1) and 4-19(d) (the level P2 of sample S2).

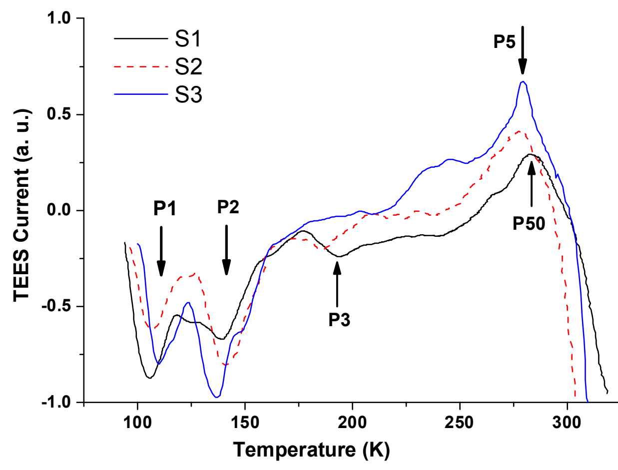

(a)

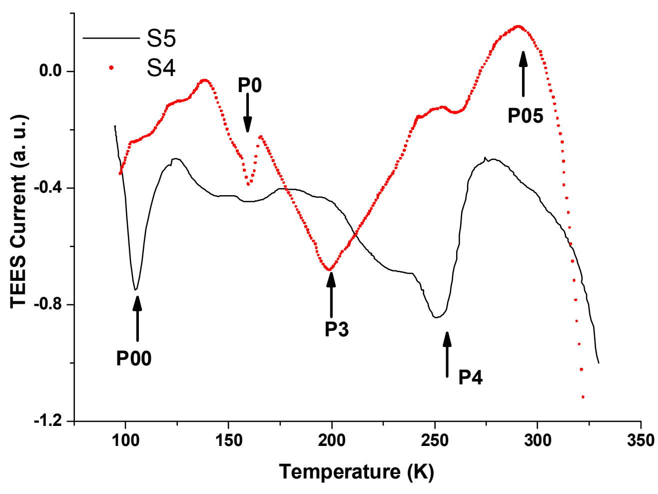

(b)

Fig. 4-18. (a) TEES spectra from samples S1 at 0.083 K/s, S2 at 0.166 K/s, and S3 at 0.25 K/s. (b) TEES spectra from samples S4 at 0.25K/s, and S4 at 0.183 K/s. Samples illuminated at 90K by 1.96eV photons for 1200s.

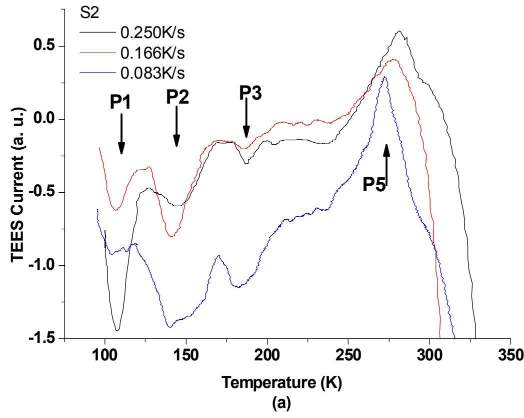

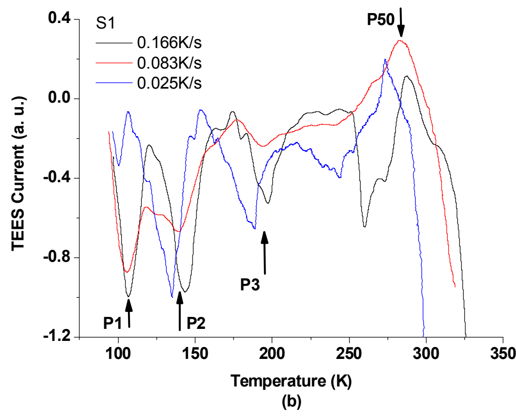

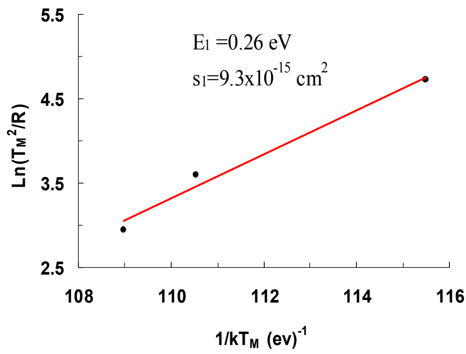

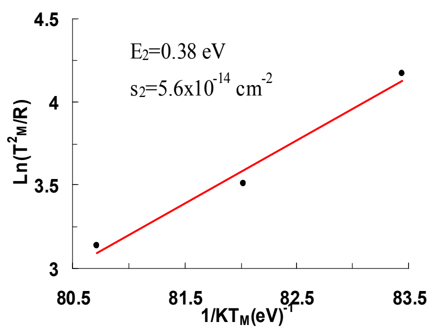

(c) (d)

Fig. 4-19. (a), (b) TEES spectra at various different rates on samples S1, S2 respectively. (c), (d) Arrhenius plots from which the energy and capture cross section of the defect levels P1 of S1, P2 of S2 are calculated.

The TEES data measured with a variable heating rate on samples S3 and S4 are presented in Figure 4-20 (a) and (b) respectively. They are characterized by 3 defect levels – P1, P2 and P5 in the sample S3 and P0, P3 and P05 in the sample S4. The values of the ionization energy and capture-cross section of the observed defect levels were calculated using Arrhenius method and listed in Table 4.7. The Arrhenius plots from which the energy and capture cross section of the trap levels P5 (sample S3) and P3 (sample S4) were calculated are presented in Figure 4.-20(c) and 4-20(d).

The TEES spectra of sample S5 (Fig. 4-18) are characterized by two defect levels – P00 and P4. The summary of results is given in Table 4.7.

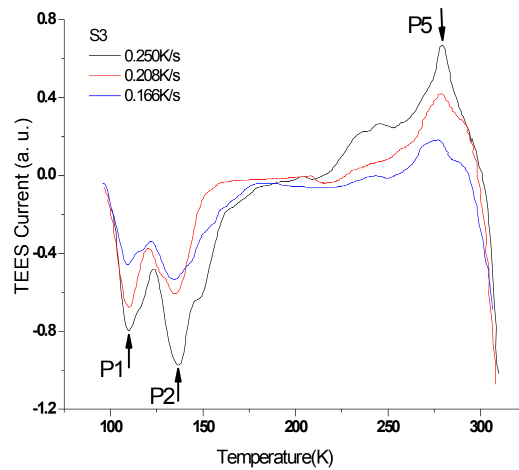

(a)

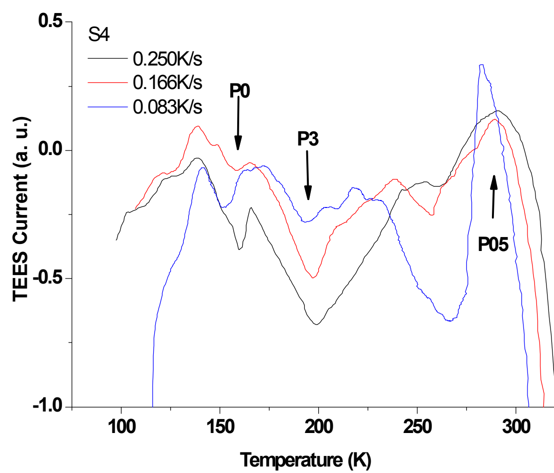

(b)

Figure 4-20. (a) and (b) Variable heating rate on samples S3 and S4 respectively.

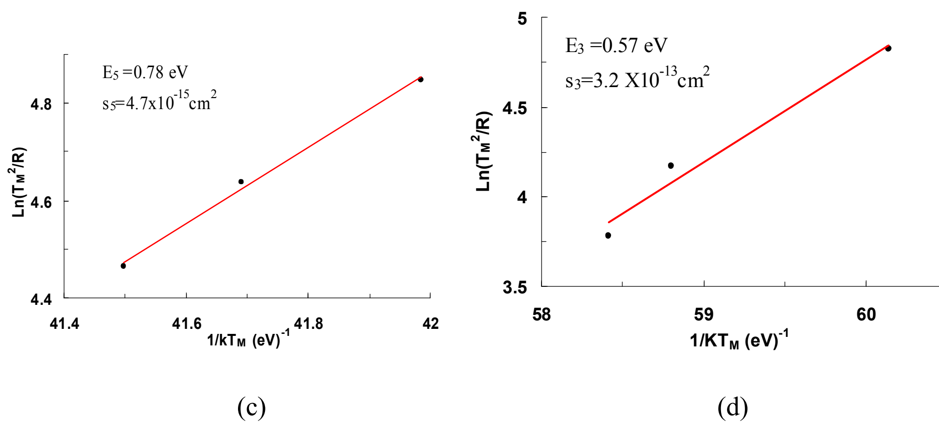

Figure 4-20. (c) and (d) Arrahnius plots showing the energy and capture cross section of the defect levels P5 in S3, P3 in S4 respectively.

Table 4.7. Thermal ionization energies E(eV), Sign, and capture cross section s(cm^2) of the defect levels in the studied samples by TEES method.

	P00	P0	P1	P2	P3	P4	P05	P5	P50
S1			0.26, e 9.3x10^{-15}	0.40, e 2.4x10^{-13}	0.63, e 9x10^{-12}				0.87, h 6.9x10^{-14}
S2			0.25, e 3.8x10^{-15}	0.38, e 5.6x10^{-14}	0.59, e 9x10^{-12}			0.80, h 9.6x10^{-15}	
S3			0.27, e 1.2x10^{-14}	0.39, e 7.5x10^{-13}				0.78, h 4.7x10^{-15}	
S4		0.28, e 1.1x10^{-18}			0.57, e 3.2x10^{-13}		0.73, h 1.1x10^{-16}		
S5	0.15, e 2.7x10^{-20}					0.68,e 1.2x10^{-15}			

4.4.2 Origin of the traps

The level labeled P1 observed in the first 3 samples has energy 0.25-0.27 eV. A level with the same energy was reported by TEES method in Ref. [11]. It was assigned there to the second ionization level of Cd vacancy. This assignment seems to be questionable, because this peak is negative and should be therefore calculated in respect to the conduction band and not to the valence band, as in Ref. [11]. We therefore identify this level as an electron trap 0.25-0.27eV from the conduction band. The P0 defect observed in the sample S3 has practically the same energy as the defect P1, but its capture-cross section is four orders of magnitude smaller. It has therefore a different macroscopic origin. The ab initio calculations have shown the first ionization level of tellurium antisite $(Te_{Cd})^{0/+}$ at energy E_C ~0.35eV. Taking into account a possible interaction with the lattice during the thermal transition as well as the experimental and theoretical error, the P0 or P1 levels could be tentatively interpreted as related to the first ionization level of Te_{Cd}. We also attribute the electron trap level P00 (0.15 eV) observed in the sample S5 to intrinsic defects related to dislocations , which is in agreement with the defect level of the same energy observed in Ref [90].

The level P2 was observed in three samples, all coming from crystal A. It was not present in samples from crystal B and C. We attribute this trap to some foreign impurity or a complex including a foreign impurity atom.

Level P3 was observed in several studied samples. A level (~0.6eV) in CdTe was based on ab-initio calculations [11] attributed to the second ionization energy of tellurium antisite $(Te_{Cd})^{+/2+}$.

The P4 level was only observed in sample S5, coming from crystal C. It is therefore probably related to some impurity or a complex including a foreign impurity atom. Ref. [11] predicts one of the transitions related to the $(Te_{Cd}$-$V_{Cd})$ complex at ~ 0.70 eV, too.

Several deep levels near the midgap (0.73-0.87eV) were observed in different samples. The origin of the levels (named P05, P5 and P50 in Table I) can be attributed to a complex of Cd vacancy with donors [80]. Complexes with different donors will result in slightly different defect energies, which is in agreement with our experiment. Ab initio calculations in Ref. [11] found also energy of a complex of Cd vacancy and Te antisite at this energy. It is important from the point of view of electron transport in detectors, that all observed deep levels near the midgap are hole traps. Therefore, they are mostly filled with electrons at equilibrium and do not influence the electron lifetime substantially.

4.4.3 Traps and the charge collections properties.

Correlation between the measured TEES and the mobility-lifetime product of electrons was looked for. The highest mobility-lifetime product $\mu\tau_e$~10^{-4}cm^2/Vs had the sample S3, while the $\mu\tau_e$ was smaller than 10^{-5}cm^2/Vs in case of the other 4 samples.

Comparison of results of TEES measurements shows, that the main difference among detecting sample S3 and not-detecting samples S1, S2, S4 and S5 was the absence of electron traps of energy E_t~0.6-0.7eV (P3 and P4). The capture cross-section of the P3 trap is very high (~10^{-12}cm^2) acting as a typical "lifetime killer" even at very low concentrations. The electron capture cross-section of the P4 trap is smaller; however the trap is deeper than the P3 trap and can therefore effectively trap electrons as well. This explains the low mobility-lifetime product of sample S5.

The results of TEES measurements together with data of mobility-lifetime product of electrons enable to make rough estimates of maximum concentrations of deep levels in some samples. We will at first assume that the midgap level P5 is fixing the Fermi level

and is therefore partially occupied by electrons at equilibrium. Using the simple formula for trapping time of the level $\tau^+=1/\sigma_n v_{th}(N_t-n_t)$ results in N_t~$4x10^{13}cm^{-3}$ for $\mu\tau^+= 10^{-4}cm^2/Vs$ observed in sample S3 (supposing 50% trap occupation in equilibrium). Taking into account, that the P2 trap present in the sample can also participate in electron trapping without returning the electron back to the conduction band, this value represents an upper concentration estimate.

Apparently the most deteriorating effect on detector performance will have the level P3, because it is localized above the Fermi level. It is therefore almost empty and has a large capture cross-section for electrons. It is present in samples having the $\mu\tau^+<10^{-5}cm^2/Vs$. Here the calculations lead to $N_t\geq 6x10^{11}cm^{-3}$ to explain the observed mobility-lifetime product. Taking into account that also other deep levels trapping electrons are present, this value represents again the upper estimate.

This analysis shows, that electron traps P3 and P4 with energy E_t=0.4-0.7eV in CdTe:In and a very low concentration of ~10^{11}-$10^{12}cm^{-3}$ may be responsible for the deterioration of the electron mobility lifetime product in CdTe:In semi-insulating materials. On the other hand, the midgap level P5, which is fixing the Fermi level can be present at 1-2 orders of magnitude higher concentration, before it starts to influence the charge collection efficiency substantially. This is caused by a higher filling factor of the level, which is apparent from the fact, that this midgap trap appears as a hole trap in the TEES experiment.

4.4.4 Summary

The high resistivity CdTe In doped samples were characterized using thermoelectric effect spectroscopy. The thermal ionization energies and capture cross-sections were calculated using the variable heating method. Comparison of results of TEES shows, that deterioration of the mobility-lifetime product of electrons can be caused by electron traps at E_C-0.6-0.7eV and E_C-0.4eV. Recently published ab-initio calculations show a complex of Te antisite and Cd vacancy at ~E_C-0.7eV. Maximum concentrations of these levels in the samples were estimated based on a combination of TEES and mobility-lifetime product measurements.

4.5 Photoluminescence study of CdTe:Sn and CdTe:In by Ti-sapphire laser and HgCdTe detector

Unfortunately, the detection properties of the deep-donor-doped, e. g. Sn and Ge, crystals are normally not good; the trapping time is too short due to the high capture cross section and high concentration of the midgap level introduced by such donors. It was observed, section 4.1, that both deep donors (Sn, Ge) have a high capture cross section of electrons, which is negative for detection properties of the detector. The situation was improved (section 4.3) when the Fermi level converted these electronic deep level into hole one in the higher resistivity samples. One the other hand, the correlation between deep levels in shallow donor doped CdTe and ability of detection is not fully clear.

Photoluminescence (PL) reflects the intensity of capture of carriers and thus the loss of photo-generated carriers in detectors. PL is a popular optical method for investigation the defect levels in semiconductors. It has been used to investigate shallow levels in many studies, however, a relatively low number of studies was devoted to PL study of deep levels in semiinsulating CdTe.

The purpose of this chapter is to make a comparative study of deep PL in seminsulating CdTe doped by shallow donor (In) and deep donor (Sn), and to correlate it to their ability to detect radiation. Two groups of samples were included in this study. One group was doped with Sn having a deep level near the middle of the forbidden gap, the samples of this group obtained from the crystals investigated in section 4.2. The second group was doped with In, the samples were obtained from the crystals studied in the previous section, 4.4.

4.5.1 Experimental Results

Summary of results of all studied samples is shown in Table 4.8. Two groups of samples were subject of investigation. The first group consists of 4 samples doped by shallow donors (In). Figure 4-21 shows a spectral region of deep traps (0.5-1eV). Samples No.1 and 3 have only a very weak signal from deep levels. Sample No.2 has also a weak PL signal; there is a measurable signal from a transition centered at 0.77eV. Sample No.4 has a relatively strong PL signal centered at 0.87eV. Together three levels (0.63eV, 0.77eV and 0.87eV) with a varying intensity were observed in CdTe:In samples in the spectral range of 0.5-1eV.

Results of measurement in the spectral range <0.5eV for sample No.4 are shown in Fig. 4-22. The measurement of sample No.1 and 3 is practically a straight line with a small peak at 0.28eV. Sample No.2 has practically the same course of PL in this spectral range. Two regions of peaks can be seen in the PL spectra, a series of sharp transitions at 0.36-0.38eV and a peak centered at 0.4eV. Sample No.2 has similar character of the PL signal as sample No.4 shown in Fig.2-22. Sharp transitions at 0.36-0.38eV probably correspond to internal transitions of some transitional element. Similar series of lines was observed in CdTe:Fe at ~0.28eV [145].

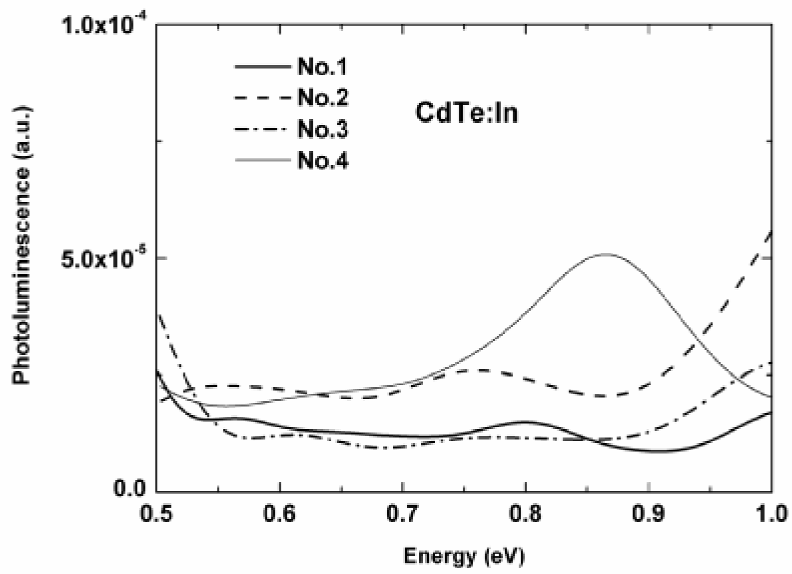

Fig.4-21. Typical PL spectra in 0.5-1 eV range of the CdTe:In studied samples.

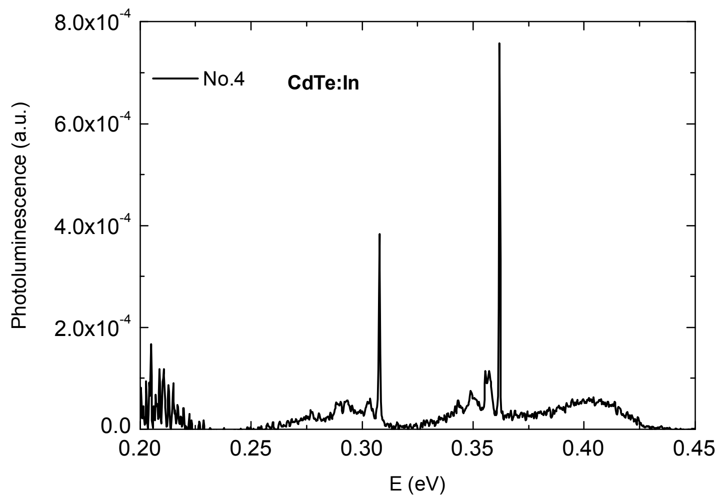

Fig.4-22. Typical PL spectra in the range < 0.5 eV of CdTe:In sample No.4.

In order to compare PL intensity in CdTe doped by shallow donors and by impurities having a deep level in the bandgap, measurements were performed under the same experimental conditions on several CdTe:Sn samples. The results are shown on Fig.4-23. A very intensive PL luminescence on deep levels is observed in case of these samples. The intensity is approximately two orders of magnitude higher, than in In doped samples. The substantially higher recombination traffic through deep levels can be caused by a higher concentration of corresponding defects or their higher capture cross-section. It fully corresponds to the very low mobility-lifetime product of free electrons, which is demonstrated by the fact, that these samples practically do not detect gamma radiation (Table 4.8).

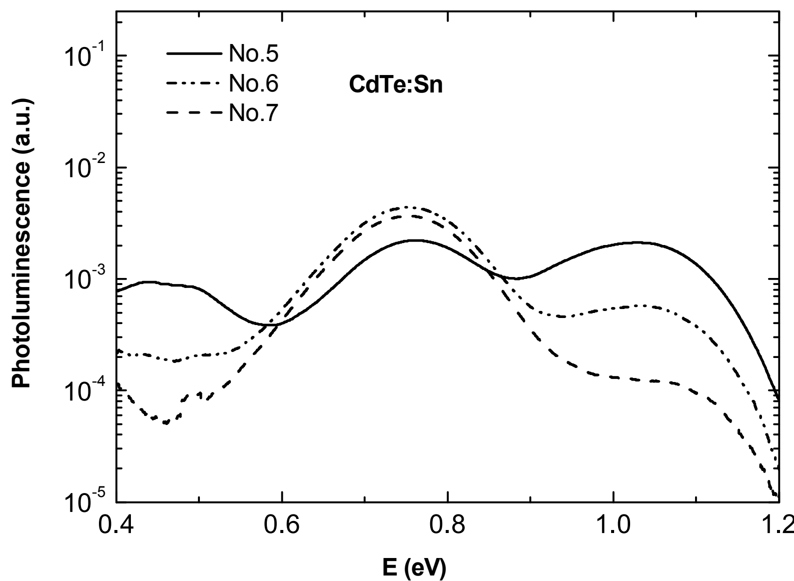

Fig. 4-23. Typical PL spectra in 0.4-1.2 eV range of the CdTe:Sn studied samples

The photoluminescence signal was integrated in the whole measured spectral region (0.5-1.6eV). The results are shown in Table 4.8. The integral PL intensity of In doped samples is very similar ~$2x10^{-3}$a.u. Also the integral PL intensity of CdTe:Sn samples is approximately the same ($1\text{-}7x10^{-3}$a.u.). This result shows that the recombination activity through non-radiative channels differs only slightly among the studied samples. The goal of the integration was to obtain a simple parameter characterizing recombination activity on deep levels in each sample. Using such a parameter in further considerations is substantiated by the assumption, that loss of photo-generated carriers by recombination and trapping in X- and gamma ray detectors is caused by the deep levels contributing to

integral PL intensity. This assumption is valid for samples having a similar intensity of non-radiative transitions.

The results for all measured samples are summarized in Table 4.8 together with the overview of observed PL maxima and their intensities. Comparison of the radiative recombination activity through deep levels (0.3-1.2eV) with the total PL signal (0.3-1.6eV) shows that approx. 0.2-1% of radiative recombination occurs through deep levels in case of CdTe:In samples and 7-15% in case of CdTe:Sn.

Table 4.8. Summary of the PL study of CdTe:In and CdTe:Sn samples

No.	Energy (eV) PL intensity (a.u)	Energy (eV) PL intensity (a.u)	Energy (eV) PL intensity (a.u)	Energy (eV) PL intensity (a.u)	Energy (eV) PL intensity (a.u)	Integrated PL (a.u) (0.5-1.6eV)	Integrated PL(a.u) (0.5-1eV)	Integrated PL(a.u) (0.5-1.2eV)	$\mu\tau_e$ (cm^2/Vs)
1-In			0.8 $1.6x10^{-5}$			$2.8x10^{-3}$	$6.7x10^{-6}$		$1x10^{-4}$
2-In	0.4 $6x10^{-4}$		0.77 $2.6x10^{-5}$			$2.0x10^{-3}$	$1.26x10^{-5}$		$\sim 10^{-5}$
3-In		0.63 $1.2x10^{-5}$				$2.5x10^{-3}$	$7.1x10^{-6}$		$1x10^{-4}$
4-In	0.4 $6.1x10^{-4}$			0.86 $5.1x10^{-5}$		$1.8x10^{-3}$	$1.47x10^{-5}$		10^{-5}
5-Sn	0.47 $9x10^{-4}$		0.77 $5.4x10^{-4}$		1.03 $2.0x10^{-3}$	$1.6x10^{-3}$		$1.1x10^{-4}$	$<10^{-6}$
6-Sn			0.76 $4x10^{-3}$		1.05 $5.0x10^{-4}$	$2.4x10^{-3}$		$6.7x10^{-4}$	$<10^{-6}$
7-Sn			0.76 $3.5x10^{-3}$		1.05 $1.2x10^{-4}$	$6.7x10^{-3}$		$6.5x10^{-4}$	$<10^{-6}$

The fact that a high PL in the spectral range of deep levels observed in case of CdTe:Sn can serve as an indicator of poor charge collection efficiency is certainly not surprising taking into account the relatively high difference of the integral PL from deep levels between CdTe:Sn and CdTe:In samples group (Table 4.8). More interesting is the apparent correlation between the integral PL intensity of deep levels and the charge collection efficiency in case of CdTe:In samples, i.e. in the case when the total PL signal in the range of 0.5-1 eV is very low. This comparison was done on samples No1-4 originating from the same crystal. The spectra were normalized with respect to the intensity of PL at the energy of free exciton. Two studied samples (No.1 and No.3) being able to detect gamma radiation ($\mu\tau_e \sim 10^{-4} cm^2/Vs$) had the lowest integral PL ($\sim 5\text{-}7x10^{-6}$a.u), while the PL signal of other CdTe:In samples was in the range of ($1.2\text{-}2x10^{-5}$a.u.). Therefore the integral PL in the spectral range of deep levels could indicate the sample quality from the point of view of its suitability for detectors of gamma and X-ray radiation.

The integral PL is certainly only a rough guide and a more detailed analysis of the PL spectra is desirable. Deep levels below midgap are mostly occupied by electrons at equilibrium and do not trap photo-generated electrons. The levels in the upper part of the gap are free and act as strong electron traps. These traps were investigated in details in

section 4.4. by TEES method. Therefore the level at 0.4eV and 0.6 eV are probably mostly responsible for the poor charge collection efficiency of CdTe:In samples No 2., No.4.

Correlation analysis of PL intensity of CdTe:In samples No.1-4 in the range of 1.3-1.48eV (A centers) (Fig.4-24) and 0.5-1.2eV (deep levels) was performed. A-centers are shallow complexes of Cd vacancy and shallow donors (In). It was observed in our laboratory in the past, that samples having a high concentration of A-centers are bad detectors. This result was difficult to understand. A-centers are hole traps being located ~150meV from the valence band. They should have therefore a negligible effect on transport of electrons being practically fully occupied at operating conditions. The results of correlation are presented in Fig.4-25. They clearly show that with an increasing PL signal from A-centers the PL of deep levels also increases. In this sense high radiative recombination at A-centers indicates presence of deep levels influencing the charge collection efficiency of electrons. The observed correlation can be explained by the assumption that deep levels in CdTe:In samples are also complexes. Krustok at el. [146] studied in detail CdTe:Cu:Cl samples by PL in the spectral range 0.6-1.2eV, they observed two deep levels (0.72eV and 0.81eV). Based on the behavior of the integral PL of each of the bands with annealing Te or Cd overpressure they came to the conclusion, that these levels are formed by donor-acceptor complexes. It is supposed, that at high pressures of Te (Cd) acceptors (donors) are neutralized due to the shifts of high temperature Fermi level. As a result of neutralization of one of the partners complexes are not formed at high Te and Cd pressures. Therefore optimal annealing and cooling conditions (Te overpressure and cooling speed) could lead to a reduced concentration of deep levels and thus to fabrication of detector-grade material.

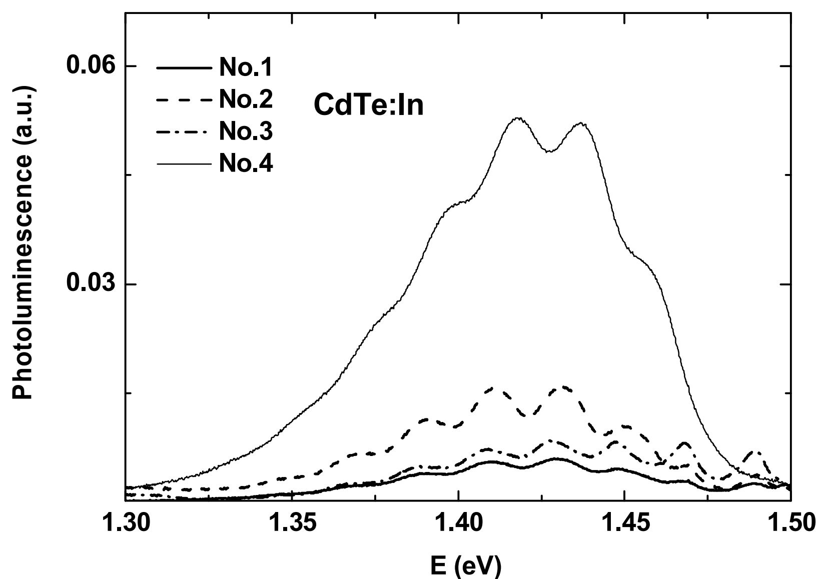

Fig.4-24. Typical PL spectra in the A-center range (1.3-1.5 eV) of the CdTe:In studied samples No.1-4.

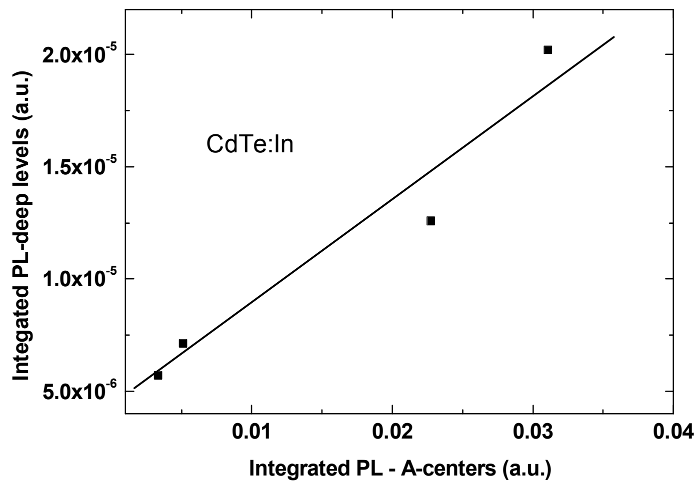

Fig. 4-25. Correlation between the integral PL in the deep levels and A-centers spectral range.

We can conclude from this comparative study of deep PL in semi-insulating CdTe doped shallow donor (In) and deep donor (Sn) the following:

1. Very intensive PL luminescence on deep levels is observed in case of CdTe:Sn samples. The intensity is approximately two orders of magnitude higher, than in In doped samples.
2. Correlation between the detection ability and the integral PL intensity at deep levels was observed.
3. Correlation between integral PL intensity of A-centers and deep levels in CdTe:In samples was found out. This fact supports the idea, that deep levels in these samples are primarily complexes formed together with A-centers.
4. The integral PL in the spectral range of deep levels can serve as an indicator of sample quality from the point of view of their suitability for detectors of gamma and X-ray radiation.

4.6 Numerical simulation of TEES

In the previous sections in the results and discussion part, the properties of the deep defect level like their energy, sign, capture cross section for the dominate carrier, origin, ionization states, rough estimation of the their densities and their correlation to the charge collection properties of the different studied material were looked for.

The densities of shallow impurities, over a limited range of concentrations, have been evaluated using PL measurements (e. g.[147, 148]) and by Hall-technique (e.g. [149]), however, still no easy way to evaluate the accurate densities of deep traps, and to our knowledge, no information about the trap capture cross section for the minority carrier have been published.

In this part of study, TEES simulation model is presented, which can give a lot of information about the defect traps in the bandgap. Comparison of the simulated TEES and experimental results will be one of our future activities. Here, we will show outline of the model and some influence of the trap's parameters on the TEES spectra.

4.6.1 Outlines of the model

4.6.1.1 Theory

The change of concentration of electrons (n) in conduction band, concentration of electrons on centers (n_t), and holes (p) in valence due to the generation-recombination process are described by the following kinetic equations (see 4.1):

$$dn/dt = G + v_e \sum_j S_{ej} n_{tj} n_{lj} - v_e n \sum_j S_{ej}(N_{tj} - n_{tj}) + C_B(n_i^2 - np) \quad (4.5)$$

$$dp/dt = G + v_h \sum_j S_{hj}(N_{tj} - n_{tj}) p_{lj} - v_h p \sum_j S_{hj} n_{tj} + C_B(n_i^2 - np) \quad (4.6)$$

$$dn_{tj}/dt = v_e n S_{ej}(N_{tj} - n_{tj}) - v_e S_{ej} n_{tj} n_{lj} + v_h S_{hj}(N_{tj} - n_{tj}) p_{lj} - v_h p S_{hj} n_{tj} \quad (4.7)$$

And neutrality condition

$$\Delta \mathrm{n} + \sum_j \Delta \mathrm{n}_{\mathrm{tj}} = \Delta \mathrm{p} \quad (4.8)$$

There

S_{ej} (S_{hj}) are capture cross sections of j-th level for electrons (holes).

v_e (v_h) is electron (hole) thermal velocity ($= \sqrt{\frac{8kT}{\pi m^*_{e(h)}}}$).

n_{lj} (p_{lj}) are electron (hole) concentrations when $E_f = E_{tj}$

G is the generation rate; C_B is the direct *G-R* rate between *VB* and *CB*.

Fortran code for numerical solution of this set of equations (4.5-4.8) was composed (author R. Grill) and the time evolution of *n, p,* and n_{tj} are obtained for given N_{tj}, S_{ej}, and S_{hj}.

4.6.1.2 Model output

The model is to calculate the thermal current (I_{TEE}) as a function of temperature by computing the conductivity σ and the thermoelectric power K, using the following equations [99]

$$I_{TEE} = \frac{K_e\sigma_e + K_h\sigma_h}{\sigma_e + \sigma_h}\frac{dT}{dx} = \frac{K_e\mu_e n + K_h\mu_h p}{\mu_e n + \mu_h p}\frac{dT}{dx} \tag{4.9}$$

Where

$$K_e = -\frac{k}{e}[r + \ln(\frac{N_C}{n})] \quad , \qquad K_p = \frac{k}{e}[r + \ln(\frac{N_V}{p})] \tag{4.10}$$

r is a parameter depending on the scattering mechanism. r =5/2 corresponding to low-temperature optical phonon scattering is used in the code. Due to the fact that only relative quantities are watched in the experiment, r has a minor effect on the results and it is not studied in detail in this thesis.

- Concentrations *n, p* come from the numerical solution of the equations (4.5-4.7),
- Drift motilities $\mu=\mu(T)$, obtained by fitting of experimental data in CdTe, [150], have the form

$$\mu_e = 5.632(T)^{1/2}[\exp(261/T) - 1.33] \quad (\text{cm}^2/\text{Vs})$$

$$\mu_h = 57[\exp(252/T) - 1] \quad (\text{cm}^2/\text{Vs})$$

- N_c (N_v) is the effective density of states in the conduction band (valence band)

$$N_{C,V} = 4.829\times10^{15}[T(K)m^*_{e,h}/m_0]^{3/2} \quad (\text{cm}^{-3}), \qquad m^*_e = 0.096m_0\,,\ m^*_h = 0.83m_0\,.$$

4.6.1.3 Model Inputs

- Position of Fermi level relative to CB.
- Number of levels, their position from CB, densities and capture cross sections for both electrons and holes.
- Gap energy $E_g(T)$, In CdTe, [52], has the form

$$E_g(T) = 1.622 - 3.5x10^{-4}T - 1.1x10^{-7}T^2$$

- Heating rate

Note: For each *N* levels, there are as maximum *N-1* peaks. The last depleted level is filled automatically within previous heating due to the necessity to fulfill the neutrality condition (4.8), i.e. to get peak for midgap level it is necessary to include two midgap levels at least.

4.6.1.4 Model Approximations

1- Illumination is assumed to be homogenous. Otherwise, if a strong recombination center exists in the sample, the generated carriers recombine on that and do not penetrate into the sample.
2- Both donor- acceptor (DA) and other inter-defect transitions are neglected. Otherwise, relaxation of the generated trapped charge would take place from the beginning.

4.6.2 Validity of the some glow curves evaluations methods:

By comparing the values of the input trapping parameters with that obtained from the analysis of the output TEES curve, one can check the validity of different evaluation methods. The validity of methods presented in section 2.3 is checked here.
Fig. 4-26 represents the TEES simulated signal at four different heating rates, from acceptor level at $E_A=E_V+0.3Eg$ ($=E_C-0.7Eg$), when a midgap level and Fermi level are located in the middle of the bandgap (-0.5Eg). The input parameters are:
1-Hole trap at $E_A=E_V+0.3Eg$, (i.e. 0.465eV), with concentration $N_A = 1x10^{12}cm^{-3}$ and equal capture cross sections for both electrons and holes as $S_e=10^{-17}= S_h=10^{-17}cm^2$
2-Deep level (hidden) at (-0.5Eg) with $N_t=10^{14}cm^{-3}$, $S_e=10^{-15}$ $cm^{2,}$ and $S_h=10^{-17}$.

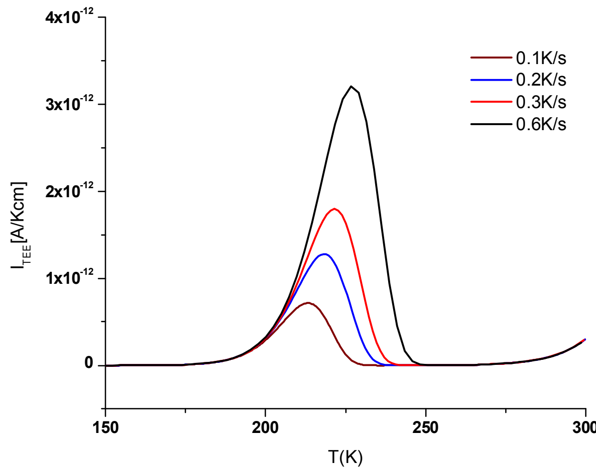

Fig. 4-26 TEES simulated signal at different heating rates. Emission takes place from acceptor level at $E_A=E_V+0.3Eg$, when a midgap level and Fermi level are in the middle of the gap $E_t= -0.5Eg = E_F$

Analysis of the curves in the above figure to evaluate the energy and capture cross section by different method was done; the result is presented in Table 4.9.

Table 4.9: shows the Ionization Energy, E_t, and the capture cross section ,S_h ,obtained by several analyzing method from the simulated TEES curves of Fig. 4-26.

Method	Description	E_t(eV)	S_h(cm^2)
1-Grossweiner[105]	no retrapping (recombination)	0.498	*5.9E^{-17}*
2-Variable heating rate[106]	no retrapping (recombination)	0.466	1.1E^{-17}
3-Initial rise[107]	Independent of recombination	*0.363*	Not included
4-Haering& Adams[108]	Independent of recombination and no/fast retrapping assumed	0.467	Not included

Comparing the different values in the table with the input energy, 0.465eV, and input capture cross section, 1x10^{-17} cm^2, one can note that, the methods that assumed no retrapping process, while recombination occurs give a very good agreement with the input parameters. Therefore, the trapping of conduction electron back to the defect trap has a very low probability in the studied experiment. On the other hand, the result from the initial rise method, which is independent of the recombination kinetic, is in bad agreement with the input values. Therefore recombination processes via the trap defect should be taken into account.

From the experimental view, the variable heating rate method is one of the best methods to analyze the TEES curves, due to the fact that the evaluated values come from the plot of many TEES curves at different heating rate, while the other methods used T_M, T_1, and T_2 from the glow curve, see 2.3. Therefore any errors in these values could cause very big error in the evaluated values

4.6.3 Study the influences of trapping parameters on the TEES signal.

4.6.3.1 The influence of the concentration of the traps on their TEES signals.

Three levels are supposed to be in the bandgap:

- Midgap level (hidden) at E_t = E_F=-0.5Eg, and N_t= 10^{12}cm^{-3}, with equal capturing radii for electrons and holes S_e=S_h=10^{-15}cm$^{2.}$
- Donor level at position -0.2Eg, with S_e=10^{-15} cm^2, and S_h=10^{-16} cm^2.
- Acceptor level at -0.65Eg with S_e=10^{-16} cm^2, and S_h=10^{-15} cm^2.

The calculations have been done for different concentration of the donor and acceptor levels, in the range of $N_D= N_A=10^{11}$ - 10^{14} $cm^{-3.}$ The output spectra are presented in Fig. 4-27. One can see that:

1- As the density of the level increases, its signal increases, and the peak position is shifted to a higher temperature
2- Even if the deep level has equal values of the capturing radii for electrons and holes, electron peak is larger than the hole one. This might be explained by about 10 times larger mobility of electrons than that of holes, and with the filling of the midgap level E_t, by electrons excited from donor level which enhances the capturing of holes excited from acceptor level at higher T.

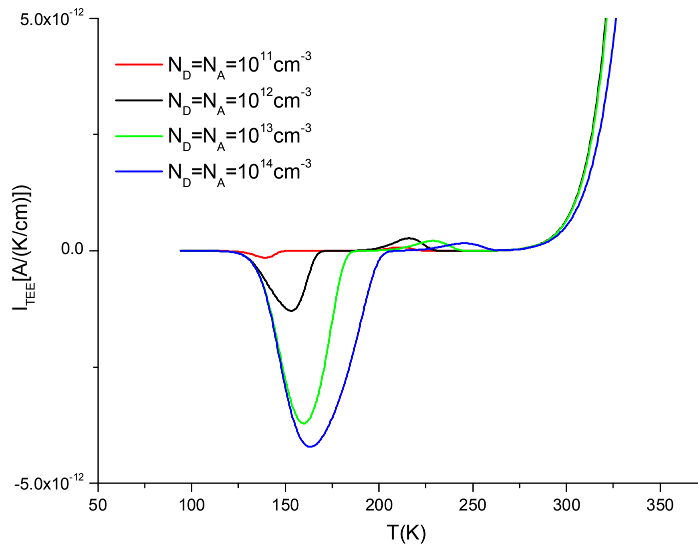

Fig.4-27. The TEES simulated spectra from donor level at E_C- 0.2Eg and acceptor level at E_C-0.65Eg, for different densities of the donor and the acceptor

4.6.3.2 The influences of the capture radii of the deep level on the TEES signal from donor and acceptor level.

Three levels are suggested to be in the bandgap, as

- Donor level at -0.2Eg, with N_D= 2x10^{12} cm^{-3}, S_e=10^{-15} cm^2, and S_h=10^{-16} cm^2.
- Acceptor level at -0.65Eg with N_A= 2x10^{12} cm^{-3} , S_e=10^{-16} cm^2, and S_h=10^{-15} cm^2.
- Midgap level (hidden) at E_t = E_F=-0.5Eg, and N_t= $10^{12}cm^{-3}$

The calculations have been done for different values of capture radii of the midgap level. The output spectra are presented in Fig. 4-28, one can note that the midgap level capture cross section value has a strong influence on the signal from both donor and acceptor levels. The value of 10^{-15} cm^2 capture cross section of the midgap level was enough to cancel the signal from both the donor and acceptor levels.

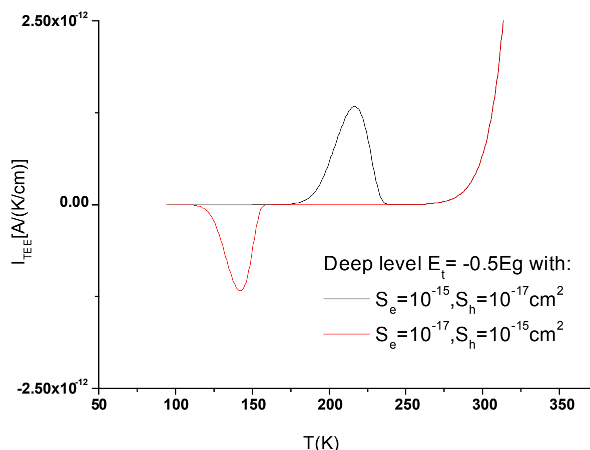

Fig. 4-28. the TEES simulated signal from donor level at E_D=-0.2Eg, and acceptor level at E_A=-0.65Eg. The spectra simulated for different deep level capturing radii for electron, S_e, and holes, S_h, when E_t= E_F =-0.5Eg

4.6.3.3 Influences of the midgap level position on the TEES signal from donor and acceptor level.

Three levels are supposed to be in the bandgap, as

- Donor level at -0.2Eg with N_D=2x10^{12}cm^{-3} , S_e=10^{-15} cm^2 and S_h=10^{-16}cm^2
- Acceptor level at -0.65Eg with N_A=2x10^{12}cm^{-3}, S_e=10^{-16} cm^2 and S_h=10^{-15} cm^2.
- Midgap level with N_t= 8x10^{13}cm^{-3}, and Se=S_h=10^{-16} cm^2

The calculations were done at different positions of the midgap level, E_t, between -0.45Eg and -0.55Eg. The output is shown in Fig. 4-29, where $\delta = E_t - E_F$ .We can note that:

For δ>0 (E_t above E_F) i.e. the midgap level is closer to the donor level than the acceptor level,

1-The signal from the acceptor level, hole signal, is higher than the that from the donor level, and as δ increases the maximum of the hole peak increases while it decreases for electronic one.

2- The conduction at higher temperature is dominated by holes.

3- The peak position is shifted to higher temperature as its maximum increases.

For δ≤0 (E_t at or E_F) i.e. the midgap level is closer to the acceptor level than the donor level,

1-The TEES signal from the donor level, electron signal, is higher than that from the acceptor level, and as δ increases (in –ve) the maximum of the electron peak increases while it decreases for the hole one.

2- The conduction at higher temperatures is dominated by electrons.

3- The peak position is shifted to higher temperatures as its maximum increases.

These results might be explained if we suggest that the capturing probability of midgap level for carriers increases when it becomes closer to their level position and decreases when it will be away from this position. Higher capturing probability of the midgap level for one carrier decreases its signal, and let the other carrier to be dominant.

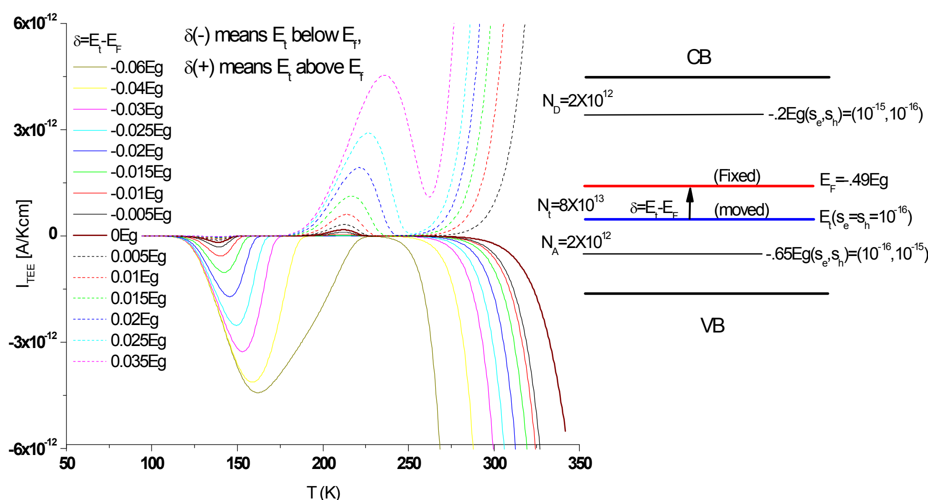

Fig.4-29. TEES simulated spectra from donor level at 0.2Eg, and acceptor level at -0.65Eg for different midgap level positions, with $Se = S_p = 10^{-16}$ cm^2 , and E_F =-0.49Eg.

4.6.4 Summary

TEES simulation model based on the numerical solution of a set of kinetic equations introduced in the SR model to describe the generation –recombination process through a set of defect levels in the bandgap is presented. Using this model, it is concluded that:

1- Checking the validity of different method for analyzing glow curves, showed that the Variation of the heating rate method which ignored the retrapping process is one of the best methods to analyze the TEES glow cures.
2- As the concentration of a bandgap level increase, the intensity of the TEES signal from this level increases, and position of its maximum temperature moves towards the higher concentration, while the ionization energy of the level remains the same.

3- Not all the bandgap levels can show TEES signal. If there is a midgap level with a higher carrier capture cross section, it can deteriorate the TEES signal of this carrier.
4- The area under the TEES signal from bandgap level doesn't depend on his properties only, but on the relative positions of the midgap level and Fermi level. The positions of these two levels are also found to be responsible for the conductivity type at room temperature.

CONCLUSION

Defect structure in high resistivity CdTe samples doped with shallow (In, Cl) and deep (Sn, Ge) donors from crystals grown by vertical gradient freeze method have been investigated by several characterizing techniques. Different trapping parameters of these defect levels and their correlation to the charge collection properties of the material are evaluated to identify which defects act as strong traps or recombination centers that deteriorate the mobility-lifetime product ($\mu\tau$) of the carriers in order to eliminate them from the technological process.

Comparative study by TEES and PICTS methods of various samples have shown that near midgap levels in samples doped with shallow donors (Cl, In) have a low value of capture cross-section and are hole traps. Samples doped with a deep donor (Ge, Sn) have higher capture cross section of the midgap level, and act as electron trap which results in a substantial deterioration of detector performance. TEES measurement using Fermi-level scanning revealed the conversion of the Sn defect from the electron trap in the lower resistivity sample to the hole trap in the higher resistivity one

A complex investigation by several complementary techniques of the CdTe samples doped with different concentration of Sn showed that the Sn impurity strongly influences the material properties. The concentration of Sn must be equal to or higher than the total concentration of uncompensated acceptors to reach precise compensation, and therefore resistivity of 10^{10} Ω cm can be achieved. The middle-gap donor level of Sn located, at E_C–0.85 eV found to be responsible for pinning of Fermi-level and for both compensation and photoconductivity.

Two deep acceptor levels located lower in the band gap than the Sn donor level at E_V + (0.66 to 0.7) eV and E_V + 0.39 eV, are identified and found to be responsible for the photoconductivity at room temperature. Two deep electron traps at E_C-0.47 eV and E_C-0.52 eV, which deteriorate the detector ability of CdTe were identified as native complex defects.

The high resistivity In doped CdTe samples were in detail characterized using TEES and mobility-lifetime measurements. Comparison of results of the studied samples showed, that deterioration of the mobility-lifetime product of electrons can be caused by electron traps at E_C-(0.6-0.7) eV. This clarifies why some In doped CdTe sample is good detector and others are not detecting samples. This electron trap was identified as a native defect complex of Te antisite and Cd. Therefore, annealing effect is expected to eliminate it from the technological process and this way to improve the yield of usable material. Maximum concentrations of these levels in the samples were estimated based on a combination of TEES and mobility-lifetime product measurements.

Since the photoluminescence reflects the loss of carries in a radiative recombination, and therefore the detection properties of the material, a comparative study of CdTe:Sn and CdTe:In have done. A very intensive PL luminescence on deep levels is observed in case of CdTe:Sn samples. The intensity is almost two orders of magnitude higher, than in In doped samples. Approximately 7-15% of radiative recombination occurs through deep levels in case of CdTe:Sn samples and 0.2-1% in case of CdTe:In . A correlation between the detection ability and the integral PL intensity at deep levels was observed. Therefore integral PL in the spectral range of deep levels can serve as an

indicator of sample quality from the point of view of their suitability for detectors of gamma and X-ray radiation.

A correlation between integral PL intensity of A-centers and deep levels in CdTe:In samples was found out. This fact supports the idea, that deep levels in these samples are primarily complexes formed together with A-centers.

The TEES simulation model is presented based on the numerical solution of a set of kinetic equations introduced in the SR model to describe the generation – recombination process through a set of defect levels in the bandgap. The influences of trap parameters on the simulated TEES are observed. Checking the validity of different methods for analyzing glow curves showed that the Variation of the heating rate method which ignored the retrapping process is one of the best methods to analyze the TEES glow curves.

List of publications related to the thesis

A. International Journals

1- **H. Elhadidy**; J. Franc, E. Belas, P. Hlídek , P. Moravec: Thermoelectric Effect Spectroscopy and Photoluminescence of High resistivity CdTe:In. *Journal of Electronic Materials,* (2008*), **Accepted**.*

2- J. Franc, P. Hlídek, E. Belas, J. Kubát, **H. Elhadidy** and R. Fesh : Comparative Study of Deep Levels Defect in Semi-insulating CdTe by Photoluminescence. *Nuclear Instruments and Methods in Physics Research Section A, (2008), **Accepted**.*

3- E. Saucedo, J. Franc, **H. Elhadidy**, P. Horodysky, N. V. Sochinskii: Investigation of the origin of deep levels in CdTe doped with Bi. *Journal of Applied Physics*, **103** (2008) p. 094901-6

4- V. Babentsov, J. Franc, **H. Elhadidy**, A. Fauler, M. Fiederle and R.B. James: Dependence of the $Sn^{0/2+}$ charge state on the Fermi level in semi-insulating CdTe*. Journal of Materials Research**, 22*** (2007), 3249-3254*.*

5- **H. Elhadidy**, J. Franc, P. Moravec, P. Höschl and M. Fiederle: Deep Level Defects in CdTe Materials Studied by Thermoelectric Effect Spectroscopy and Photo-induced Current Transient Spectroscopy. *Semiconductor Science and Technology,* **22** (2007) *537-542.*

6- J. Franc, **H. Elhadidy**, V. Babentsov, A. Fauler, M. Fiederle. Comparative Study of Vertical Gradient Freeze Grown CdTe with Variable Sn Concentration. *Journal of Materials Research,* **21**(2006) 1025-1032

B. International conferences

1- **H. Elhadidy**; J. Franc, E. Belas, P. Hlídek , P. Moravec: Thermoelectric Effect Spectroscopy and Photoluminescence of High resistivity CdTe:In: *Proceeding of the II-VI workshop, Baltimore , Maryland, USA*. Oct. 30- Nov. 1, 2007.

2- J. Franc, P. Hlídek, E. Belas, **H. Elhadidy** and R. Fesh: Deep Level Photoluminescence in Semiinsulating CdTe(In) and CdTe(Sn), *Proceeding of the 9th International Workshop on Radiation Imaging Detectors* (9th IWORID), Erlangen, Germany, July 22-26, 2007.

3- J. Franc, P. Hlídek, E. Belas, J. Kubát, **H. Elhadidy**, and R. Fesh: Photoluminescence Study of Deep Levels in High-resistivity CdTe **,** *Proceeding of the 07 IMAPS CS International Conference, Brno, Czech Republic*, Sept. 20-21, 2007.

4- **H. Elhadidy**, J. Franc, R. Girll, and P. Moravec: Thermoelectric Effect Spectroscopy of Deep Levels in CdTe**, *Invited Paper*:** *Proceeding of the 06 IMAPS CS International Conference. Brno, Czech Republic*, Sept. 14-15, 2006, PP XXVII-XXXII.

5- P. Praus, **H. Elhadidy**, J. Franc, R. Grill and P. Moravec: Control System of Thermal Electron Emission Spectroscopy – Experimental Setup for Study of Deep Levels in High-resistivity CdTe Semiconductor: *Proceeding of the 4th International Conference on Computing, Communications and Control Technologies", CCCT, Orlando, Florida, USA*, July 20-23, 2006

References

1. Zanio, K., *Cadmium Telluride*, in *Semiconductors and Semimetals*, ed. R.K. Willardson and A.C. Beer (Academic Press: New York) Vol. **13** (1978) p. 235
2. Triboule.R, Y. Marfaing, A. Cornet, and P. Siffert, *Undoped High-Resistivity Cadmium Telluride for Nuclear Radiation Detectors.* Journal of Applied Physics. **45** 6 (1974) p. 2759-2765.
3. Szeles, C., *CdZnTe and CdTe materials for X-ray and gamma ray radiation detector applications.* Physica Status Solidi B-Basic Research. **241** 3 (2004) p. 783-790.
4. Luke, P.N., *Single-Polarity Charge Sensing in Ionization Detectors Using Coplanar Electrodes.* Applied Physics Letters. **65** 22 (1994) p. 2884-2886.
5. Barrett, H.H., J.D. Eskin, and H.B. Barber, *Charge - transport in arrays of semiconductor gamma-ray detectors.* Physical Review Letters. **75** 1 (1995) p. 156-159.
6. Shor, A., Y. Eisen, and I. Mardor, *Optimum spectroscopic performance from CZT gamma- and X-ray detectors with pad and strip segmentation.* Nuclear Instruments & Methods in Physics Research Section a-Accelerators Spectrometers Detectors and Associated Equipment. **428** 1 (1999) p. 182-192.
7. Szeles, C. and M.C. Driver, *Growth and properties of semi-insulating CdZnTe for radiation detector applications.* Proceedings of SPIE. **3446** (1998) p. 2-9.
8. Amman, M., J.S. Lee, and P.N. Luke, *Electron trapping nonuniformity in high-pressure-Bridgman-grown CdZnTe.* Journal of Applied Physics. **92** 6 (2002) p. 3198-3206.
9. Berding, M.A., *Annealing conditions for intrinsic CdTe.* Applied Physics Letters. **74** 4 (1999) p. 552-554.
10. Wei, S.H. and S.B. Zhang, *Chemical trends of defect formation and doping limit in II-VI semiconductors: The case of CdTe.* Physical Review B. **66** 15 (2002) p. 155211-1-10.
11. Soundararajan, R., K.G. Lynn, S. Awadallah, C. Szeles, and S.H. Wei, *Study of defect levels in CdTe using thermoelectric effect spectroscopy.* Journal of Electronic Materials. **35** 6 (2006) p. 1333-1340.
12. Du, M.H., H. Takenaka, and D.J. Singh, *Carrier compensation in semi-insulating CdTe: First-principles calculations.* Physical Review B. **77** (2008) p. 094122-1-5.
13. Meyer, B.K., P. Omling, E. Weigel, and G. Mullervogt, *F-Center in CdTe.* Physical Review B. **46** 23 (1992) p. 15135-15138.
14. Emanuelsson, P., P. Omling, B.K. Meyer, M. Wienecke, and M. Schenk, *Identification of the Cadmium Vacancy in CdTe by Electron-Paramagnetic-Resonance.* Physical Review B. **47** 23 (1993) p. 15578-15580.
15. Tessaro, G. and P. Mascher, *Point defect characterization of Zn- and Cd-based semiconductors using positron lifetime spectroscopy.* Journal of Crystal Growth. **197** 3 (1999) p. 581-585.
16. Castaldini, A., A. Cavallini, B. Fraboni, P. Fernandez, and J. Piqueras, *Deep energy levels in CdTe and CdZnTe.* Journal of Applied Physics. **83** 4 (1998) p. 2121-2126.
17. Huang, Z.C., E. Eissler, and C.R. Wie, *Role of Cadmium Vacancy-Related Defects in CdTe Nuclear-Detectors.* Nuclear Instruments & Methods in Physics Research Section B-Beam Interactions with Materials and Atoms. **100** 4 (1995) p. 507-510.
18. Szeles, C., Y.Y. Shan, K.G. Lynn, and A.R. Moodenbaugh, *Trapping properties of cadmium vacancies in* $Cd_{1-x}Zn_xTe$*.* Physical Review B. **55** 11 (1997) p. 6945-6949.

19. Krsmanovic, N., A.W. Hunt, K.G. Lynn, P.J. Flint, and H.L. Glass, *Studies of deep trapping levels in undoped and Sn-doped $Cd_{1-x}Zn_xTe$ by thermoelectric effect spectroscopy and thermally stimulated current.* Proceedings of SPIE. **4141** (2000) p. 11-22.
20. Krsmanovic, N., K.G. Lynn, M.H. Weber, R. Tjossem, T. Gessmann, C. Szeles, E.E. Eissler, J.P. Flint, and H.L. Glass, *Electrical compensation in CdTe and $Cd_{0.9}Zn_{0.1}Te$ by intrinsic defects.* Physical Review B. **62** 24 (2000) p. R16279-R16282.
21. Hage-Ali, M. and P. Siffert, *Growth Methods of CdTe Nuclear Detector Materials*, in *Semiconductors for room temperature nuclear detector applications* ed. T.E. Schlesinger and R.B. James (Academic Press: New York) Vol. **43** (1995) p. 219-255
22. Ye, C.P. and J.H. Chen, *Studies of Defects in N-Type CdTe by Charge Transient Spectroscopy.* Journal of Applied Physics. **67** 5 (1990) p. 2475-2481.
23. Corbel, C., L. Baroux, F.M. Kiessling, C. Gelysykes, and R. Triboulet, *Positron Trapping at Native Vacancies in CdTe Crystals - in Doping Effect.* Materials Science and Engineering B-Solid State Materials for Advanced Technology. **16** 1-3 (1993) p. 134-138.
24. Chang, Y.C. and R.B. James, *Theoretical studies of Cd vacancies and vacancy-chlorine complexes in CdTe and $Cd_{1-x}Zn_xTe$.* Proceedings of SPIE **3768** (1999) p. 381-391.
25. Debbag, F., G. Bastide, and M. Rouzeyre, *Thermal Ionization and Photoionisation Properties of Deep Traps in N-Type CdTe.* Solid State Communications. **67** 1 (1988) p. 1-5.
26. Fiederle, M., D. Ebling, C. Eiche, D.M. Hofmann, M. Salk, W. Stadler, K.W. Benz, and B.K. Meyer, *Comparison of CdTe, $Cd_{0.9}Zn_{0.1}Te$ and $CdTe_{0.9}Se_{0.1}$ Crystals - Application for Gamma-Ray and X-Ray-Detectors.* Journal of Crystal Growth. **138** 1-4 (1994) p. 529-533.
27. Isett, L.C. and P.K. Raychaudhuri, *Deep Levels in N-CdTe.* Journal of Applied Physics. **55** 10 (1984) p. 3605-3612.
28. Chibani, L., M. HageAli, and P. Siffert, *Electrically active defects in detector-grade CdTe:Cl and CdZnTe materials grown by THM and HPBM.* Journal of Crystal Growth. **161** 1-4 (1996) p. 153-158.
29. Allachen, K., M. Tapiero, Z. Guellil, J.P. Zielinger, and J.C. Launay, *Photoconductivity studies in vanadium-doped CdTe and $Cd_{1-x}Zn_xTe$.* Journal of Crystal Growth. **185** (1998) p. 1142-1146.
30. Moravec, P., M. Hageali, L. Chibani, and P. Siffert, *Deep Levels in Semiinsulating CdTe.* Materials Science and Engineering B-Solid State Materials for Advanced Technology. **16** 1-3 (1993) p. 223-227.
31. Toney, J.E., B.A. Brunett, T.E. Schlesinger, E. Cross, F.P. Doty, and R.B. James, *Optical and Electrical Characterization of Copper- and Chlorine-Doped Cadmium Zinc Telluride.* Proceedings of Material Research Society. **487** (1998) p. 59-65.
32. Babii, P.I., V.V. Slynko, Y.P. Gnatenko, P.N. Bukivskii, M.I. Ilashchuk, and O.A. Parfenyuk, *Isoelectronic Substitutional Sc and Ti Impurities in CdTe.* Soviet Physics Semiconductors-Ussr. **24** 8 (1990) p. 904-906.
33. Molva, E., J.M. Francou, J.L. Pautrat, K. Saminadayar, and L.S. Dang, *Electrical and Optical-Properties of Au in Cadmium Telluride.* Journal of Applied Physics. **56** 8 (1984) p. 2241-2249.
34. Hendorfer, G., G. Brunthaler, W. Jantsch, J. Reisinger, and H. Sitter, *Photo-EPR and DLTS of CdTe-Co.* Journal of Crystal Growth. **86** 1-4 (1988) p. 497-501.

35. Godlewski, M. and J.M. Baranowski, *Electron-Paramagnetic-Res Measurements of Chromium Impurity Photo-Ionization Transitions in CdTe.* Physica Status Solidi B-Basic Research. **97** 1 (1980) p. 281-287.
36. Molva, E., J.P. Chamonal, and J.L. Pautrat, *Shallow Acceptors in Cadmium Telluride.* Physica Status Solidi B-Basic Research. **109** 2 (1982) p. 635-644.
37. Sarem, A., B.A. Orlowski, and S. Kuzminski, *Surface Photovoltage Spectroscopy of $Cd_{0.97}Fe_{0.03}Se$ and $Cd_{0.97}Fe0.03Te$ Crystals.* Acta Physica Polonica A. **79** 2-3 (1991) p. 183-186.
38. Jantsch, W., G. Brunthaler, and G. Hendorfer, *Constant photo-EPR: A new method for DEEP level charachterization.* Materials Science Forum. **10-12** (1986) p. 515-520.
39. Lischka, K., G. Brunthaler, and W. Jantsch, *Deep Donor Levels Due to Isolated Fe in CdTe.* Journal of Crystal Growth. **72** 1-2 (1985) p. 355-359.
40. Tovstyuk, K.D., V.G. Deybuk, S.V. Melnichuk, and N.K. Tovstyuk, *3d-Impurity Levels in CdTe and ZnSe.* Physica Status Solidi B-Basic Research. **130** 2 (1985) p. K153-K156.
41. Zerrai, A. and G. Bremond, *Properties of the titanium related level in $Cd_{0.96}Zn_{0.04}Te$ crystals.* Journal of Applied Physics. **84** 10 (1998) p. 5554-5559.
42. Christmann, P., B.K. Meyer, J. Kreissl, R. Schwarz, and K.W. Benz, *Vanadium in CdTe: An electron-paramagnetic-resonance study.* Physical Review B. **53** 7 (1996) p. 3634-3637.
43. Caldas, M.J., A. Fazzio, and A. Zunger, *A Universal Trend in the Binding-Energies of Deep Impurities in Semiconductors.* Applied Physics Letters. **45** 6 (1984) p. 671-673.
44. Zerrai, A., G. Marrakchi, and G. Bremond, *Electrical and optical characteristics of deep levels in vanadium-doped $Cd_{0.96}Zn_{0.04}Te$ materials by photoinduced current, capacitance, and photocapacitance transient spectroscopies.* Journal of Applied Physics. **87** 9 (2000) p. 4293-4302.
45. Neumark, G.F., *Are Impurities the Cause of Self-Compensation in Large-Band-Gap Semiconductors.* Journal of Applied Physics. **51** 6 (1980) p. 3383-3387.
46. Shcherbak, L., P. Feichouk, P. Fochouk, and O. Panchouk, *Self-compensation studies in Cd-saturated in-doped CdTe.* Journal of Crystal Growth. **161** 1-4 (1996) p. 219-222.
47. Stadler, W., D.M. Hofmann, H.C. Alt, T. Muschik, and B.K. Meyer, *Optical Investigations of Defects in $Cd_{1-x}Zn_xTe$.* Physical Review B. **51** 16 (1995) p. 10619-10630.
48. Bassani, F., S. Tatarenko, K. Saminadayar, N. Magnea, R.T. Cox, A. Tardot, and C. Grattepain, *Indium Doping of Cdte and $Cd_{1-x}Zn_xte$ by Molecular-Beam Epitaxy - Uniformly and Planar-Doped Layers, Quantum-Wells, and Superlattices.* Journal of Applied Physics. **72** 7 (1992) p. 2927-2940.
49. Gelysykes, C., C. Corbel, and R. Triboulet, *Positron Trapping in Vacancies in Indium Doped CdTe Crystals.* Solid State Communications. **80** 1 (1991) p. 79-83.
50. Krause-Rehberg, R., H.S. Leipner, T. Abgarjan, and A. Polity, *Review of defect investigations by means of positron annihilation in II-VI compound semiconductors.* Applied Physics A-Materials Science & Processing. **66** 6 (1998) p. 599-614.
51. Espinosa, F.J., J.M. de Leon, S.D. Conradson, J.L. Pena, and M. Zapata-Torres, *Local atomic structure of CdTe : In at high In concentrations.* Physical Review B. **61** 11 (2000) p. 7428-7432.

52. Grill, R., J. Franc, P. Hoschl, I. Turkevych, E. Belas, and P. Moravec, *Semi-insulating Te-saturated CdTe.* Ieee Transactions on Nuclear Science. **52** 5 (2005) p. 1925-1931.
53. Lee, E.Y. and R.B. James, *Effect of electron transport properties on unipolar CdZnTe radiation detectors: LUND, SpectrumPlus, and coplanar grid.* Journal of Electronic Materials. **28** 6 (1999) p. 843-849.
54. Franc, J., V. Babentsov, M. Fiederle, E. Belas, R. Grill, K.W. Benz, and P. Hoschl, *Defect structure of high resistive CdTe : In prepared by vertical gradient freeze method.* IEEE Transactions on Nuclear Science. **51** 3 (2004) p. 1176-1181.
55. Hofmann, D.M., P. Omling, H.G. Grimmeiss, B.K. Meyer, K.W. Benz, and D. Sinerius, *Identification of the Chlorine-A center in CdTe.* Physical Review B. **45** 11 (1992) p. 6247-6250.
56. Panchuk, O., A. Savitskiy, P. Fochuk, Y. Nykonyuk, O. Parfenyuk, L. Shcherbak, M. Ilashchuk, L. Yatsunyk, and P. Feychuk, *IV group dopant compensation effect in CdTe.* Journal of Crystal Growth. **197** 3 (1999) p. 607-611.
57. Scharager, C., P. Siffert, P. Hoschl, P. Moravec, and M. Vanecek, *Characterization of Germanium-Doped CdTe Crystals.* Physica Status Solidi a-Applied Research. **66** 1 (1981) p. 87-92.
58. Chibani, L., M. Hageali, J.P. Stoquert, J.M. Koebel, and P. Siffert, *Carbon and Silicon in Traveling Heater Method Grown Semiinsulating CdTe.* Materials Science and Engineering B-Solid State Materials for Advanced Technology. **16** 1-3 (1993) p. 202-206.
59. Jantsch, W. and G. Hendorfer, *Characterization of Deep Levels in CdTe by Photo-EPR and Related Techniques.* Journal of Crystal Growth. **101** 1-4 (1990) p. 404-413.
60. Bilbe, R.M., J.E. Nicholls, and J.J. Davies, *Electron-Paramagnetic Resonance Investigation of Pb-Doped and Ge-Doped CdTe.* Physica Status Solidi B-Basic Research. **121** 1 (1984) p. 339-344.
61. Kremer, R.E. and W.B. Leigh, *Deep Levels in CdTe.* Journal of Crystal Growth. **86** 1-4 (1988) p. 490-496.
62. Franc, J., M. Fielderle, V. Babentsov, A. Fauler, K.W. Benz, and R. James, *Defect structure of Sn-doped CdTe.* Journal of Electronic Materials. **32** 7 (2003) p. 772-777.
63. Francou, J.M., K. Saminadayar, and J.L. Pautrat, *Shallow Donors in CdTe.* Physical Review B. **41** 17 (1990) p. 12035-12046.
64. Molva, E., K. Saminadayar, J.L. Pautrat, and E. Ligeon, *Photo-Luminescence Studies in N, P, Arsenic Implanted Cadmium Telluride.* Solid State Communications. **48** 11 (1983) p. 955-960.
65. Stadler, W., D.M. Hofmann, B.K. Meyer, R. Krauserehberg, A. Polity, T. Abgarjan, M. Salk, K.W. Benz, and M. Azoulay, *Compensation Models in Chlorine Doped CdTe Based on Position Annihilation and Photoluminescence Spectroscopy.* Acta Physica Polonica A. **88** 5 (1995) p. 921-924.
66. Park, C.H. and D.J. Chadi, *First-Principles Study of DX-Centers in CdTe, ZnTe, and* Cd_xZn_{1-x} *Te Alloys.* Physical Review B. **52** 16 (1995) p. 11884-11890.
67. Ido, T., A. Heurtel, R. Triboulet, and Y. Marfaing, *Deep Level Structure and Compensation Mechanism in in-Doped CdTe Crystals.* Journal of Physics and Chemistry of Solids. **48** 9 (1987) p. 781-790.
68. Molva, E., J.L. Pautrat, K. Saminadayar, G. Milchberg, and N. Magnea, *Acceptor States in CdTe and Comparison with ZnTe - General Trends.* Physical Review B. **30** 6 (1984) p. 3344-3354.

69. Look, D.C., Z.Q. Fang, J.W. Hemsky, and P. Kengkan, *Identification of electron-irradiation defects in semi-insulating GaAs by normalized thermally stimulated current measurements.* Physical Review B. **55** 4 (1997) p. 2214-2218.
70. Bube, R.H., *Photoconductivity and Crystal Imperfections in Cadmium Sulfide Crystals .2. Determination of Characteristic Photoconductivity Quantities.* Journal of Chemical Physics. **23** 1 (1955) p. 18-25.
71. Santic, B. and U.V. Desnica, *Thermoelectric Effect Spectroscopy of Deep Levels - Application to Semi-Insulating Gaas.* Applied Physics Letters. **56** 26 (1990) p. 2636-2638.
72. Lang, D.V., *Deep-Level Transient Spectroscopy - New Method to Characterize Traps in Semiconductors.* Journal of Applied Physics. **45** 7 (1974) p. 3023-3032.
73. Mooney, P.M., *Photo-Deep Level Transient Spectroscopy - A technique to Study Deep Levels in Heavily Compensated Semiconductors.* Journal of Applied Physics. **54** 1 (1983) p. 208-213.
74. Eiche, C., D. Maier, M. Schneider, D. Sinerius, J. Weese, K.W. Benz, and J. Honerkamp, *Analysis of Photoinduced Current Transient Spectroscopy (PICTS) Data by a Regularization Method.* Journal of Physics-Condensed Matter. **4** 28 (1992) p. 6131-6140.
75. Vonwindheim, J.A. and M. Cocivera, *Hall-Effect Measurements on CdTe Electrodeposited from Tri-N-Butylphosphine Telluride.* Journal of Physics and Chemistry of Solids. **53** 1 (1992) p. 31-38.
76. Lee, E.Y., *Thermoelectric voltage spectroscopy for studying compensation in semi-insulating wide energy band gap materials.* Solid State Communications. **112** 1 (1999) p. 31-34.
77. Ayoub, M., M. Hage-Ali, J.M. Koebel, A. Zumbiehl, F. Klotz, C. Rit, R. Regal, P. Fougeres, and P. Siffert, *Annealing effects on defect levels of CdTe : Cl materials and the uniformity of the electrical properties.* Ieee Transactions on Nuclear Science. **50** 2 (2003) p. 229-237.
78. Zerrai, A., M. Dammark, and G. Bremond. *Deep level characterization of Ti and V doped $Cd_{96\%}Zn_{4\%}Te$ crystals for semi-insulating and photorefractiveapplications*. in *Semiconducting and Semi-Insulating Materials Conferance*. (Toulouse, France, 1996) p. 127-130.
79. Saucedo, E., C.M. Ruiz, V. Bermudez, E. Dieguez, E. Gombia, A. Zappettini, A. Baraldi, and N.V. Sochinskii, *Photoluminescence and photoconductivity in CdTe crystals doped with Bi.* Journal of Applied Physics. **100** 10 (2006) p. 104901-1-6.
80. Castaldini, A., A. Cavallini, B. Fraboni, P. Fernandez, and J. Piqueras, *Midgap traps related to compensation processes in CdTe alloys.* Physical Review B. **56** 23 (1997) p. 14897-14900.
81. Cavallini, A., B. Fraboni, W. Dusi, and M. Zanarini, *Defective states induced in CdTe and CdZnTe detectors by high and low energy neutron irradiation.* Journal of Applied Physics. **94** 5 (2003) p. 3135-3142.
82. Samimi, M., B. Biglari, M. Hageali, J.M. Koebel, and P. Siffert, *About the Origin of the 0.15 to 0.20 eV Defect Level in Cadmium Telluride.* Physica Status Solidi A-Applied Research. **100** 1 (1987) p. 251-258.
83. Cavallini, A., B. Fraboni, and W. Dusi, *Compensation processes in CdTe-based compounds.* IEEE Transactions on Nuclear Science. **52** (2005) p. 1964-1967.
84. Bao, X.J., T.E. Schlesinger, R.B. James, R.H. Stulen, C. Ortale, and L. Vandenberg, *Investigation of Copper Electrodes for Mercuric Iodide Detector Applications.* Journal of Applied Physics. **67** 12 (1990) p. 7265-7267.

85. Bao, X.J., T.E. Schlesinger, R.B. James, G.L. Gentry, A.Y. Cheng, and C. Ortale, *Study of Semitransparent Palladium Contacts on Mercuric Iodide by Photoluminescence Spectroscopy and Thermally Stimulated Current Measurements.* Journal of Applied Physics. **69** 8 (1991) p. 4247-4252.
86. Lee, E.Y., J.C. Lund, N.R. Hilton, B.A. Brunett, and R.B. James, *Device Simulation of a Unipolar Gamma-Ray Detector.* Proceedings of Material Research Society. **487** (1998) p. 537-545.
87. Fougeres, P., M. Hage-Ali, J.M. Koebel, P. Siffert, S. Hassan, A. Lusson, R. Triboulet, G. Marrakchi, A. Zerrai, K. Cherkaoui, R. Adhiri, G. Bremond, O. Kaitasov, M.O. Ruault, and J. Crestou, *Properties of $Cd_{1-x}Zn_xTe$ crystals grown by high pressure Bridgman for nuclear detection.* Journal of Crystal Growth. **185** (1998) p. 1313-1318.
88. Lee, E.Y., B.A. Brunett, R.W. Olsen, J.M. Van Scyoc III, H. Hermon, and R.B. James, *Detection of electron and hole traps in CdZnTe radiation detectors by thermoelectric emission spectroscopy and thermally stimulated conductivity.* Proceedings of SPIE. **3446** (1998) p. 40-48.
89. Desnica, U.V., M. Pavlovic, Z.Q. Fang, and D.C. Look, *Thermoelectric effect spectroscopy of deep levels in semi-insulating GaN.* Journal of Applied Physics. **92** 7 (2002) p. 4126-4128.
90. Awadalla, S.A., A.W. Hunt, T.B. Tjossem, K.G. Lynn, C. Szeles, and M. Bliss, *Evidence for dislocations or related defects present in CdTe and $Cd_{1-x}Zn_xTe$ Crystals.* Proceedings of SPIE. **4507.** (2001.) p. 264-272.
91. Szeles, C., Y.Y. Shan, K.G. Lynn, and E.E. Eissler, *Deep electronic levels in high-pressure Bridgman $Cd_{1-x}Zn_xTe$.* Nuclear Instruments & Methods in Physics Research Section A-Accelerators Spectrometers Detectors and Associated Equipment. **380** 1-2 (1996) p. 148-152.
92. Lynn, K.G., M. Weber, H. Glass, J. Flint, and C. Szeles, *Improved CdZnTe Detectors Grown by Vertical Bridgman Process.* Proceedings of Material Research Society **487** (1998) p. 229-239.
93. Awadalla, S.A., K.G. Lynn, S.H. Wei, and C. Szeles, *Effect of Zn on the cation vacancy-isoelectronic oxygen pair in $Cd_{1-x}Zn_xTe$ crystals.* Physical Review B. **70** 24 (2004) p. 245213-1-3.
94. Saucedo, E., J. Franc, H. Elhadidy, P. Horodysky, C.M. Ruiz, V. Bermúdez, and N.V. Sochinskii, *Investigation of the origin of deep levels in CdTe doped with Bi.* Journal of Applied Physics. **103** (2008) p. 094901-6.
95. Cavallini, A., B. Fraboni, and W. Dusi, *Compensation processes in CdTe-based compounds.* Nuclear Science Symposium Conference Record, 2004 IEEE. **7** (2004) p. 4247- 4250.
96. Franc, J., P. Horodysky, R. Grill, J. Kubat, E. Saucedo, and N.V. Sochinskii, *Characterization of optical and electrical properties of CdTe : Yb co-doped with Ge.* Journal of Crystal Growth. **286** 2 (2006) p. 384-388.
97. Shockley, W. and W.T. Read, *Statistics of the Recombinations of Holes and Electrons.* Physical Review. **87** 5 (1952) p. 835-842.
98. Marfaing, Y., *Handbook of semiconductor,* Vol. **2** (1980) p. 418-445.
99. Böer, K.W., *Survey of Semiconductor Physics,* (Van Nostrand Reinhold: New York) Vol. **II** (1992) p. 757
100. Goudon, T., V. Miljanovic, and C. C. Schmeiser, *On the Shockley–Read–Hall model: Generation-Recombination in Semiconductors.* SIAM J. APPL. MATH. **67** 4 (2007) p. 1183–1201.

101. Balland, J.C., J.P. Zielinger, M. Tapiero, J.G. Gross, and C. Nogue, *Investigation of deep levels in high-resistivity bulk materials by Photoinduced current transient spectrocopy. 2. Evaluation of various signal-proceeing methods.* Journal of Physics D-Applied Physics. **19** 1 (1986) p. 71-87.

102. Tapiero, M., N. Benjelloun, J.P. Zielinger, S. Elhamd, and C. Noguet, *Photoinduced Current Transient Spectroscopy in High-Resistivity Bulk Materials - Instrumentation and Methodology.* Journal of Applied Physics. **64** 8 (1988) p. 4006-4012.

103. Nicholas, K.H. and J. Woods, *Evaluation of Electron Trapping Parameters from Conductivity Glow Curves in Cadmium Sulphide.* British Journal of Applied Physics. **15** 7 (1964) p. 783-795.

104. Pagonis, V., *Evaluation of activation energies in the semi-localized transition model of thermoluminescence.* Journal of Physics D-Applied Physics. **38** 13 (2005) p. 2179-2186.

105. Grossweiner, L.I., *A note on the Analysis of 1st-Order Glow Curves.* Journal of Applied Physics. **24** 10 (1953) p. 1306-1307.

106. Booth, A.H., *Calculation of Electron Trap Depth from Thermoluminescence Maxima.* Canadian Journal of Chemistry-Revue Canadienne De Chimie. **32** 2 (1954) p. 214-215.

107. Garlick, G.F.J. and A.F. Gibson, *The Electron Trap Mechanism of Luminescence in Sulphide and Silicate Phosphors.* Proceedings of the Physical Society of London. **60** 342 (1948) p. 574-590.

108. Haering, R.R. and E.N. Adams, *Theory and Application of Thermally Stimulated Currents in Photoconductors.* Physical Review. **117** 2 (1960) p. 451-454.

109. Stibal, R., J. Windscheif, and W. Jantz, *Contactless Evaluation of Semiinsulating Gaas Wafer Resistivity Using the Time-Dependent Charge Measurement.* Semiconductor Science and Technology. **6** 10 (1991) p. 995-1001.

110. Ayoub, M., M. Hage-Ali, A. Zumbiehl, R. Regal, J.M. Koebel, C. Rit, P. Fougeres, and P. Siffert, *Study of the resistivity mapping in CdTe : Cl - Correlation with annealing and Te-precipitates.* Ieee Transactions on Nuclear Science. **49** 4 (2002) p. 1954-1959.

111. Rudolph, P. and M. Muhlberg, *Basic Problems of Vertical Bridgman Growth of CdTe.* Materials Science and Engineering B-Solid State Materials for Advanced Technology. **16** 1-3 (1993) p. 8-16.

112. Kroger, F.A., *Defect Structure of CdTe.* Revue De Physique Appliquee. **12** 2 (1977) p. 205-210.

113. Matveev, O.A. and A.I. Terent'ev, *Basic principles of postgrowth annealing of CdTe : Cl ingot to obtain semi-insulating crystals.* Semiconductors. **34** 11 (2000) p. 1264-1269.

114. Fiederle, M., C. Eiche, M. Salk, R. Schwarz, K.W. Benz, W. Stadler, D.M. Hofmann, and B.K. Meyer, *Modified compensation model of CdTe.* Journal of Applied Physics. **84** 12 (1998) p. 6689-6692.

115. Fiederle, M., V. Babentsov, J. Franc, A. Fauler, K.W. Benz, R.B. James, and E. Cross, *Defect structure of Ge-doped CdTe.* Journal of Crystal Growth. **243** 1 (2002) p. 77-86.

116. Brunthaler, G., W. Jantsch, U. Kaufmann, and J. Schneider, *Electron-Spin-Resonance Analysis of the Deep Donors Lead, Tin, and Germanium in CdTe.* Physical Review B. **31** 3 (1985) p. 1239-1243.

117. Savitskii, A.V., K.D. Tovstyuk, and O.E. Panchuk, *Impurity Intraction in CdTe Dynamic Lattice.* Fizika Tverdogo Tela. **27** 11 (1985) p. 3248-3253.

118. Fochuk, P.M., L.P. Shcherbak, P.I. Feichuk, and O.E. Panchuk, *Spectrum of point defects in quenched crystals of Sn-doped CdTe.* Inorganic Materials. **31** 12 (1995) p. 1383-1384.
119. Illgner, M. and H. Overhof, *Electronic structure and hyperfine interactions of 3d transition element sons in CdTe.* Semiconductor Science and Technology. **11** 7 (1996) p. 977-982.
120. Savitskii, A.V., O.A. Parfenyuk, M.I. Ilashchuk, and P.A. Pavlin, *Compensating Effect of Lead Impurity in Cadmium Telluride.* Inorganic Materials. **25** 11 (1989) p. 1564-1567.
121. Gorlei, P.N., O.A. Parfenyuk, M.I. Ilashchuk, K.S. Ul'yanitskii, V.R. Burachek, and S.N. Chupyra, *Photosensitive centers in CdTe < Ge >, CdTe < Sn >, and CdTe < Pb >*. Inorganic Materials. **39** 11 (2003) p. 1127-1131.
122. Franc, J., H. Elhadidy, V. Babentsov, A. Fauler, and M. Fiederle, *Comparative study of vertical gradient freeze grown CdTe with variable Sn concentration.* Journal of Materials Research. **21** 4 (2006) p. 1025-1032.
123. Grosch, G.H., B. Freytag, K.J. Range, and U. Rossler, *Stability of $Cd_xSn_{1-x}Te$ in Rock-Salt Structure - A Study of Zero-Flux Surfaces and Bonding Character.* Journal of Chemical Physics. **101** 8 (1994) p. 6782-6789.
124. Blackmore, G.W., S.J. Courtney, A. Royle, N. Shaw, and A.W. Vere, *Boron-Segregation in Czochral ski-grown CdTe.* Journal of Crystal Growth. **85** 3 (1987) p. 335-340.
125. Oldekop, E., V. Eyert, F. Niedermeyer, M. Wienecke, and W.D. Zeitz, *The behaviour of B-12 in CdTe studied with beta-NMR techniques.* Materials Science Applications of Ion Beam Techniques. **248-** (1997) p. 267-270.
126. Pal, U., P. Fernandez, J. Piqueras, N.V. Sochinskii, and E. Dieguez, *Cathodoluminescence Characterization of Ge-Doped CdTe Crystals. Journal of Applied Physics.* Journal of Applied Physics. **78** 3 (1995) p. 1992-1995.
127. Yu, Z.H., S.G. Hofer, N.C. Giles, T.H. Myers, and C.J. Summers, *Interpretation of near-Band-Edge Photoreflectance Spectra from CdTe.* Physical Review B. **51** 19 (1995) p. 13789-13792.
128. Hageali, M. and P. Siffert, *Status of Semiinsulating Cadmium Telluride for Nuclear Radiation Detectors.* Nuclear Instruments & Methods in Physics Research Section A-Accelerators Spectrometers Detectors and Associated Equipment. **322** 3 (1992) p. 313-323.
129. Rose, A., *Concepts in photoconductivity and allied problems,* (Robert E. Krieger Publishing: New York) (1978) p. 43
130. Bube, R.H., *Photoconductivity of solids,* (John Wiley & Sons: New York) (1960) p. 325
131. Mathew, X., *Photo-induced current transient spectroscopic study of the traps in CdTe.* Solar Energy Materials and Solar Cells. **76** 3 (2003) p. 225-242.
132. Fougeres, P., P. Siffert, M. Hageali, J.M. Koebel, and R. Regal, *CdTe and $Cd_{1-x}Zn_xTe$ for nuclear detectors: facts and fictions.* Nuclear Instruments & Methods in Physics Research Section A-Accelerators Spectrometers Detectors and Associated Equipment. **428** 1 (1999) p. 38-44.
133. Takebe, T., J. Saraie, and H. Matsunami, *Detailed Characterization of Deep Centers in CdTe - Photo-Ionization and Thermal Ionization Properties.* Journal of Applied Physics. **53** 1 (1982) p. 457-469.
134. Sitter, H., D. As, J. Humenberger, and A. Lopezotero, *Investigation of Deep Levels in Epitaxially Grown CdS and CdTe Layers.* Journal of Crystal Growth. **59** 1-2 (1982) p. 229-233.

135. Khattak, G.M. and C.G. Scott, *Characteristics of DEEP Levels in n-type CdTe.* Journal of Physics-Condensed Matter. **3** 44 (1991) p. 8619-8634.
136. Eiche, C., W. Joerger, M. Fiederle, D. Ebling, R. Schwarz, and K.W. Benz, *Investigation of CdTe-Cl Grown from the Vapor-Phase under Microgravity Conditions with Time-Dependent Charge Measurements and Photoinduced Current Transient Spectroscopy.* Journal of Crystal Growth. **146** 1-4 (1995) p. 98-103.
137. Balcioglu, A., R.K. Ahrenkiel, and F. Hasoon, *Deep-level impurities in CdTe/CdS thin-film solar cells.* Journal of Applied Physics. **88** 12 (2000) p. 7175-7178.
138. Becker, U., P. Rudolph, R. Boyn, M. Wienecke, and I. Utke, *Characterization of p-type CdTe bridgman crystal by infrared extinction spectra.* Physica Status Solidi A-Applied Research. **120** 2 (1990) p. 653-660.
139. Fiederle, M., A. Fauler, J. Konrath, V. Babentsov, J. Franc, and R.B. James, *Comparison of undoped and doped high resistivity CdTe and (Cd,Zn)Te detector crystals.* Ieee Transactions on Nuclear Science. **51** 4 (2004) p. 1864-1868.
140. Astles. M.G., ed. EMIS Datareviews Series 10 (INSPEC: LONDON) (1994) p.494-500.
141. Babentsov, V., V. Corregidor, J.L. Castano, E. Dieguez, M. Fiederle, T. Feltgen, and K.W. Benz, *Compensation in semi-intrinsic CdTe based materials.* Proceedings of SPIE. **4355** (2001) p. 238-251.
142. Lee, E.Y., R.B. James, R.W. Olsen, and H. Hermon, *Compensation and trapping in CdZnTe radiation detectors studied by thermoelectric emission spectroscopy, thermally stimulated conductivity, and current-voltage measurements.* Journal of Electronic Materials. **28** 6 (1999) p. 766-773.
143. Franc, J., R. Grill, J. Kubat, P. Hlidek, E. Belas, P. Moravec, and P. Hoschl, *Influence of space charge on lux-ampere characteristics of high-resistivity CdTe.* Journal of Electronic Materials. **35** 5 (2006) p. 988-992.
144. Elhadidy, H., J. Franc, P. Moravec, P. Hoschl, and M. Fiederle, *Deep level defects in CdTe materials studied by thermoelectric effect spectroscopy and photo-induced current transient spectroscopy.* Semiconductor Science and Technology. **22** 5 (2007) p. 537-542.
145. Vogel, E.E., O. Mualin, M.A. Deorue, J. Riverairatchet, M.L. Flores, U.W. Pohl, H.J. Schulz, and M. Thiede, *Infrared Luminescence and Application of a Vibronic-Coupling Hamiltonian to the Level Structure of Cdte-*Fe^{2+}. Physical Review B. **50** 8 (1994) p. 5231-5238.
146. Krustok, J., A. Loo, and T. Piibe, *Deep-Level Photoluminescence of Doped CdTe in the 0.8eV Region.* Journal of Physics and Chemistry of Solids. **52** 8 (1991) p. 1037-1038.
147. Colley, P.M. and E.C. Lightowlers, *Calibration of the Photoluminescence Technique for Measuring B, P and Al Concentrations in Si in the Range* 10^{12} *to* 10^{15} cm^{-3} *Using Fourier-Transform Spectroscopy.* Semiconductor Science and Technology. **2** 3 (1987) p. 157-166.
148. Tajima, M., *Recent Advances in Photo-Luminescence Analysis of Si - Application to an Epitaxial Layer and Nitrogen in Si.* Japanese Journal of Applied Physics. **21** 1 (1982) p. 113-119.
149. Wolfe, C.M., G.E. Stillman, and J.O. Dimmock, *Ionized Impurity Density in n-Type GaAs* . Journal of Applied Physics. **41** 2 (1970) p. 504-509.
150. Turkevych, I., R. Grill, J. Franc, E. Belas, P. Hoschl, and P. Moravec, *High-temperature electron and hole mobility in CdTe.* Semiconductor Science and Technology. **17** 10 (2002) p. 1064-1066.